THE UNIVERSITY OF QUEENSLAND

AUSTRALIA

Effects of reagents and solid particles on drainage and stability of liquid film, foam and froth

Jianlong Wang

B.Eng., M.Eng.

A thesis submitted for the degree of Doctor of Philosophy at

The University of Queensland in 2015

School of Chemical Engineering

Abstract

The objective of this study is to explore the interrelated mechanisms governing foam drainage and stability by modeling the foam column kinetics, measuring the interfacial properties of the air-water interface and conducting forced drainage experiments. Studies on foams are usually divided into four length scales: (i) a gas-liquid interface (molecular scale), (ii) a liquid film (nanometer scale), (iii) a bubble (millimeter scale), and (iv) a foam (meter scale). Although much progress has been made in each length scale, the correlation between the different length scales remains poorly understood and quantified. The present study seeks to address this problem. In many industrial processes, such as froth flotation and foam fractionation, careful control of the foam or froth stability is required to optimize the process performance. Therefore, an understanding of the correlation between the different length scales is of paramount interest for industrial applications. The present study can be divided into three different parts: (1) foam column kinetics, (2) mechanisms governing foamability and foam stability, and (3) foam drainage in the presence of solid particles.

The first part models foam column kinetics to predict the evolution of foam growth, liquid fraction, the transport of liquid and gas in growing foams and foam collapse by analogy with chemical kinetics. First, a modeling framework was formulated to categorize the foam or froth growth models into zeroth, first and second order, according to the dependence of the foam collapse rate on the foam volume or height. Then, a novel kinetic model was developed based on the mass balance of gas and liquid in the foam column to simulate the foam column kinetics. Finally, the simulation results were compared with the reported experimental data. Good agreement between model predictions and published experimental results confirms the validity of the analogy between foam column kinetics and reaction kinetics.

Mechanisms governing the foamability and foam stability are crucial to understanding foam behaviors. The foamability and foam stability of surfactant blend and surfactant solutions in different electrolyte concentrations were examined to elucidate the different mechanisms that collectively determine foamability and foam stability. The foam growth kinetic model developed in the previous section was also applied here. First, the foamability of sodium dodecyl sulfate (SDS)-dodecanol (DOH)

solutions was investigated to test the conventional theories that apply to a single surfactant of pre-critical micelle concentration (CMC). The remarkable decrease in the foamability of SDS solutions caused by the addition of DOH could not be easily explained by the theories of surface tension and surface viscoelasticity. Instead, alternative mechanisms were proposed. Second, findings regarding the foamability of SDS-DOH solutions were extended to froth flotation, that is, the effect of a nonpolar collector (diesel oil) on the foamability of frother solutions (methyl isobutyl carbinol, MIBC). The results showed that the presence of diesel oil, even in trace amounts (e.g., 2 ppm), could effectively decrease the foam growth rate by accelerating the foam collapse process. Two mechanisms were proposed to explain the antifoam effect of diesel oil: (i) the spreading of the diesel oil droplets at the liquid film interface and (ii) the molecular interactions between the diesel oil and the frother molecules. Finally, the rupture of standing aqueous foams stabilized by SDS-DOH and SDS-NaCl mixtures was examined to obtain different values of the surface viscoelasticity and surface potential to elucidate the roles of surface rheology and intermolecular forces in foam stability.

Foam drainage in the presence of solid particles is relevant to the field of froth flotation, where the wash water is commonly applied to the froth layer to improve the product's grade. Forced drainage experiments were conducted to study the liquid flow within the foam stabilized by hexadecyltrimethylammonium bromide (CTAB) with glass beads. Two foam drainage models for aqueous foams were applied to simulate and interpret the experimental results. The simulation results showed that the presence of solid particles in foams increases the rigidity of the interfaces and the viscous losses in the channels (Plateau borders) of the foams, which consequently resulted in a decrease in the foam permeability.

In summary, the present study focuses on modeling foam column kinetics, the effects of interfacial properties on the foamability and foam stability of surfactant solutions, and the effect of solid particles on foam drainage. To further understand the mechanisms governing foamability and foam stability, the interplay and magnitude of these mechanisms on the different stages of foam life should be addressed in future studies.

Declaration by author

This thesis is composed of my original work, and contains no material previously published or written by another person except where due reference has been made in the text. I have clearly stated the contribution by others to jointly-authored works that I have included in my thesis.

I have clearly stated the contribution of others to my thesis as a whole, including statistical assistance, survey design, data analysis, significant technical procedures, professional editorial advice, and any other original research work used or reported in my thesis. The content of my thesis is the result of work I have carried out since the commencement of my research higher degree candidature and does not include a substantial part of work that has been submitted to qualify for the award of any other degree or diploma in any university or other tertiary institution. I have clearly stated which parts of my thesis, if any, have been submitted to qualify for another award.

I acknowledge that an electronic copy of my thesis must be lodged with the University Library and, subject to the policy and procedures of The University of Queensland, the thesis be made available for research and study in accordance with the Copyright Act 1968 unless a period of embargo has been approved by the Dean of the Graduate School.

I acknowledge that copyright of all material contained in my thesis resides with the copyright holder(s) of that material. Where appropriate I have obtained copyright permission from the copyright holder to reproduce material in this thesis.

Publications during candidature

Peer-reviewed papers submitted

1. **Wang, J.**, Nguyen, A. V. and Farrokhpay, S., A Critical Review of the Growth, Drainage and Collapse of Foams. Advances in Colloid and Interface Science, 2015
2. **Wang, J.**, Nguyen, A. V. and Farrokhpay, S., Foam Column Kinetics – Analogy to Reaction Kinetics. Chemical Engineering Science, 2015
3. **Wang, J.**, Nguyen, A. V. and Farrokhpay S., Foamability of Sodium Dodecyl Sulfate Solutions: Anomalous Effect of Dodecanol Unexplained by Conventional Theories. Colloids and Surfaces, A: Physicochemical and Engineering Aspects, 2015
4. **Wang, J.**, Nguyen, A. V. and Farrokhpay, S., Effects of Nonpolar Collector on Foam Stability, International Journal of Mineral Processing, 2015
5. **Wang, J.**, Nguyen, A. V. and Farrokhpay S., Effects of Surface Rheology and Surface Potential on Foam Stability. Journal of Colloid and Interface Science, 2015
6. **Wang, J.**, Nguyen, A. V. and Farrokhpay S., Foam Drainage in the Presence of Solid Particles. European Physical Journal E: Soft Matter, 2015

Publications included in this thesis

Wang, J., Nguyen, A. V. and Farrokhpay, S., A Critical Review of the Growth, Drainage and Collapse of Foams. Advances in Colloid and Interface Science, 2015. - incorporated as Chapter 2.

Contributor	Statement of contribution
Author Jianlong Wang (Candidate)	Wrote the paper (70%)
Author Anh Nguyen	Wrote and edited paper (20%)
Author Saeed Farrokhpay	Wrote and edited paper (10%)

Wang, J., Nguyen, A. V. and Farrokhpay, S., Foam Column Kinetics – Analogy to Reaction Kinetics. Chemical Engineering Science, 2015. - incorporated as Chapter 3.

Contributor	Statement of contribution
Author Jianlong Wang (Candidate)	Analyzed and interpreted data (80%) Wrote the paper (70%)
Author Anh Nguyen	Analyzed and interpreted data (20%) Wrote and edited paper (20%)
Author Saeed Farrokhpay	Wrote and edited paper (10%)

Wang, J., Nguyen, A. V. and Farrokhpay, S., Foamability of Sodium Dodecyl Sulfate Solutions: Anomalous Effect of Dodecanol Unexplained by Conventional Theories. Colloids and Surfaces, A: Physicochemical and Engineering Aspects, 2015. - incorporated as Chapter 4.

Contributor	Statement of contribution
Author Jianlong Wang (Candidate)	Designed experiments (80%) Conducted experiments (100%) Analyzed and interpreted data (80%) Wrote the paper (70%)
Author Anh Nguyen	Designed experiments (20%) Analyzed and interpreted data (20%) Wrote and edited paper (20%)
Author Saeed Farrokhpay	Wrote and edited paper (10%)

Wang, J., Nguyen, A. V. and Farrokhpay, S., Effects of Nonpolar Collector on Foam Stability, International Journal of Mineral Processing, 2015. – incorporated as Chapter 5.

Contributor	Statement of contribution
Author Jianlong Wang (Candidate)	Designed experiments (80%) Conducted experiments (100%) Analyzed and interpreted data (80%) Wrote the paper (70%)
Author Anh Nguyen	Designed experiments (20%) Analyzed and interpreted data (20%) Wrote and edited paper (20%)
Author Saeed Farrokhpay	Wrote and edited paper (10%)

Wang, J., Nguyen, A. V. and Farrokhpay, S., Effects of Surface Rheology and Surface Potential on Foam Stability. Journal of Colloid and Interface Science, 2015. - incorporated as Chapter 6.

Contributor	Statement of contribution
Author Jianlong Wang (Candidate)	Designed experiments (80%) Conducted experiments (100%) Analyzed and interpreted data (80%) Wrote the paper (70%)
Author Anh Nguyen	Designed experiments (20%) Analyzed and interpreted data (20%) Wrote and edited paper (20%)
Author Saeed Farrokhpay	Wrote and edited paper (10%)

Wang, J., Nguyen, A. V. and Farrokhpay, S., Foam Drainage in the Presence of Solid Particles. European Physical Journal E: Soft Matter, 2015. - incorporated as Chapter 7.

Contributor	Statement of contribution
Author Jianlong Wang (Candidate)	Designed experiments (80%) Conducted experiments (100%) Analyzed and interpreted data (80%) Wrote the paper (70%)
Author Anh Nguyen	Designed experiments (20%) Analyzed and interpreted data (20%) Wrote and edited paper (20%)
Author Saeed Farrokhpay	Wrote and edited paper (10%)

Contributions by others to the thesis

Contributions to the conception and design of the project were provided by Professor Anh V Nguyen. Professor Anh V Nguyen contributed to providing advice on the mathematical model design, drafting and writing in an advisory capacity.

Statement of parts of the thesis submitted to qualify for the award of another degree

None.

Acknowledgements

First of all, I would like to extend my sincerest thanks and appreciation to my supervisors, Professor Anh Nguyen and Dr. Saeed Farrokhpay for their valuable guidance, expertise and encouragement throughout my Ph.D. study.

I would like to thank Dr. Reinhard Miller and the Max Planck Institute for Colloid and Surface Science in Potsdam, for giving me the opportunity to stay and learn the interfacial viscoelasticity measurements.

I would like to extend my appreciation to Professor Johannes Cilliers (Department of Earth Science and Engineering, Imperial College London, UK) for his advices and encouragement on the model of foam column kinetics in Chapter 3.

The financial supports from the University of Queensland UQI tuition fee scholarship and China Scholarship Council (CSC) are greatly appreciated.

I would like to thank all the staff and students at the School of Chemical Engineering, for providing both technical and administrative assistance when required.

I would like to thank Dong-xia Feng for the help of calculation of contact angle in Chapter 7.

My thanks also go to all my friends for their understanding and support through the good times and the bad ones.

I especially would like to thank my parents for their unconditional love and support.

Keywords

foam, foam growth, foam drainage, foam collapse, foamability, foam stability, antifoams, surface viscoelasticity, solid particle, foam model

Australian and New Zealand Standard Research Classifications (ANZSRC)

ANZSRC code: 030603, Colloid and Surface Chemistry, 40%
ANZSRC code: 090499, Chemical Engineering not elsewhere classified, 30%
ANZSRC code: 091404, Mineral Processing/Beneficiation, 30%

Fields of Research (FoR) Classification

FoR code: 0306, Physical Chemistry (incl. Structural), 40%
FoR code: 0904, Chemical Engineering, 30%
FoR code: 0914, Resources Engineering and Extractive Metallurgy, 30%

TABLE OF CONTENTS

List of Figures

Chapter 2

Chapter 3

Chapter 4

Chapter 5

Chapter 6

Chapter 7

List of Tables

Chapter 1: Introduction

Foams are highly concentrated dispersions of (dispersed phase) gas in a (continuous phase) liquid [1]. Because of their lightness and large specific surface area, foams are widely applied in our daily lives and in industry. Examples of applications in which foams are used include food, cosmetics, cleaning, surface treatment, building materials, reducing pollution and the extraction of natural resources, e.g., froth flotation [2]. This immense practical and industrial interest inevitably inspires fundamental studies of foams. Although many research efforts have been focused on foams [2, 3], numerous research questions remain unanswered. For example, what are the mechanisms that govern foam growth and collapse? What is the relationship between these processes? How do the interfacial properties influence the foaming capacity of a solution (foamability) and the lifetime of a foam (foam stability)? How does the presence of solid particles affect in foam drainage? In this chapter, the background of this project is introduced, followed by the research objectives and hypotheses of this work. Finally, a brief description of the thesis organization is presented.

1. Background

Since being commercially introduced early in the 20th century, froth flotation has become the most important and widely used separation method for minerals. In mineral flotation, the ore is first ground into particles of a certain size to liberate the valuable minerals from the gangue. A suspension of solid particles and water is then subjected to vigorous mixing in the flotation cell, followed by the introduction of fine bubbles that selectively attach to hydrophobic particles and carry them to the bulk surface. A froth phase is then formed above the surface, which transports the particles to the concentrate. Frothers and collectors are added to the suspension during froth flotation to make the particles hydrophobic and facilitate the formation of the froth phase by reducing the bubble coalescence rate in the pulp and froth phases. In froth flotation, two distinct zones have thus been recognized: the pulp zone and the froth zone. The overall performance of flotation relies on the collective results of these two zones.

Although the importance of the froth phase in flotation performance has been recognized [4-26], the behavior of the froth zone has not yet been fully described and quantified by universal models because of the complexity of the processes occurring in it [27]. In practice, “the production and maintenance of a satisfactory froth phase at different stages of a flotation process has been an art rather than a science and is often a problem to flotation operators” [27]. Therefore, it is crucially important to understand the mechanisms governing froth stability in order to manipulate it to optimize the flotation performance. However, the

presence of solid particles in the flotation froth makes it very difficult to study these mechanisms. Despite the absence of solid particles, studies on the aqueous foam properties, such as foam column kinetics, foamability, foam stability and foam drainage, will undoubtedly set the benchmark to study more complex three-phase flotation froths.

This project aims to develop a better understanding of the foam column kinetics, the mechanisms governing the foamability and foam stability, and the role of solid particles in the liquid drainage in foams by developing mathematical models, providing important data and elucidating mechanisms.

2. Objectives of the thesis

The overall objective of this project is to elucidate the different mechanisms that collectively determine foam properties. More specifically, the objectives of this project are the following:

- To develop mathematical models to simulate foam column kinetics and interrelate the growth, drainage and collapse of foams by analogy with reaction kinetics.
- To elucidate the different mechanisms (e.g., surface tension, surface viscoelasticity, double-layer interactions, antifoam effects of nonionic surfactant and nonpolar collectors) that collectively determine foamability and foam stability.
- To investigate the role of solid particles in foam drainage by conducting forced drainage experiments and applying drainage equations for aqueous foams.

3. Hypotheses of the thesis

- Foam column kinetics is determined by the competition between foam formation and foam collapse and can be simulated via analogy to reaction kinetics.
- Different mechanisms collectively determine the foamability and foam stability, and each mechanism is only dominant for a certain foam system and stage of the foam life.
- The presence of solid particles affects foam drainage by altering the interfacial properties of foams.

4. Structure of the thesis

The thesis consists of eight chapters. Chapter 1 is a brief introduction of the background, objectives and hypotheses of the project. Chapter 2 provides a literature review on foam column kinetics, the mechanisms governing foamability and foam stability, and foam drainage in the presence of solid particles. Chapter 3 develops a mathematical model to

simulate foam column kinetics and interrelate the growth, drainage and collapse of foams by analogy with reaction kinetics. Chapter 4 explores the anomalous foam behaviors of surfactant blend foams and elucidates novel mechanisms. Chapter 5 investigates the effects of a nonpolar collector (i.e., diesel) that has been widely used in froth flotation on the foamability and foam stability of methyl isobutyl carbinol (MIBC) solutions (a common frother used in froth flotation). Chapter 6 focuses on the effects of surface rheology and double-layer interactions on the foam stability of surfactant blend foams. Chapter 7 presents the role of solid particles in the liquid drainage through the froth phase, which is relevant for froth flotation because the wash water is commonly applied to the froth layer to improve the product grade. The final chapter summarizes the conclusions and provides recommendations for future work.

References

[1] A. Bhakta, E. Ruckenstein, Decay of standing foams: drainage, coalescence and collapse, Advances in Colloid and Interface Science, 70 (1997) 1-124.

[2] I. Cantat, S. Cohen-Addad, F. Elias, F. Graner, R. Hohler, O. Pitois, F. Rouyer, A. Saint-jalmes, Foams: Structure and Dynamics, CPI Group (UK) Ltd, Croydon, 2013.

[3] D. Weaire, S. Hutzler, The Physics of Foams, Clarendon Press, Oxford, 1999.

[4] S. Farrokhpay, The significance of froth stability in mineral flotation — A review, Advances in Colloid and Interface Science, 166 (2011) 1-7.

[5] S. Ata, Phenomena in the froth phase of flotation — A review, International Journal of Mineral Processing, 102–103 (2012) 1-12.

[6] N. Barbian, E. Ventura-Medina, J.J. Cilliers, Dynamic froth stability in froth flotation, Minerals Engineering, 16 (2003) 1111-1116.

[7] N. Barbian, K. Hadler, E. Ventura-Medina, J.J. Cilliers, The froth stability column: linking froth stability and flotation performance, Minerals Engineering, 18 (2005) 317-324.

[8] N. Barbian, K. Hadler, J.J. Cilliers, The froth stability column: Measuring froth stability at an industrial scale, Minerals Engineering, 19 (2006) 713-718.

[9] S.J. Neethling, J.J. Cilliers, Predicting air recovery in flotation cells, Minerals Engineering, 21 (2008) 937-943.

[10] Z. Aktas, J.J. Cilliers, A.W. Banford, Dynamic froth stability: Particle size, airflow rate and conditioning time effects, International Journal of Mineral Processing, 87 (2008) 65-71.

[11] K. Hadler, J.J. Cilliers, The relationship between the peak in air recovery and flotation bank performance, Minerals Engineering, 22 (2009) 451-455.

[12] K. Hadler, C.D. Smith, J.J. Cilliers, Recovery vs. mass pull: The link to air recovery, Minerals Engineering, 23 (2010) 994-1002.

[13] K. Hadler, M. Greyling, N. Plint, J.J. Cilliers, The effect of froth depth on air recovery and flotation performance, Minerals Engineering, 36–38 (2012) 248-253.

[14] P.R. Brito-Parada, S.J. Neethling, J.J. Cilliers, The advantages of using mesh adaptivity when modelling the drainage of liquid in froth, Minerals Engineering, 33 (2012) 80-86.

[15] K. Cole, P.R. Brito-Parada, A. Morrison, I. Govender, A. Buffler, K. Hadler, J.J. Cilliers, Using positron emission tomography (PET) to determine liquid content in overflowing foam, Chemical Engineering Research and Design, 94 (2015) 721-725.

[16] R.M. Rahman, S. Ata, G.J. Jameson, Froth recovery measurements in an industrial flotation cell, Minerals Engineering, 53 (2013) 193-202.

[17] G. Bournival, Z. Du, S. Ata, G.J. Jameson, Foaming and gas dispersion properties of non-ionic frothers in the presence of hydrophobized submicron particles, International Journal of Mineral Processing, 133 (2014) 123-131.
[18] M. Zanin, E. Wightman, S.R. Grano, J.P. Franzidis, Quantifying contributions to froth stability in porphyry copper plants, International Journal of Mineral Processing, 91 (2009) 19-27.
[19] J.G. Wiese, P.J. Harris, D.J. Bradshaw, The effect of increased frother dosage on froth stability at high depressant dosages, Minerals Engineering, 23 (2010) 1010-1017.
[20] J. Wiese, P. Harris, D. Bradshaw, The effect of the reagent suite on froth stability in laboratory scale batch flotation tests, Minerals Engineering, 24 (2011) 995-1003.
[21] S. Farrokhpay, M. Zanin, An investigation into the effect of water quality on froth stability, Advanced Powder Technology, 23 (2012) 493-497.
[22] M. Alvarez-Silva, J. Wiese, C.T. O'Connor, An investigation into the role of froth height and depressant dosage in the recovery of chromite in the flotation of UG2 ore using a laboratory column, Minerals Engineering, 55 (2014) 125-131.
[23] K.C. Corin, J.G. Wiese, Investigating froth stability: A comparative study of ionic strength and frother dosage, Minerals Engineering, 66–68 (2014) 130-134.
[24] G.W. Cutting, S.P. Barber, S. Newton, Effects of froth structure and mobility on the performance and simulation of continuously operated flotation cells, International Journal of Mineral Processing, 16 (1986) 43-61.
[25] S.M. Feteris, J.A. Frew, A. Jowett, Modelling the effect of froth depth in flotation, International Journal of Mineral Processing, 20 (1987) 121-135.
[26] M.A. Vera, J.P. Franzidis, E.V. Manlapig, Simultaneous determination of collection zone rate constant and froth zone recovery in a mechanical flotation environment, Minerals Engineering, 12 (1999) 1163-1176.
[27] A.V. Nguyen, H.J. Schulze, Colloidal science of flotation, Marcel Dekker, New York, 2004.

Chapter 2: Literature Review: A Critical Review of the Growth, Drainage and Collapse of Foams

Jianlong Wang[1], Anh V Nguyen[1*] and Saeed Farrokhpay[2]
[1]School of Chemical Engineering, University of Queensland, Brisbane, Queensland 4072, Australia
[2]JKMRC, University of Queensland, Brisbane, Queensland 4072, Australia

[*]Correspondence: anh.nguyen@eng.uq.edu.au

Highlights:

- Foam growth and collapse are poorly quantified in the literature
- Mechanisms governing foamability and foam stability are reviewed
- Foamability and foam stability are jointly determined by many factors
- Solid particles significantly affect foam drainage
- Modelling foam drainage with solid particles is limited

Abstract

This chapter focuses on the current knowledge regarding the (i) quantification of foam growth and collapse, (ii) the mechanisms governing foamability and foam stability, and (iii) foam drainage in the presence of solid particles. Limitations of the existing models of foam column kinetics are discussed. Special attention is paid to the interrelation between the growth and collapse of the foam column. Different mechanisms governing foamability and foam stability are reviewed to elucidate different length scales of foam properties. The current understanding of the effects of solid particles on foam drainage is discussed to highlight gaps in our present level of understanding.

Keywords: foam, foam stability, foam drainage, foamability, solid particle

1. Foam column kinetics

Foam column kinetics describes the transient behaviors of foams, including the growth, drainage and collapse of foams. Foam column kinetics is crucially important for many industrial applications. For example, the precise control over the froth phase becomes particularly important in froth flotation because of the strong dependence of its performance on the froth stability. Foam column kinetics has been used to predict the froth rising velocity, which can be linked to a key parameter in froth modeling and plant operation, that is, the fraction of bubbles bursting on the top surface of the froth [1-3]. Foam column kinetics has also been applied in glass-melting furnaces [4-7].

1.1 Models of equilibrium foam height

1.1.1 Hrma's model

Bikerman introduced the concept of "unit of foaminess" as follows [8, 9]:

$$\Sigma = \frac{H_{\max}}{j_g} \tag{1}$$

where $H_{\max}$ is the equilibrium foam height under the superficial gas velocity, j_g. Despite its wide application to represent the foam or froth stability [1-3, 5, 10, 11], this expression is limited by its dependence on the gas flow rate [5, 12]. An equation has been proposed to express the foam height as a function of the bubble radius, r; the critical gas flux, j_c, beyond

which the foam will grow without limit; the minimum gas flux required to generate foam, j_m; and the gas flux, j, as follows [5]:

$$H_{\max} = 2r\left[\left(j_c - j_m\right)/\left(j_c - j\right)\right] j / j_m \tag{2}$$

When $j \ll j_c$, Eq. (2) can be expressed as $H_{\max} / 2r = j / j_m$, where $\Sigma \approx 2r / j_m$ such that a liquid with a low gas velocity threshold is more "foamable".

1.1.2 Hartland's model

The first attempt to predict the equilibrium foam height dates back to 1974 [13]. In this model, the foam height, h, is related to the critical liquid film thickness, δ, in terms of the liquid density, ρ, viscosity, μ, surface tension, σ, gas velocity, v, and bubble diameter, d, by the following expression:

$$\frac{H_{\max}}{d} = \frac{0.55\left(\mu v d\right)^{5/4}}{\left(\rho g\right)^{1/4} \sigma \delta^{7/4}} \tag{3}$$

This model successfully predicts that the foam height will increase as the viscosity, gas velocity and bubble size increase but decrease as the density, surface tension and film thickness increase. However, the model assumes that the drainage of the films is represented by the axisymmetric drainage of liquid from between two flat discs, which allows the Reynolds equation to be applied. The problem with this assumption is that the interfaces are assumed to be rigid, whereas in reality, the interfaces of liquid films are mobile or partially mobile [14-16]. The assumption that the liquid film rupture occurs when the critical film thickness is reached is also problematic. It has been found that liquid films do not necessarily burst when their critical thickness is reached. Instead, the lifetime of a liquid film can be expressed as a function of two characteristic times: (i) the characteristic time of drainage, τ_d, and (ii) the lifetime of the critically thin film, τ_c [4, 5, 17]:

$$\tau_f = \tau_d + \tau_c \tag{4}$$

Only when the foam is evanescent, $\tau_c = 0$. Even if the evanescent foam assumption is correct, in a real foam, the films are unlikely to burst at a single exerted pressure or critical thickness but will instead exhibit a distribution of bursting probabilities [18].

1.1.3 Pilon's model

An equation for the equilibrium foam height of highly viscous fluids has been proposed based on dimensional analysis [7]:

$$\frac{H_{\max}}{r} = \frac{2905}{Ca}\left(\frac{Fr}{\mathrm{Re}}\right)^{1.80} \tag{5}$$

where Re, Fr, and Ca are the Reynolds, Froude, and Capillary numbers, respectively, which are defined as:

$$\mathrm{Re} = \frac{\rho\left(j - j_m\right)r}{\mu} \tag{6}$$

$$Fr = \frac{\left(j - j_m\right)^2}{gr} \tag{7}$$

$$Ca = \frac{\mu\left(j - j_m\right)}{\sigma} \tag{8}$$

by identifying two dimensionless numbers:

$$\Pi_1 = \frac{\rho g r^2}{\mu\left(j - j_m\right)} \tag{9}$$

$$\Pi_2 = \frac{\mu H_{\max}\left(j - j_m\right)}{\sigma r} \tag{10}$$

Please note that the relationship between Π_1 and ε was established to compare the published forced drainage data [19, 20]. In these equations, ρ is the liquid density, r is the average bubble radius, j_m is the minimum superficial gas velocity for the onset of foaming [21], μ is the liquid viscosity, σ is the surface tension and g is the acceleration due to gravity. Because Eq. (5) neglects both bubble coalescence and inter-bubble gas diffusion, its application is limited to highly viscous liquids. Consider a third dimensionless number to represent the Ostwald ripening that occurs in surfactant foams:

$$\Pi_3 = \frac{DS_o}{r\left(j - j_m\right)} = \frac{\tau_c}{\tau_d} \tag{11}$$

where D is the diffusion coefficient, S_o is the Ostwald solubility coefficient, and τ_c and τ_d are the characteristic times of the contact and permeation between bubbles, respectively. Therefore, the expression of equilibrium foam height in Eq. (5) was generalized as follows [22]:

$$H_{\max} = 118 \frac{\sigma}{r^{1.64}} \frac{\mu^{0.8} \left(j - j_m \right)^{1.76}}{\left(\rho g \right)^{1.8} \left(DS_o \right)^{0.96}} \tag{12}$$

1.1.4 Limitations of the models for equilibrium foam height

All of the above models assume that there is no bubble coalescence on the top of the foam before the equilibrium foam height is reached. Based on this assumption, the foam will reach its equilibrium height as soon as the bubbles burst at the top of the foam. However, a gentler transition from not bursting to bursting is much more common in growing foam or froth [1-3, 18]. This relatively gentle transition indicates that rupture of liquid films or bubbles of foams do not occur at the same time but instead exhibit a distribution of bursting probabilities [18]. Therefore, predicting the change in foam height with time becomes more important than the equilibrium foam height.

1.2 Models of foam growth

Modeling foam growth has mainly focused on the collapse of standing foams [18, 23-27]. A mass balance for the bubbling gas in a foam column has been introduced and rewritten as [27, 28]:

$$\frac{dH}{dt} = \frac{j_g}{1-\varepsilon} - \frac{dH_{collapse}}{dt} \tag{13}$$

where j_g is the superficial gas flow rate, H is the foam height, ε is the volumetric liquid fraction and $H_{collapse}$ is the collapsed foam height. The first term on the right-hand side of Eq. (13) represents the foam growth rate of stable foams (i.e., no bubble coalescence), and the second term is the foam collapse rate. The growth rate of transient foams, therefore, equals the growth rate of stable foam minus the foam collapse rate. In this section, the models of foam growth are categorized based on the treatment of the foam collapse rate: (i) the foam collapse rate is not considered; (ii) the foam collapse rate is expressed empirically; and (iii) the foam collapse rate is related to the critical film thickness or Plateau border size.

1.2.1 Models without consideration of foam collapse

An equation has been proposed to express the foam height as a function of the superficial gas velocity and average foam porosity (gas fraction), $\bar{\phi}(t)$ [4]:

$$H = \frac{j_g}{\bar{\phi}(t)} t \quad \text{if} \quad t \le \tau \tag{14}$$

where τ is the time for the foam height to reach its equilibrium value and

$$\bar{\phi}(t) = \frac{1}{H}\int_0^H \phi(z,t)dz \tag{15}$$

The local foam porosity distribution has been represented as a second-order polynomial:

$$\phi(z,t) = a_0 + a_1\left[\frac{z}{H}\right] + a_2\left[\frac{z}{H}\right]^2 \tag{16}$$

where the coefficients a_0, a_1, and a_2 are determined based on the boundary conditions at the top and bottom of the foam layer, and the final expression of $\bar{\phi}(t)$ is obtained from Eqs. (15) and (16):

$$\bar{\phi}(t) = \frac{2\phi_1(t) + \phi_2(t)}{3} \tag{17}$$

where $\phi_1(t)$ is the foam porosity on the top surface and $\phi_2(t)$ is the foam porosity at the bottom of the foam, which equals 0.74 and corresponds to the maximum packing of spherical bubbles of the same size[27, 29]. $\phi_1(t)$ has been treated as follows [4]: (i) constant porosity at the top, (ii) an exponential function of time, and (iii) obtained based on an approximate solution of the drainage equation. A similar model for the build-up and breakdown of foam in a glass melt has also been derived based on the hydrodynamics of the drainage of liquid lamellae [6]. Please note that the application of the two models is limited to the assumption that there is no foam collapse before the time τ.

1.2.2 Empirical expressions of the foam collapse rate

The half decay time ($t_{1/2}$) was found by expressing the foam collapse rate as [30]:

$$\frac{dH}{dt} = -k / t \tag{18}$$

Integrating Eq. (18), the expression for the change of foam height with time becomes:

$$H / H_0 = -\alpha \ln\left(t / t_{1/2}\right) + 0.5 \tag{19}$$

where H_0 is the original foam height, $t_{1/2}$ is the half foam decay time, and α is a constant. Because the relationship between H and t is known, $t_{1/2}$ can be obtained by fitting the foam collapse data [28].

An empirical equation for the froth growth in froth flotation has also been proposed [1-3]:

$$H(t) = H_{\max}\left(1 - e^{-t/\tau}\right) \tag{20}$$

$\beta(H)$ is the fraction of air remaining in the froth at a given froth height H, which is a crucial parameter in froth modeling and plant operation involving froth flotation; it is expressed as:

$$\beta(H) = \frac{dH(t)}{dt}\frac{A}{Q} = \frac{\left(H_{\max} - H(t)\right)}{\tau}\frac{A}{Q} \tag{21}$$

where $H_{\max}$ is the equilibrium foam height; τ is the average bubble lifetime, which equals the unit of foaminess, Σ, defined by Eq. (1); A is the column cross-sectional area; and Q is the gas flow rate to the flotation cell [2]. The growth rate of the froth height can be deduced from Eq. (20) as follows:

$$\frac{dH}{dt} = j_g - \frac{1}{\tau}H \tag{22}$$

assuming that the liquid content is low. By comparing Eq. (22) with Eq. (13), we can see that the foam collapse rate is proportional to the foam height.

Although Eq. (19) and Eq. (20) have been proposed to describe the change in foam or froth height with time, these two empirical equations were developed without any fundamental basis.

1.2.3 Expression for the foam collapse rate and the critical Plateau border size

Figure 1 shows an example of how the foam collapse rate is related to the critical Plateau border size, which is represented by the critical cross-sectional Plateau border area, A_{crit} [18]. It was assumed that the foam grows initially with no bubble bursting inside the foam or at the top surface. That is, the growth rate of the foam equals the superficial gas velocity when the liquid content is low:

$$\left(\frac{dH}{dt}\right)_{Initial} = v_g \tag{23}$$

Once the Plateau border size at the top of the foam attains its critical value, bubble coalescence begins. The foam collapse rate for standing foams has been expressed as [18]:

$$\left(\frac{dH}{dt}\right)_{Burst} = -k_1 A_{crit} \tag{24}$$

where

$$k_1 = \frac{\rho g}{3 C_{PB} \mu} \tag{25}$$

If the gas flow rate is high enough, the foam will continue to grow at a reduced growth rate:

$$\left(\frac{dH}{dt}\right)_{Final} = -k_1 A_{crit} + v_g \tag{26}$$

in which ρ is the liquid density, g is the acceleration due to gravity, C_{PB} is the Plateau border drag coefficient and μ is the liquid viscosity [31]. Additionally, the critical Plateau border area can be obtained based on the foam growth curve if the gas flow rate is sufficiently high:

$$A_{crit} = \frac{1}{k_1}\left(\left(\frac{dH}{dt}\right)_{Initial} - \left(\frac{dH}{dt}\right)_{Final}\right) \tag{27}$$

Otherwise, the foam will attain its equilibrium height.

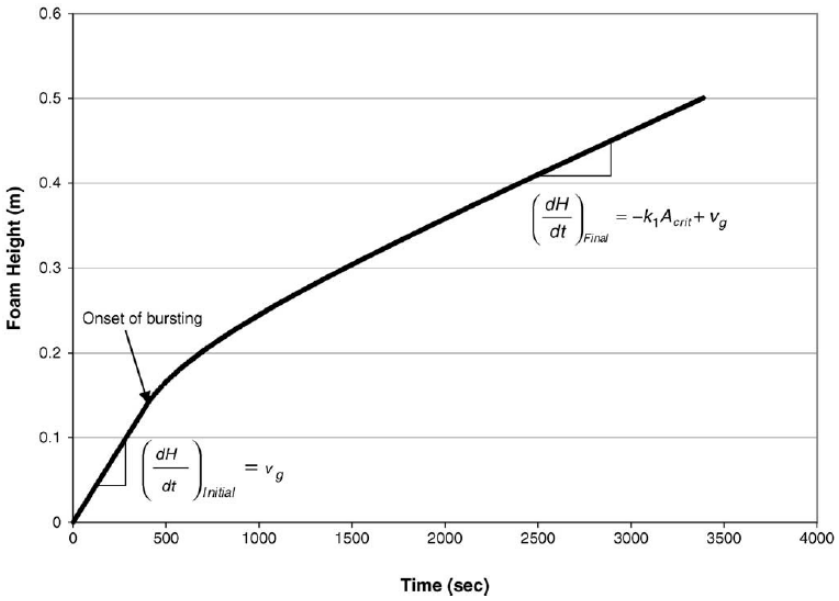

Figure 1. A typical simulated relationship between foam height and time for a gas rate that is sufficiently high such that the foam will grow indefinitely [18].

Although the fundamental physics governing the foam collapse process have been considered, a considerable discrepancy between the simulated and experimental results for growing and collapsing foams or froth remains [1-3, 18]. This discrepancy has been explained as follows: "In a real foam, the films are unlikely to burst at a single exerted pressure, but rather are likely to exhibit a distribution in the bursting probabilities….This distribution in the film stabilities probably accounts for the more gentle transition from not bursting to bursting seen in the experiments [18]." However, this distribution is still not well understood or quantified.

1.3 Summary

The equations to describe the equilibrium foam height and foam growth reported in the literature are summarized in Table 1.

Table 1. Summary of equations for the equilibrium foam height and foam or froth growth

Source	Equation	Note
	Equations for equilibrium foam height	
[5]	$H_{\max} = 2r\left[\left(j_c - j_m\right)/\left(j_c - j\right)\right] j / j_m$	-
[13]	$\frac{H_{\max}}{d} = \frac{0.55\left(\mu v d\right)^{5/4}}{\left(\rho g\right)^{1/4} \sigma \delta^{7/4}}$	Rigid interface assumption
[7]	$\frac{H_{\max}}{r} = \frac{2905}{Ca}\left(\frac{Fr}{\mathrm{Re}}\right)^{1.80}$	For highly viscous fluids
[22]	$H_{\max} = 118\frac{\sigma}{r^{1.64}}\frac{\mu^{0.8}\left(j - j_m\right)^{1.76}}{\left(\rho g\right)^{1.8}\left(DS_o\right)^{0.96}}$	Applied for surfactant foams
	Equations for foam or froth growth	
[4]	$H = \frac{j_g}{\bar{\phi}(t)} t$	No bubble coalescence
[30]	$H / H_0 = -\alpha \ln\left(t / t_{1/2}\right) + 0.5$	Empirical equation
[1]	$H\left(t\right) = H_{\max}\left(1 - e^{-t/\tau}\right)$	Empirical equation
[18]	$\left(\frac{dH}{dt}\right)_{Final} = -k_1 A_{crit} + v_g$	After onset of bursting

2. Mechanisms governing foamability and foam stability

Foamability and foam stability are two main foam properties of surfactant solutions. Foamability is a surfactant solution's overall capacity to produce foams, whereas foam stability refers to the lifetime of a foam column. These two terms are interrelated. For example, the foamability of a transient foam is believed to depend on its stability. Although these two terms are commonly used in the literature, there are no universal physical parameters to quantify them. Foam height and foam lifetime have been applied to characterize foamability and foam stability [8, 9, 30]. However, these two criteria are not satisfactory because they are not only dependent on the foaming solution but also on how foams are generated. Moreover, a general theory to explain the mechanisms of foam formation and stability for all types of foam system does not exist [32-34] because the magnitude and mutual importance of the different types of effects can vary significantly

depending on the stage of foam life and the conditions of its existence [33]. Bearing in mind the complicated interplay of various mechanisms, here, we review the existing theories that describe the mechanisms governing foam formation and stability.

2.1 Effects of interfacial properties on foam properties

The adsorption of surfactant molecules on the air-water interface alters the interfacial properties, and the foam properties change accordingly.

2.1.1 Surface tension and foamability

It is clearly evident that the decrease in surface tension ensues as a result of the adsorption of surfactant molecules on the air-water interface. In the first stage of foam formation, bubbles are split into smaller ones because of the external forces that the bulk liquid subjects them to. The splitting of bubbles results in an increase in the specific surface area and surface energy. If the external energy imposed to generate the foams is constant, then lower surface tensions are achieved and higher surface areas can be produced. In other words, a lower surface tension will enhance the foamability of a solution as a function of the surface energy. Except for the surface energy, the critical Weber number, $We = \rho u^2 r_b / \sigma$, is also introduced to predict the maximum stable bubble size for bubbles in the bulk phase [35-38]. It is also evident that a lower surface tension corresponds to a smaller bubble size, indicating a better foamability with a constant (assumed) Weber number.

Although surface tension and foamability are dependent on surface energy and Weber number, choosing an appropriate characteristic time at which the dynamic surface tension should be applied remains difficult. Several research efforts using different designs have investigated the effect of dynamic surface tension on the foamability. For example, the relationship between foam formation and the dynamic surface tension of non-ionic and anionic surfactants has been studied using a rotor test, in which air is introduced to the surfactant solutions with the help a special stirring device [39]. A good correlation between foam formation and the dynamic surface tension values at $t = 100\ ms$, which is expressed as the relative surface pressure, has been found (Figure 2). Despite the choice of the characteristic time, $t = 100\ ms$, the authors found that the average lifetime of the bubbles at the solution-air interface should be chosen as the reference adsorption time. The relationship between foam formation and dynamic surface tension has also been investigated using the Ross-Miles test [40-42]. Recently, the foam formation at a sparger was related to the dynamic surface tension [43]. In that paper, the authors summarized the results from [42] and

correlated the foam height with the surface tension reduction rate, which is defined as [42, 43]:

$$R_{1/2} = \frac{\sigma_0 - \sigma_m}{2t^*} \tag{28}$$

where σ_0 is the surface tension of the solvent, σ_m is the meso-equilibrium surface tension at which the decrease rate of the surface tension is smaller than 1 mN/m per 30 seconds, and t^* is the time when the surface tension is equal to $(\sigma_0 - \sigma_m)/2$. Here, we note that the surface tension reduction rate in Eq. (28) derived from [42, 44] lacks a fundamental basis. Therefore, the correlation between the foam formation and the surface tension reduction developed in [43] is limited.

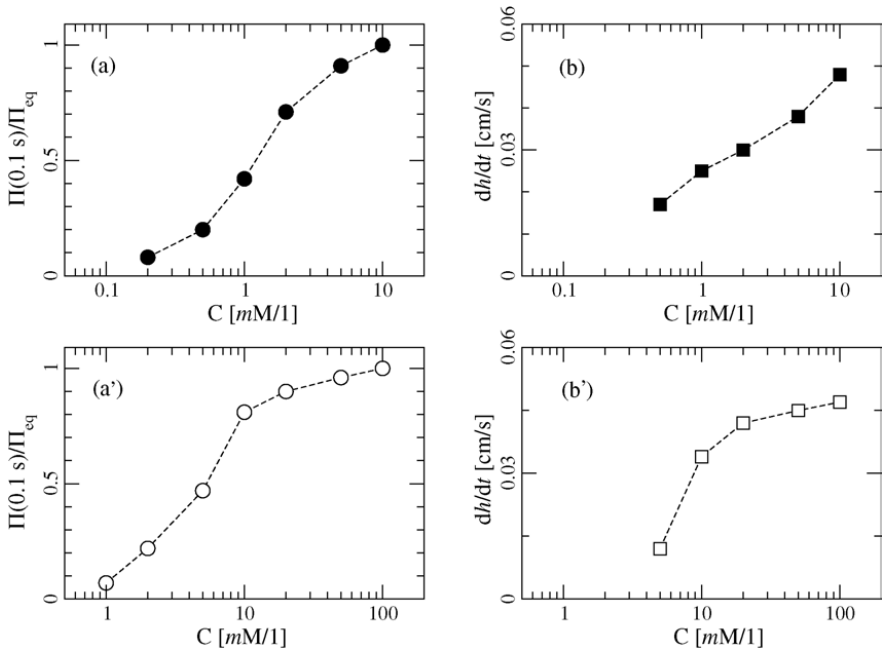

Figure 2 The relative dynamic pressure at $t = 100\ ms$ and the rate of foam formation for the non-ionic surfactant $C_{12}(EO)_6$ (a, b) and the anionic surfactant $C_{12}SO_3Na$ (a', b'). The rate of foam formation refers to a rotor speed of 900 min^{-1}. The graphs are reproduced from [39].

2.1.2 Surface viscoelasticity and foam properties

The adsorption of surfactant molecules on the air-water interface can not only decrease the surface tension, but also generate the surface viscoelasticity. Surface viscoelasticity is related to the non-equilibrium state of the adsorption layer [45]. A distortion of its existing equilibrium state and the absence of adsorption equilibrium at a freshly created interface are

the two main reasons underlying the non-equilibrium state of the adsorption layer. Because the interface has not yet attained its equilibrium adsorption coverage during foam generation, surface viscoelasticity plays a significant role in foamability. Moreover, regarding foam drainage, the surface tension gradients induced at the air-water interface can stabilize the foam films by retarding drainage [46].

A century ago the significance of the surface tension gradients for foam stability were described by Gibbs and Marangoni [47]. The first theory to discuss the surface tension gradient in terms of surface dilational elasticity was presented by Levich in 1941 [48]. It is to note that the new methodology for measuring the dilational rheology via a harmonically oscillating bubble in 1970 [49] paves the way for the first commercial instrument for routine experiments of the dilational surface elasticity [50], based on oscillating drops and bubbles. Various special aspects of surface viscoelasticity has been reviewed [51-55] and a book that is completely devoted to surface viscoelasticity has been published recently [56].

The dilational elasticity modulus, E, has been defined as the ratio of the surface tension change, $\Delta\sigma$, to the relative increase in surface area, $\Delta A/A$, i.e., $E = d\sigma / d\ln A$. Regarding the film elasticity, its value should be two times the value of E, indicating the presence of two film interfaces. It should be noted that an analogy between the Gibbs elasticity and the surface dilational modulus has been made [57]. The Gibbs elasticity refers to the increase in the film's surface tension resulting from a decrease in the surfactant concentration within the interlamellar solution caused by the small extension of the film relative to the film size. In the Gibbs mechanism, the film elasticity originates from the deterioration of the interstitial surfactant solution with the assumption that the thickness of the lamellae is very small. The Marangoni elasticity, as related to the Marangoni effect, originates from the transport of surfactant molecules from the adjacent bulk phase to the interface for the case of the non-equilibrium state of thick foam films [58]. For soluble surfactants, the magnitude of the elasticity modulus depends on the frequency of external disturbances or the oscillation frequency. The adsorption layer will behave as an insoluble monolayer when the frequency is sufficiently high and the Marangoni dilational modulus reaches its limiting value, E_M [59, 60]. At low frequencies, the adsorption layer behaves as a viscoelastic surface because of relaxation processes, i.e., diffusional exchange that occurs in and near the interface. Therefore, the modulus E has both elastic and viscous components. A review paper has analyzed the surface viscoelasticity of adsorption layers and the origin of the dilational

viscosity [61]. The dilational surface viscosity has been categorized as follows: (i) “true” dilational surface viscosity, which originates only from the transport of surfactant molecules at the interface, and (ii) “apparent” dilational surface viscosity caused by the surfactant diffusion from the bulk solution.

A good correlation between the liquid film or foam stability and the surface viscoelasticity has been reported [60, 62-78]. However, questions remain unanswered: Is the good correlation between film stability and surface rheology indicative of a similar correlation with foam stability? Are measurements at the interfaces (i.e., surface viscoelasticity) and on a single film (i.e., film stability) sufficient to understand and predict the foamability and foam stability [79]? What is the appropriate frequency at which the surface viscoelasticity can correlate with the foamability and foam stability? For the first and second questions, because the foams cannot be considered as a simple combination of foam films, the correlation between film stability and surface rheology cannot be directly applied to foam stability. Moreover, it is challenging to correlate the foam column stability with the liquid film stability [80, 81]. This discrepancy has been explained as “the conditions of the existence of the foams and of the single film were quite different and, therefore, the different types of forces could operate there [33].” For the last question, on the one hand, the frequency of the measurements of the surface viscoelasticity should be relevant to the surface age during foam generation (0.1–1 s) in terms of foamability. On the other hand, the two main processes that determine the foam lifetime, that is, Ostwald ripening and bubble coalescence, have been shown to be controlled by the low- and high-frequency surface elasticities, respectively [69]. Nevertheless, the roles of surface viscoelasticity in the foamability and foam stability remain poorly understood. The effects that contribute to the link between surface viscoelasticity and foam properties are summarized in a recent textbook as follows [79]:

- Because a large dilational surface elastic modulus results in a smaller strain for a given applied stress, the foam film will stretch less and is less likely to rupture when subjected to certain disturbances.
- The film elasticity will restore the interface by bringing back surfactants and by limiting the stretch of the interface.
- The Marangoni effect will draw surfactants back to the interface and liquid into the film, thereby reducing the possibility of liquid film rupture.

- On the one hand, a value of surface viscoelasticity that is too low facilitates the stretching of the interface, resulting in liquid film rupture. On the other hand, a surface viscoelasticity that is too high will cause a solid-like response of the interface, leading to the possibility of fracture.
- Surface elasticity modifies the process of drainage in the films and Plateau borders.
- Surface elasticity controls the appearance of bell-shaped liquid drops that have a destabilizing effect on films.

2.2 Effects of liquid film properties on foam properties

Any foam is made of single liquid film. Therefore, the link between liquid film properties and foam properties is most obvious. The fundamentals of the present knowledge in the field of foam films had been discovered by pioneers like Boyle, Hooke [82], Newton [83], Plateau [84] and Gibbs [47, 85] during $17 - 19^{th}$ centuries. The history of the scientific research on foam films has been compiled as the "chronicles" of foam films very recently [86]. The introduction of the disjoining pressure to the foam film and development of DLVO theory to describe the liquid film stability are considered as milestones in the theoretical development of foam films.

When two bubbles meet in foams, forces act between the two interfaces. These forces determine the stability of the liquid film that separates the foam bubbles. The disjoining pressure, Π_d, was introduced by Derjaguin in the late 1930s to characterize the force per unit area between the two interfaces of a liquid film [87, 88]. Π_d is based on the following attractive and repulsive interactions [35, 89-94].

- *London-van der Waals interactions* originate from the interaction between two molecules. The attractive contribution of the London-van der Waals forces to the disjoining pressure is quantified as:

$$\Pi_{vdW} = -\frac{A_h}{6\pi h^3} \tag{29}$$

where A_h is the Hamaker constant and h is the film thickness. It should be noted that van der Waals forces always make a film unstable. Therefore, repulsive forces induced by the presence of surfactant molecules are needed to balance this attractive force to stabilize the liquid film.

- The *electrostatic interaction* becomes evident when the interfaces are electrically charged in the presence of ionic surfactants. The repulsion between the two charged

interfaces stabilizes the liquid film. However, the presence of an ionic solution such as NaCl will screen this repulsion. The Debye length defines the effective range of the electrostatic potential, Ψ, of a charged interface (Figure 3):

$$\lambda_D = \sqrt{\frac{\varepsilon k_B T}{8\pi n e^2}} \tag{30}$$

where ε is the relative permittivity of the fluid, k_B is Boltzmann's constant, T is the absolute temperature, n is the charged density, and e is the elementary charge. The repulsion can be clearly observed when the film thickness h falls below $2\lambda_D$. The contribution of electrostatic interactions to the disjoining pressure has been found to be approximately:

$$\Pi_{el} \sim \exp\left(-h/\lambda_D\right) \tag{31}$$

- The steric repulsion becomes evident when the liquid film thickness falls below the distance equal to the size of a few surfactant molecules. Therefore, the total disjoining pressure in a liquid film is the sum of the van der Waals, electrostatic, and steric contributions:

$$\Pi_d = \Pi_{vdW} + \Pi_{el} + \Pi_{ste} \tag{32}$$

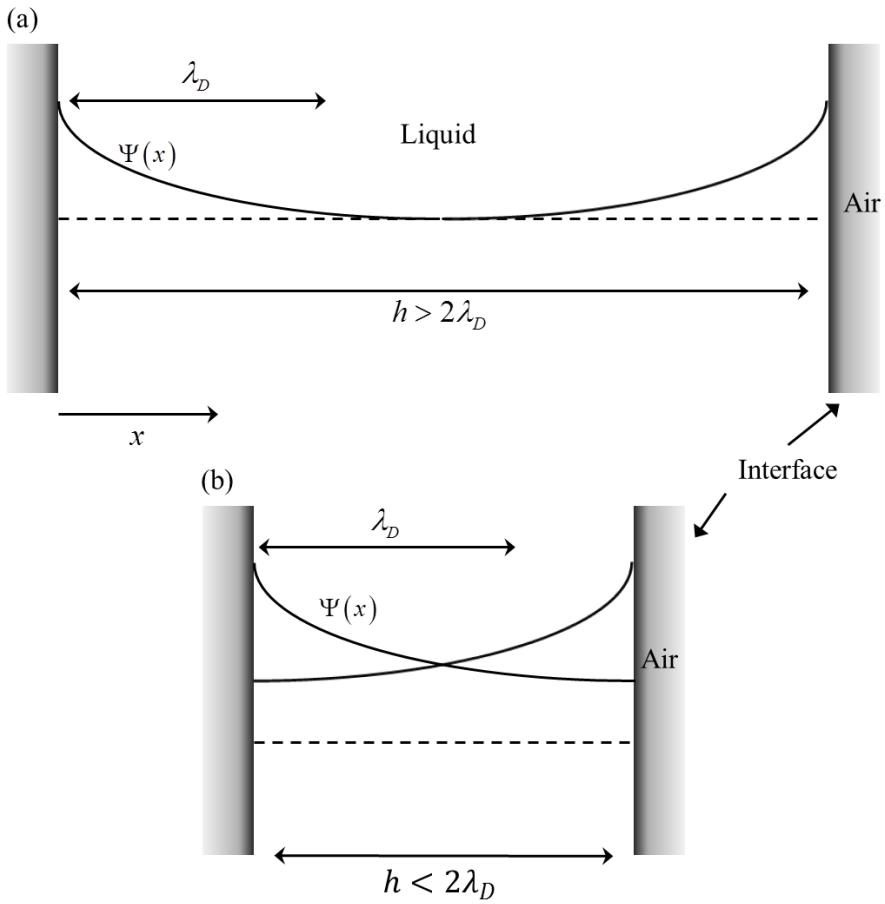

Figure 3. Electrostatic potential $\Psi(x)$ of two charged thin film interfaces at a separation distance of h. λ_D is the effective range of the electrostatic potential Ψ. (a) There is no repulsive interaction as long as $h > 2\lambda_D$. At the center of the film, we can determine the electrostatic potential of the bulk (dash line). (b) For $h < 2\lambda_D$, the electrostatic potential in the film is nowhere equal to that in the bulk. The concentration of counter ions is greater than in the bulk, and this excess of counter ions is responsible for the repulsive force between the thin film interfaces. Reproduced from [79].

The combination of Π_{vdW} and Π_{el} forms the famous DLVO theory [95-97]. The action of the disjoining pressure in foam films and the DLVO theory had been experimentally proved afterwards [98-103], especially with the help of the methodology of the microscopic foam film by Scheludko and Exerowa [104, 105]. A positive disjoining pressure in the film is fundamental to film stability and the existence of a foam. Therefore, a strong and long-range repulsive interaction in the film is necessary for good foamability and foam stability.

2.3 Effects of antifoam behaviors on foam properties

Antifoams are oils, hydrophobic solid particles or a mixture of both that are present in the solution and prevent the formation of a foam [106, 107]. Antifoams have been widely used in many industrial applications, such as pulp and paper production, food processing, textile dyeing, fermentation, wastewater treatment, and the oil industry [97, 106, 108-110]. In the froth flotation of naturally hydrophobic minerals, such as coal, graphite, sulfur and molybdenite, nonpolar collectors are used [111, 112]. They are commonly petroleum-based hydrocarbon liquids, such as diesel oil. Therefore, nonpolar collectors potentially exhibit antifoam behaviors and affect the froth stability (Chapter 5). Moreover, some nonionic surfactants, such as dodecanol, can also influence the foam properties by exerting antifoam actions (Chapter 4). In this section, the mechanisms of liquid antifoam actions and the effects of surfactants on antifoam activity are discussed. Systematic reviews discussing antifoams are available in the literature [106-108]. It should be noted that the terms "fast antifoams" and "slow antifoams" have been previously introduced [107]. The former term denotes "the antifoams whose globules are able to enter the surfaces of the foam films and to destroy these films in the early stages of film thinning", whereas the latter indicates "antifoams whose globules first leave the foam films and destroy the foam after entering the walls of the PBs." [107]. Here, only the mechanisms of "fast antifoams" are discussed on the basis that the antifoams used in this study belong to this category.

2.3.1 Entry barrier

Antifoams must enter the liquid film to destroy a liquid film or foam layer. Antifoams with a low entry barrier completely collapse the foam in seconds, whereas antifoams with a high entry barrier require hours to destroy the foam. The interaction energy per unit area in an asymmetric oil-water-air film [113] and the so-called generalized entry coefficient [114-117] have been introduced to represent the entry barrier. However, the determination of their values is very difficult [107]. Alternatively, the capillary pressure of the air-water interface at the moment of oil drop entry, P_C^{CR}, has been proposed as a quantitative characteristic of the entry barrier because it is related to antifoam efficiency [118-126]. The film trapping technique (FTT) has also been developed to precisely measure the value of P_C^{CR} [127, 128].

Because the antifoam activity strongly depends on the magnitude of the entry barrier [107], it is crucially important to understand the factors that affect the entry barrier. Here, the

two main points made in [107] concerning the factors that affect the entry barrier of an oil droplet are summarized.

- *Entry coefficient*

  Antifoam activity has been correlated with the entry coefficient [106, 108]:

  $$E = \sigma_{AW} + \sigma_{OW} - \sigma_{OA} \tag{33}$$

  where σ_{AW}, σ_{OW} and σ_{OA} are the surface tensions of an air-water interface, oil-water interface and oil-air interface, respectively. From the thermodynamic perspective, the condition for the emergence of an oil droplet at the air-water interface is $E > 0$. However, it has been correctly stated that a positive value of E does not guarantee high antifoam performance because, from the perspective of kinetics, the entry barrier also plays a crucial role [97, 106-109, 129-131]. Regarding their contributions to antifoam performance, the relationship between the entry coefficient E and the entry barrier is analogous to chemical thermodynamics and kinetics [107].

- *Surfactant concentration*

  The effect of surfactant concentration on the entry barrier has been studied previously [122]. Figure 4 shows that the entry barrier increases as the surfactant concentration increases. It should be noted that the effect of the surfactant concentration has not yet to be fully understood [107].

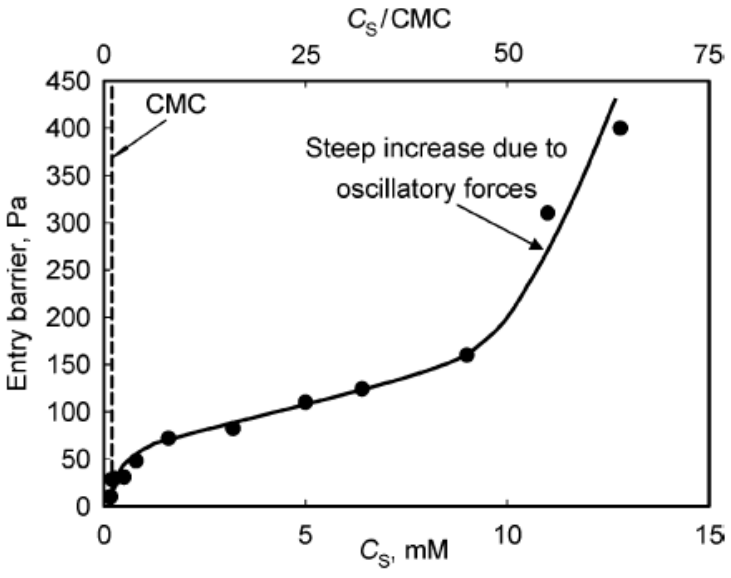

Figure 4. Entry barrier of hexadecane drops, P_c^{CR}, as a function of the SDDBS concentration, C_S [122]. Reproduced from [107].

2.3.2 Role of oil spreading in antifoam performance

When an oil droplet emerges at the air-water interface, depending on the sign of the spreading coefficient, $S = \sigma_{AW} - \sigma_{OW} - \sigma_{OA}$ [132], it either spreads out ($S > 0$) or bridges the two interfaces ($S < 0$) [129, 131, 133-140]. Both outcomes result in rupture of the liquid film. Similar to the entry coefficient, E, S is also a thermodynamic property. A positive initial spreading coefficient S_{IN} (defined using σ_{AW} without the spreading oil) has been shown to contribute to antifoam performance [138, 141]. Because the calculation of S requires the value of the oil-water surface tension, σ_{OW}, which is difficult to measure, the spreading pressure, $\Delta\sigma_{AW} = \sigma^i - \sigma^f$, which is defined as the reduction in the equilibrium surface tension of the air-water interface caused by the addition of an antifoam to the aqueous surface, was introduced [140]. σ^f and σ^i are the equilibrium surface tensions of surfactant solutions with and without antifoams, respectively. A positive value of $\Delta\sigma_{AW}$ indicates that it is thermodynamically favorable for antifoams to spread on the surface of the surfactant solution.

2.3.3 Effect of adsorption kinetics of surfactants on the antifoam performance

Some antifoams have been found to only affect the foamability and exert no influence on foam stability [120, 121, 142]. For example, Figure 5 shows that in the presence of antifoams, the initial foam volume (foamability) generated by shaking AOT solutions (Bartsch) is several times larger than that of APG solutions. However, the foam stability of APG foams is much higher than that of AOT foams. Solutions without antifoams exhibit both good foamability and foam stability. The different effects of antifoams on the foam stability of AOT and APG are explained by the different entry barrier values ($P_C^{CR} > 125$ Pa for APG solutions, and $P_C^{CR} \approx 3$ Pa for AOT solutions). The much higher entry barrier for APG solutions makes the entry of antifoams into the liquid film more difficult and results in more stable foams relative to AOT solutions. However, during foam generation, the antifoams become more active for the APG solutions because of the slow adsorption kinetics of APG molecules (Figure 6). The unsaturated adsorption layers make the entry of antifoams much easier relative to the fully saturated surfaces. It should be noted that the possible higher

surface viscoelasticity deduced from the slow adsorption kinetics of APG molecules may also contribute to the higher foam stability of APG foams relative to AOT foams. Additionally, the fast adsorption of AOT molecules on the air-water interface may facilitate foam formation and result in a higher foamability than the APG solutions (see Section 2.1.1).

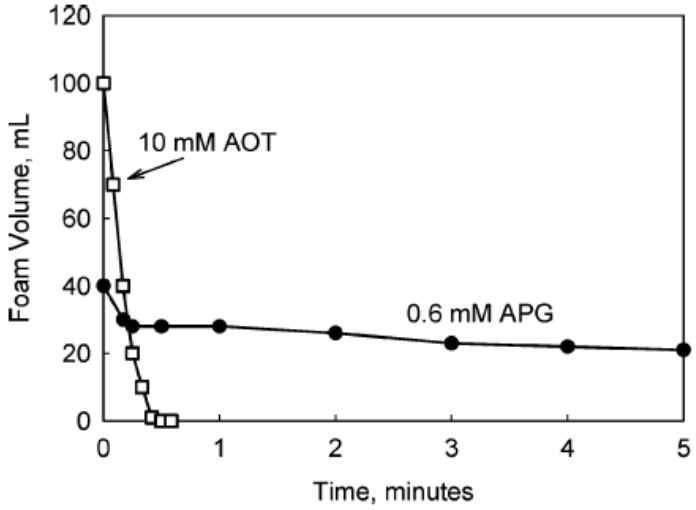

Figure 5. Foam volume vs. time for two surfactant solutions—10 mM AOT and 0.6 mM APG—containing 0.01 wt% PDMS-silica compound (Bartsch test). For comparison, in the absence of an antifoam, the initial foam volume was 180 ± 10 mL for AOT and 100 ± 10 mL for APG, and the foam was stable for the duration of this experiment [120]. Reproduced from [107].

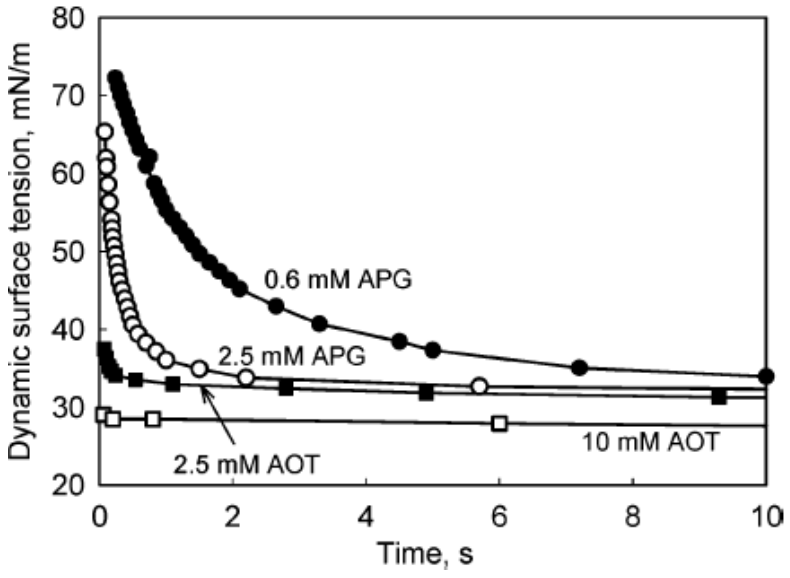

Figure 6. Dynamic surface tension of AOT and APG solutions measured by MBPM: 10 mM AOT and 0.6 mM APG were used in the foam tests (Figure 5). For comparison, the results for equal surfactant concentrations (i.e., 2.5 mM) are also shown [120]. Reproduced from [107].

3. Foam drainage in the presence of solid particles

Foam drainage is the passage of liquid through a foam. Foam drainage is crucially important for foam stability. There are three different mechanisms governing the lifetime of a foam: (i) the foam drainage caused by gravity, (ii) the coarsening caused by the transfer of gas between bubbles induced by the capillary pressure differences, and (iii) the bubble coalescence caused by the rupture of liquid films between neighboring bubbles [79]. Among these three mechanisms, foam drainage determines the liquid fraction of a foam, which is a key parameter for both coarsening and bubble coalescence [143-155]. It should be noted that different types of drainage configurations (i.e., forced, free and pulsed drainage) have been observed [16, 32, 79, 148, 156]. Here, only the forced drainage configuration is considered.

Despite the progress made in understanding aqueous foam drainage [32, 79], foam drainage in the presence of solid particles remains poorly understood. The study of the drainage of three-phase foams or froths is crucially important from an industrial point of view. For example, in froth flotation, the wash water is commonly applied to the froth phase to flush the entrained gangue out of the froth and consequently increase the product's grade. In this section, the theories developed for the foam drainage of aqueous foams are presented. Then, the studies reported in the past 15 years on foam drainage in the presence of solid particles are reviewed. Finally, gaps in the knowledge of this topic are highlighted.

3.1 Foam drainage for aqueous foams

During foam drainage, the liquid is confined in a network of channels or *Plateau borders*, which meet at *nodes* in fours. Therefore, modeling foam drainage primarily focuses on the liquid flow in the two foam structures. It should be noted that some researchers have also considered the contribution of the liquid film to the foam drainage [157, 158]. However, the liquid films have not been found to significantly contribute to the drainage process because of the relatively small amount of liquid contained in the films relative to that in the Plateau borders and nodes [157].

Studies on foam drainage can be categorized into *microscopic* and *macroscopic* investigations [157]. The former refers to studies at the scale of a single Plateau border, whereas the latter refers to studies at the scale of at least several bubbles. The first study on the microscopic modeling of foam drainage only considered the contribution of Plateau borders to the foam drainage [159, 160]. The drainage rate is thought to be dependent upon the mobility of the Plateau border wall or the surface shear viscosity. A Plateau-dominated approach to studying foam drainage was developed by subsequent researchers, who expanded on the initial microscopic modeling attempt [161, 162]. It should be noted that Nguyen improved on the numerical calculations of foam drainage and provided a numerical solution for the liquid flow velocity in a single Plateau border as a function of surface viscosity [159, 163]. The Plateau border-dominated approach was challenged, and the assumption was modified when the contribution of nodes to the foam drainage was recognized and mobile Plateau border walls were assumed [14]. Since then, the standard foam drainage equation [159] has been modified [164], and foam drainage models that consider viscous losses from both the Plateau borders and nodes have been proposed [15, 16].

On the macroscopic level, foam drainage has been shown to be analogous to the liquid flow through a porous medium [79, 165]. However, two key differences between liquid drainage through a foam and that through a porous medium must always be considered. First, in a foam, the size of the network (i.e., Plateau borders and nodes) through which the liquid flows is not fixed but is actually dependent on the flow itself. That is to say, the bubbles can move apart to allow liquid to pass and then move back. Second, the interfaces are not completely rigid but are instead partially mobile in a foam, depending on the interfacial properties, such as surface shear viscosity. It has been demonstrated that the classic Darcy's law that describes the fluid flow through a porous medium is also applicable to aqueous foams [14, 19, 143, 165, 166]. An alternative way to study foam drainage on the macroscopic level is to adopt dimensional analysis to compare the existing foam drainage data in a consistent manner and thus simplify the analysis [19].

3.2 Foam drainage for three-phase foams or froth

Theories of foam drainage for aqueous foams have established benchmarks for the study of three-phase foams in which solid particles are present. Logically, the following questions have been raised regarding foam drainage in the presence of solid particles: Can the foam drainage equations for aqueous foams apply to foams with solid particles? How does the presence of solid particles influence foam drainage?

Not surprisingly, in the past 15 years, many studies on three-phase foams have focused on the transport or motion of solid particles in the flotation froth [167-169] or surfactant foams [170-173] because of their paramount importance for industrial applications. The solid particles in flotation froths have been divided into attached particles (i.e., hydrophobic particles), which follow the bubbles, and unattached particles (i.e., both hydrophobic and hydrophilic particles), which mainly follow the liquid [167]. On the one hand, attached or hydrophobic particles have been used to adsorb to the air-water interface and act as a barrier to prevent bubble coalescence and impede the coarsening process [174-177]. However, their effects on foam drainage remain unknown. On the other hand, studies on foam drainage in the presence of solid particles have primarily focused on the unattached or hydrophilic particles and nanoparticles [168, 171-173, 178-185]. Nevertheless, these studies contribute to our understanding of drainage behaviors in the presence of solid particles. For example, on the basis of the scaling behavior (power law) between the drainage velocity and the imposed flow rate in forced drainage experiments [180], the presence of nanoparticles has been found to induce a foam drainage transition from a node-dominated regime to a Plateau border-dominated regime. Moreover, unusual phenomena, such as large foam permeability exponents and prefactors, which have not been observed in aqueous foams, have been recorded in three-phase foams [178]. It should be noted that these phenomena in three-phase foams cannot be explained simply based on the theories developed for aqueous foams. For example, the foam regime transition in aqueous foams is usually caused by a change in the surface viscosity or interface mobility [186, 187]. However, it is difficult to make the same claim in foams containing nanoparticles because the presence of hydrophilic solid particles can change the interfacial properties to only a small extent [180].

To explain the foam drainage behaviors in the presence of hydrophilic particles, several mechanisms have been proposed, such as rheology of the powder suspension and clogging in the confined regions of the Plateau borders [172, 178, 181, 183-185]. Among them, the most important parameter controlling the drainage behaviors of foams with hydrophilic particles is the confinement parameter, $\lambda = d / d_{\lim}$, which relates the size of the particle to the maximum diameter of the circle inscribed in the Plateau border cross-section. For $\lambda > 1$, particles are trapped in the foams, and the resulting drainage velocity is severely reduced [183-185].

3.3 Gaps in the knowledge of foam drainage in the presence of solid particles

The following knowledge gaps have been identified on the basis of the current understanding of foam drainage for aqueous and three-phase foams:

- The effects of attached or hydrophobic particles on the foam drainage remain poorly understood.
- The effects of solid particles on the stress state of the gas-liquid interface of foams remain poorly understood.
- It is unclear whether the foam drainage equations for aqueous foams can be applied to three-phase foams.

4. Concluding remarks

This chapter has reviewed different models for foam column kinetics, the mechanisms governing foamability and foam stability, and the effects of solid particles on foam drainage. The interrelation of different length scales of foam properties was emphasized. Although many research efforts have been made in each length scale, the correlation between their results, which is important for understanding foam drainage and stability, remains poorly understood and quantified. A more comprehensive model that includes the growth, drainage and collapse of foams is required to quantify and understand these complex foam behaviors.

Acknowledgements

The authors gratefully acknowledge the China Scholarship Council (CSC) of the Chinese Government and The University of Queensland (UQ) for the CSC-UQ scholarship for JW.

References

[1] N. Barbian, E. Ventura-Medina, J.J. Cilliers, Dynamic froth stability in froth flotation, Minerals Engineering, 16 (2003) 1111-1116.

[2] N. Barbian, K. Hadler, E. Ventura-Medina, J.J. Cilliers, The froth stability column: linking froth stability and flotation performance, Minerals Engineering, 18 (2005) 317-324.

[3] N. Barbian, K. Hadler, J.J. Cilliers, The froth stability column: Measuring froth stability at an industrial scale, Minerals Engineering, 19 (2006) 713-718.

[4] L. Pilon, A. G. Fedorov, R. Viskanta, Analysis of transient thickness of pneumatic foams, Chemical Engineering Science, 57 (2002) 977-990.

[5] P. Hrma, Model for a steady state foam blanket, Journal of Colloid and Interface Science, 134 (1990) 161-168.

[6] J. van der Schaaf, R.G.C. Beerkens, A model for foam formation, stability, and breakdown in glass-melting furnaces, Journal of Colloid and Interface Science, 295 (2006) 218-229.

[7] L. Pilon, A.G. Fedorov, R. Viskanta, Steady-State Thickness of Liquid–Gas Foams, Journal of Colloid and Interface Science, 242 (2001) 425-436.

[8] J.J. Bikerman, Foam, Springer-Verlag, New York, 1973.

[9] J.J. Bikerman, The unit of foaminess, Transactions of the Faraday Society, 34 (1938) 634-638.

[10] S.I. Karakashev, P. Georgiev, K. Balashev, Foam production – Ratio between foaminess and rate of foam decay, Journal of Colloid and Interface Science, 379 (2012) 144-147.

[11] S.I. Karakashev, P. Georgiev, K. Balashev, On the growth of pneumatic foams, Eur. Phys. J. E, 36 (2013) 13.

[12] R. McElroy, Air release from mineral oils, Department of Pure and Applied Chemistry, Strathclyde University, 1978.

[13] S. Hartland, A.D. Barber, A model for a cellular foam, Transactions of the Institution of Chemical Engineers, 52 (1974) 43-52.

[14] S.A. Koehler, S. Hilgenfeldt, H.A. Stone, Liquid Flow through Aqueous Foams: The Node-Dominated Foam Drainage Equation, Physical Review Letters, 82 (1999) 4232-4235.

[15] S.J. Neethling, H.T. Lee, J.J. Cilliers, A foam drainage equation generalized for all liquid contents, Journal of Physics: Condensed Matter, 14 (2002) 331.

[16] S.A. Koehler, S. Hilgenfeldt, H.A. Stone, A Generalized View of Foam Drainage: Experiment and Theory, Langmuir, 16 (2000) 6327-6341.

[17] N.F. Djabbarah, D.T. Wasan, Foam stability: The effect of surface rheological properties on the lamella rupture, AIChE Journal, 31 (1985) 1041-1043.

[18] S.J. Neethling, H.T. Lee, P. Grassia, The growth, drainage and breakdown of foams, Colloids and Surfaces A: Physicochemical and Engineering Aspects, 263 (2005) 184-196.

[19] P. Stevenson, Dimensional analysis of foam drainage, Chemical Engineering Science, 61 (2006) 4503-4510.

[20] P. Stevenson, On the forced drainage of foam, Colloids and Surfaces A: Physicochemical and Engineering Aspects, 305 (2007) 1-9.

[21] L. Pilon, R. Viskanta, Minimum superficial gas velocity for onset of foaming, Chemical Engineering and Processing: Process Intensification, 43 (2004) 149-160.

[22] J.A. Attia, S. Kholi, L. Pilon, Scaling laws in steady-state aqueous foams including Ostwald ripening, Colloids and Surfaces A: Physicochemical and Engineering Aspects, 436 (2013) 1000-1006.

[23] G. Narsimhan, E. Ruckenstein, Hydrodynamics, enrichment, and collapse in foams, Langmuir, 2 (1986) 230-238.

[24] G. Narsimhan, A model for unsteady state drainage of a static foam, Journal of Food Engineering, 14 (1991) 139-165.

[25] R.J. Germick, A.S. Rehill, G. Narsimhan, Experimental investigation of static drainage of protein stabilized foams — Comparison with model, Journal of Food Engineering, 23 (1994) 555-578.

[26] A. Bhakta, E. Ruckenstein, Drainage of a Standing Foam, Langmuir, 11 (1995) 1486-1492.
[27] A. Bhakta, E. Ruckenstein, Decay of standing foams: drainage, coalescence and collapse, Advances in Colloid and Interface Science, 70 (1997) 1-124.
[28] A. Bhakta, E. Ruckenstein, Modeling of the Generation and Collapse of Aqueous Foams, Langmuir, 12 (1996) 3089-3099.
[29] G. Narsimhan, E. Ruckenstein, Effect of bubble size distribution on the enrichment and collapse in foams, Langmuir, 2 (1986) 494-508.
[30] E. Iglesias, J. Anderez, A. Forgiarini, J.-L. Salager, A new method to estimate the stability of short-life foams, Colloids and Surfaces A: Physicochemical and Engineering Aspects, 98 (1995) 167-174.
[31] S.J. Neethling, J.J. Cilliers, E.T. Woodburn, Prediction of the water distribution in a flowing foam, Chemical Engineering Science, 55 (2000) 4021-4028.
[32] D. Weaire, S. Hutzler, The Physics of Foams, Clarendon Press, Oxford, 1999.
[33] K. Malysa, K. Lunkenheimer, Foams under dynamic conditions, Current Opinion in Colloid & Interface Science, 13 (2008) 150-162.
[34] S. Farrokhpay, The significance of froth stability in mineral flotation — A review, Advances in Colloid and Interface Science, 166 (2011) 1-7.
[35] A.V. Nguyen, H.J. Schulze, Colloidal science of flotation, Marcel Dekker, New York, 2004.
[36] P.C. Duineveld, Bouncing and Coalescence of Bubble Pairs Rising at High Reynolds Number in Pure Water or Aqueous Surfactant Solutions, Flow, Turbulence and Combustion, 58 (1997) 409-439.
[37] P.C. Duineveld, Bouncing and coalescence of two bubbles in pure water, in: S. Morioka, L. Van Wijngaarden (Eds.) IUTAM Symposium on Waves in Liquid/Gas and Liquid/Vapour Two-Phase Systems, Springer Netherlands1995, pp. 151-160.
[38] S.I. Karakashev, M.V. Grozdanova, Foams and antifoams, Advances in Colloid and Interface Science, 176–177 (2012) 1-17.
[39] M. Buzzacchi, P. Schmiedel, W. von Rybinski, Dynamic surface tension of surfactant systems and its relation to foam formation and liquid film drainage on solid surfaces, Colloids and Surfaces A: Physicochemical and Engineering Aspects, 273 (2006) 47-54.
[40] T. Tamura, Y. Kaneko, M. Ohyama, Dynamic Surface Tension and Foaming Properties of Aqueous Polyoxyethylene n-Dodecyl Ether Solutions, Journal of Colloid and Interface Science, 173 (1995) 493-499.
[41] R. Varadaraj, J. Bock, P. Valint Jr, S. Zushma, N. Brons, Relationship between fundamental interfacial properties and foaming in linear and branched sulfate, ethoxysulfate, and ethoxylate surfactants, Journal of Colloid and Interface Science, 140 (1990) 31-34.
[42] M. Rosen, X. Hua, Z. Zhu, Dynamic Surface Tension of Aqueous Surfactant Solutions: IV Relationship to Foaming, in: K.L. Mittal, D.O. Shah (Eds.) Surfactants in Solution, Springer US1991, pp. 315-327.
[43] D. Kawale, A.T. van Nimwegen, L.M. Portela, M.A. van Dijk, R.A.W.M. Henkes, The relation between the dynamic surface tension and thefoaming behaviour in a sparger setup, Colloids and Surfaces A: Physicochemical and Engineering Aspects.
[44] H. Xi Yuan, M.J. Rosen, Dynamic surface tension of aqueous surfactant solutions: I. Basic paremeters, Journal of Colloid and Interface Science, 124 (1988) 652-659.
[45] S.S. Dukhin, G. Kretzschmar, R. Miller, Dynamics of adsorption at liquid interfaces, in: D. Möbius, R. Miller (Eds.) Studies in interface science, Elsevier, Amsterdam, 1995.
[46] D.A. Edwards, H. Brenner, D.T. Wasan, Interfacial transport processes and rheology, Butterworth-Heinemann, Boston, 1991.
[47] J.W. Gibbs, Collected Works, vol. 1, Dover Publishing Co. Inc, New York, 1961.
[48] V.G. Levich, The damping of waves by surface-active substances. Parts I, Acta Physicochim., 14 (1941) 307-328.

[49] G. Kretzschmar, K. Lunkenheimer, Untersuchungen zur Bestimmung der Elastizität von Adsorptionsschichten löslicher grenzflächenaktiver Stoffe, Berichte der Bunsengesellschaft für physikalische Chemie, 74 (1970) 1064-1071.
[50] J. Benjamins, A. Cagna, E.H. Lucassen-Reynders, Viscoelastic properties of triacylglycerol/water interfaces covered by proteins, Colloids and Surfaces A: Physicochemical and Engineering Aspects, 114 (1996) 245-254.
[51] F.C. Goodrich, in: J.F. Danielli, M.D. Rosenberg, D.A. Cadenhead (Eds.) Progress in Surface and Membrane Science, Academic Press, New York, 1973.
[52] L. Gupta, D.T. Wasan, Surface Shear Viscosity and Related Properties of Adsorbed Surfactant Films, Industrial & Engineering Chemistry Fundamentals, 13 (1974) 26-33.
[53] F.C. Goodrich, in: K.L. Mittal (Ed.) Solution Chemistry of Surfactants, Plenum Press, New York, 1979.
[54] R. Miller, R. Wüstneck, J. Krägel, G. Kretzschmar, Dilational and shear rheology of adsorption layers at liquid interfaces, Colloids and Surfaces A: Physicochemical and Engineering Aspects, 111 (1996) 75-118.
[55] M. A. Bos, T. van Vliet, Interfacial rheological properties of adsorbed protein layers and surfactants: a review, Advances in Colloid and Interface Science, 91 (2001) 437-471.
[56] R. Miller, L. Liggieri, Interfacial Rheology, Progress in Colloid and Interface Science Volume 1, Brill, Leiden and Boston, 2009.
[57] E.H. Lucassen-Reynders, A. Cagna, J. Lucassen, Gibbs elasticity, surface dilational modulus and diffusional relaxation in nonionic surfactant monolayers, Colloids and Surfaces A: Physicochemical and Engineering Aspects, 186 (2001) 63-72.
[58] D. Langevin, F. Monroy, Marangoni stresses and surface compression rheology of surfactant solutions. Achievements and problems, Advances in Colloid and Interface Science, 206 (2014) 141-149.
[59] K. Małysa, R. Miller, K. Lunkenheimer, Relationship between foam stability and surface elasticity forces: Fatty acid solutions, Colloids and Surfaces, 53 (1991) 47-62.
[60] K. Małysa, K. Lunkenheimer, R. Miller, C. Hempt, Surface elasticity and dynamic stability of wet foams, Colloids and Surfaces, 16 (1985) 9-20.
[61] I.B. Ivanov, K.D. Danov, K.P. Ananthapadmanabhan, A. Lips, Interfacial rheology of adsorbed layers with surface reaction: On the origin of the dilatational surface viscosity, Advances in Colloid and Interface Science, 114–115 (2005) 61-92.
[62] K.-D. Wantke, H. Fruhner, Determination of Surface Dilational Viscosity Using the Oscillating Bubble Method, Journal of Colloid and Interface Science, 237 (2001) 185-199.
[63] K.D. Wantke, J. Örtegren, H. Fruhner, A. Andersen, H. Motschmann, The influence of the sublayer on the surface dilatational modulus, Colloids and Surfaces A: Physicochemical and Engineering Aspects, 261 (2005) 75-83.
[64] H. Zhang, G. Xu, T. Liu, L. Xu, Y. Zhou, Foam and interfacial properties of Tween 20–bovine serum albumin systems, Colloids and Surfaces A: Physicochemical and Engineering Aspects, 416 (2013) 23-31.
[65] K.D. Martínez, C. Carrera Sánchez, J.M. Rodríguez Patino, A.M.R. Pilosof, Interfacial and foaming properties of soy protein and their hydrolysates, Food Hydrocolloids, 23 (2009) 2149-2157.
[66] D. Langevin, Influence of interfacial rheology on foam and emulsion properties, Advances in Colloid and Interface Science, 88 (2000) 209-222.
[67] D. Varade, D. Carriere, L.R. Arriaga, A.L. Fameau, E. Rio, D. Langevin, W. Drenckhan, On the origin of the stability of foams made from catanionic surfactant mixtures, Soft Matter, 7 (2011) 6557-6570.
[68] A. Stocco, D. Carriere, M. Cottat, D. Langevin, Interfacial Behavior of Catanionic Surfactants, Langmuir, 26 (2010) 10663-10669.
[69] D. Georgieva, A. Cagna, D. Langevin, Link between surface elasticity and foam stability, Soft Matter, 5 (2009) 2063-2071.

[70] K. Wantke, K. Małysa, K. Lunkenheimer, A relation between dynamic foam stability and surface elasticity, Colloids and Surfaces A: Physicochemical and Engineering Aspects, 82 (1994) 183-191.
[71] H. Fruhner, K.D. Wantke, K. Lunkenheimer, Relationship between surface dilational properties and foam stability, Colloids and Surfaces A: Physicochemical and Engineering Aspects, 162 (2000) 193-202.
[72] J.-L. Joye, G.J. Hirasaki, C.A. Miller, Asymmetric Drainage in Foam Films, Langmuir, 10 (1994) 3174-3179.
[73] J.-L. Joye, G.J. Hirasaki, C.A. Miller, Numerical Simulation of Instability Causing Asymmetric Drainage in Foam Films, Journal of Colloid and Interface Science, 177 (1996) 542-552.
[74] A.A. Sonin, A. Bonfillon, D. Langevin, Thinning of Soap Films: The Role of Surface Viscoelasticity, Journal of Colloid and Interface Science, 162 (1994) 323-330.
[75] V. Bergeron, Disjoining Pressures and Film Stability of Alkyltrimethylammonium Bromide Foam Films, Langmuir, 13 (1997) 3474-3482.
[76] A. Espert, R.v. Klitzing, P. Poulin, A. Colin, R. Zana, D. Langevin, Behavior of Soap Films Stabilized by a Cationic Dimeric Surfactant, Langmuir, 14 (1998) 4251-4260.
[77] C. Stubenrauch, R. Miller, Stability of Foam Films and Surface Rheology: An Oscillating Bubble Study at Low Frequencies, The Journal of Physical Chemistry B, 108 (2004) 6412-6421.
[78] E. Santini, F. Ravera, M. Ferrari, C. Stubenrauch, A. Makievski, J. Krägel, A surface rheological study of non-ionic surfactants at the water–air interface and the stability of the corresponding thin foam films, Colloids and Surfaces A: Physicochemical and Engineering Aspects, 298 (2007) 12-21.
[79] I. Cantat, S. Cohen-Addad, F. Elias, F. Graner, R. Hohler, O. Pitois, F. Rouyer, A. Saint-jalmes, Foams: Structure and Dynamics, CPI Group (UK) Ltd, Croydon, 2013.
[80] A. Bhattacharyya, F. Monroy, D. Langevin, J.-F. Argillier, Surface Rheology and Foam Stability of Mixed Surfactant−Polyelectrolyte Solutions†, Langmuir, 16 (2000) 8727-8732.
[81] C. Stubenrauch, K. Khristov, Foams and foam films stabilized by CnTAB: Influence of the chain length and of impurities, Journal of Colloid and Interface Science, 286 (2005) 710-718.
[82] R. Hook, On holes (black film) in soap bubbles, Commun. Roy. Soc (1672).
[83] I. Newton, Optics, Dover, London, 1952.
[84] J.A.F. Plateau, Statique experimentale et theoryque des liquides soumis aux seules forces molecularires, Gautier-Villars, Trubner et cie, F. Clemm, 2 Vols (1873).
[85] J.W. Gibbs, On the Equilibrium of Heterogeneous Substances, Trans. Connecticut Acad., III (1876) pp 108 - 248 and (1878) pp 343 - 524, as reprinted in The Scientific Papers of J. Willard Gibbs, Vol. I. Thermodynamics., Dover Publications, New York, 1961, pp. 302.
[86] G. Gochev, D. Platikanov, R. Miller, Chronicles of foam films, Advances in Colloid and Interface Science.
[87] B.V. Derjaguin, Theory of particles interaction in presence of double electric layers and aggregation stability of liophobic colloids and disperse systems, Bull. Acad. Sci. URSS Ser, 5 (1937) 1153-1164.
[88] B. Derjaguin, On the repulsive forces between charged colloid particles and on the theory of slow coagulation and stability of lyophobe sols, Transactions of the Faraday Society, 35 (1940) 203-215.
[89] B. Vance, Forces and structure in thin liquid soap films, Journal of Physics: Condensed Matter, 11 (1999) R215.
[90] K.J. Mysels, K. Shinoda, S. Frankel, Soap films: studies of their thinning, Pergamon Press, London, New York, Pairs, Los Angeles, 1959.
[91] S. Cosima, K. Regine von, Disjoining pressure in thin liquid foam and emulsion films—new concepts and perspectives, Journal of Physics: Condensed Matter, 15 (2003) R1197.
[92] N.V. Churaev, Derjaguin's disjoining pressure in the colloid science and surface phenomena, Advances in Colloid and Interface Science, 104 (2003) xv-xx.

[93] B.V. Derjaguin, M.M. Kussakov, Experimental investigations on solvation of surfaces with application to the development of a mathematical theory of the stability of lyophobic colloids, Bull. Acad. Sci. URSS Ser Chim, 5 (1937) 1119-1152.
[94] B.V. Derjaguin, M.M. Kussakov, Anomalous properties of thin polymolecular - films V an experimental investigation of polymolecular solvate (adsorbed) films as applied to the development of a mathematical theory of the stability of colloids, Acta Phys. URSS, 10 (1939) 25.
[95] B.V. Derjaguin, L.D. Landau, Theory of the stability of strongly charged lyophobic sols and of the adhesion of strongly charged particles in solution of electrolytes, Acta Phys. URSS, 14 (1941) 633-662.
[96] E.J.W. Verwey, Theory of the Stability of Lyophobic Colloids, The Journal of Physical and Colloid Chemistry, 51 (1947) 631-636.
[97] D. Exerowa, P.M. Kruglyakov, Foam and Foam Films - Theory, Experiment, Application, Elsevier, Amsterdam, 1998.
[98] B.V. Derjaguin, A.S. Titijevskaya, Static and kinetic stability of free films and froths, Progress in Surface Science, 43 (1993) 74-82.
[99] B.V. Derjaguin, A.S. Titijevskaia, I.I. Abricossova, A.D. Malkina, Investigations of the forces of interaction of surfaces in different media and their application to the problem of colloid stability, Discussions of the Faraday Society, 18 (1954) 24-41.
[100] J.T.G. Overbeek, BLACK SOAP FILMS1, The Journal of Physical Chemistry, 64 (1960) 1178-1183.
[101] E.M. Duyvis, The equilibrium thickness of free liquid films, University Utrecht, 1962.
[102] A. Scheludko, D. Platikanov, E. Manev, Disjoining pressure in thin liquid films and the electro-magnetic retardation effect of the molecule dispersion interactions, Discussions of the Faraday Society, 40 (1965) 253-265.
[103] J. Lyklema, K.J. Mysels, A Study of Double Layer Repulsion and van der Waals Attraction in Soap Films, Journal of the American Chemical Society, 87 (1965) 2539-2546.
[104] A. Scheludko, D. Exerowa, Über den elektrostatischen Druck in Schaumfilmen aus wässerigen Elektrolytlösungen, Kolloid-Zeitschrift, 165 (1959) 148-151.
[105] A. Scheludko, D. Exerowa, Über den elektrostatischen und van der Waalsschen zusätzlichen Druck in wässerigen Schaumfilmen, Kolloid-Zeitschrift, 168 (1960) 24-28.
[106] P.R. Garrett, The Science of Defoaming: Theory, Experiment and Applications, Surfactant science series volume, CRC Press Taylor&Francis Group, Boca Raton, 2013.
[107] N.D. Denkov, Mechanisms of Foam Destruction by Oil-Based Antifoams, Langmuir, 20 (2004) 9463-9505.
[108] P.R. Garrett, Defoaming: Theory and Industrial Applications New York, 1993.
[109] D.T. Wasan, S.P. Christiano, Foams and Antifoams: A thin film approach, in: K.S. Birdi (Ed.) Handbook of Surface and Colloid Chemistry, CRC Press, New York, 1997.
[110] R.K. Prud'homme, S.A. Khan, Foams: theory, measurements, and applications, Marcel Dekker, New York, 1996.
[111] T. Wei, Y. Peng, S. Farrokhpay, Froth stability of coal flotation in saline water, Mineral Processing and Extractive Metallurgy (Trans. Inst. Min Metall. C), (2014).
[112] M. Zanin, I. Ametov, S. Grano, L. Zhou, W. Skinner, A study of mechanisms affecting molybdenite recovery in a bulk copper/molybdenum flotation circuit, International Journal of Mineral Processing, 93 (2009) 256-266.
[113] L. Lobo, D.T. Wasan, Mechanisms of aqueous foam stability in the presence of emulsified non-aqueous-phase liquids: structure and stability of the pseudoemulsion film, Langmuir, 9 (1993) 1668-1677.
[114] V. Bergeron, M.E. Fagan, C.J. Radke, Generalized entering coefficients: a criterion for foam stability against oil in porous media, Langmuir, 9 (1993) 1704-1713.

[115] A.S. Aronson, V. Bergeron, M.E. Fagan, C.J. Radke, The influence of disjoining pressure on foam stability and flow in porous media, Colloids and Surfaces A: Physicochemical and Engineering Aspects, 83 (1994) 109-120.
[116] V. Bergeron, C.J. Radke, Disjoining pressure and stratification in asymmetric thin-liquid films, Colloid & Polymer Sci, 273 (1995) 165-174.
[117] V. Bergeron, J.E. Hanssen, F.N. Shoghl, Thin-film forces in hydrocarbon foam films and their application to gas-blocking foams in enhanced oil recovery, Colloids and Surfaces A: Physicochemical and Engineering Aspects, 123–124 (1997) 609-622.
[118] E.S. Basheva, D. Ganchev, N.D. Denkov, K. Kasuga, N. Satoh, K. Tsujii, Role of Betaine as Foam Booster in the Presence of Silicone Oil Drops, Langmuir, 16 (2000) 1000-1013.
[119] E.S. Basheva, S. Stoyanov, N.D. Denkov, K. Kasuga, N. Satoh, K. Tsujii, Foam Boosting by Amphiphilic Molecules in the Presence of Silicone Oil, Langmuir, 17 (2001) 969-979.
[120] K.G. Marinova, N.D. Denkov, Foam Destruction by Mixed Solid−Liquid Antifoams in Solutions of Alkyl Glucoside: Electrostatic Interactions and Dynamic Effects, Langmuir, 17 (2001) 2426-2436.
[121] L. Arnaudov, N.D. Denkov, I. Surcheva, P. Durbut, G. Broze, A. Mehreteab, Effect of Oily Additives on Foamability and Foam Stability. 1. Role of Interfacial Properties, Langmuir, 17 (2001) 6999-7010.
[122] A. Hadjiiski, S. Tcholakova, N.D. Denkov, P. Durbut, G. Broze, A. Mehreteab, Effect of Oily Additives on Foamability and Foam Stability. 2. Entry Barriers, Langmuir, 17 (2001) 7011-7021.
[123] K.G. Marinova, N.D. Denkov, P. Branlard, Y. Giraud, M. Deruelle, Optimal Hydrophobicity of Silica in Mixed Oil−Silica Antifoams, Langmuir, 18 (2002) 3399-3403.
[124] K.G. Marinova, N.D. Denkov, S. Tcholakova, M. Deruelle, Model Studies of the Effect of Silica Hydrophobicity on the Efficiency of Mixed Oil−Silica Antifoams, Langmuir, 18 (2002) 8761-8769.
[125] N.D. Denkov, S. Tcholakova, K.G. Marinova, A. Hadjiiski, Role of Oil Spreading for the Efficiency of Mixed Oil−Solid Antifoams, Langmuir, 18 (2002) 5810-5817.
[126] K.G. Marinova, S. Tcholakova, N.D. Denkov, S. Roussev, M. Deruelle, Model Studies on the Mechanism of Deactivation (Exhaustion) of Mixed Oil−Silica Antifoams, Langmuir, 19 (2003) 3084-3089.
[127] N.D. Denkov, K.G. Marinova, C. Christova, A. Hadjiiski, P. Cooper, Mechanisms of Action of Mixed Solid−Liquid Antifoams: 3. Exhaustion and Reactivation, Langmuir, 16 (2000) 2515-2528.
[128] A. Hadjiiski, S. Tcholakova, I.B. Ivanov, T.D. Gurkov, E.F. Leonard, Gentle Film Trapping Technique with Application to Drop Entry Measurements, Langmuir, 18 (2002) 127-138.
[129] R. Aveyard, J.H. Clint, Liquid Droplets and Solid Particles at Surfactant Solution Interfaces, J. CHEM. SOC. FARADAY TRANS., 91 (1995) 2681-2697.
[130] I.B. Ivanov, Thin liquid films: fundamentals and applications, Marcel Dekker, New York, 1988.
[131] K. Koczo, L.A. Lobo, D.T. Wasan, Effect of oil on foam stability: Aqueous foams stabilized by emulsions, Journal of Colloid and Interface Science, 150 (1992) 492-506.
[132] W.D. Harkins, A General Thermodynamic Theory of the Spreading of Liquids to Form Duplex Films and of Liquids or Solids to Form Monolayers, The Journal of Chemical Physics, 9 (1941) 552-568.
[133] S. Ross, The Inhibition of Foaming. II. A Mechanism for the Rupture of Liquid Films by Anti-foaming Agents, The Journal of Physical and Colloid Chemistry, 54 (1950) 429-436.
[134] P.R. Garrett, J. Davis, H.M. Rendall, An experimental study of the antifoam behaviour of mixtures of a hydrocarbon oil and hydrophobic particles, Colloids and Surfaces A: Physicochemical and Engineering Aspects, 85 (1994) 159-197.
[135] R. Aveyard, P. Cooper, P.D.I. Fletcher, C.E. Rutherford, Foam Breakdown by Hydrophobic Particles and Nonpolar Oil, Langmuir, 9 (1993) 604-613.

[136] R. Aveyard, B.P. Binks, P.D.I. Fletcher, T.G. Peck, C.E. Rutherford, Aspects of aqueous foam stability in the presence of hydrocarbon oils and solid particles, Advances in Colloid and Interface Science, 48 (1994) 93-120.
[137] G.C. Frye, J.C. Berg, Mechanisms for the Synergistic Antifoam Action by Hydrophobic Solid Particles in Insoluble Liquids, Journal of Colloid and Interface Science, 130 (1989) 54-59.
[138] V. Bergeron, P. Cooper, C. Fischer, J. Giermanska-Kahn, D. Langevin, A. Pouchelon, Polydimethylsiloxane (PDMS)-based antifoams, Colloids and Surfaces A: Physicochemical and Engineering Aspects, 122 (1997) 103-120.
[139] R. Aveyard, B.P. Binks, P.D.I. Fletcher, T.-G. Peck, P.R. Garrett, Entry and spreading of alkane drops at the air/surfactant solution interface in relation to foam and soap film stability, Journal of the Chemical Society, Faraday Transactions, 89 (1993) 4313-4321.
[140] B.K. Jha, S.P. Christiano, D.O. Shah, Silicone Antifoam Performance: Correlation with Spreading and Surfactant Monolayer Packing, Langmuir, 16 (2000) 9947-9954.
[141] V. Bergeron, D. Langevin, Monolayer Spreading of Polydimethylsiloxane Oil on Surfactant Solutions, Physical Review Letters, 76 (1996) 3152-3155.
[142] H. Zhang, C.A. Miller, P.R. Garrett, K.H. Raney, Mechanism for defoaming by oils and calcium soap in aqueous systems, Journal of Colloid and Interface Science, 263 (2003) 633-644.
[143] A. Saint-Jalmes, Physical chemistry in foam drainage and coarsening, Soft Matter, 2 (2006) 836-849.
[144] S. Hutzler, D. Weaire, S. Shah, Bubble sorting in a foam under forced drainage, Philosophical Magazine Letters, 80 (2000) 41-48.
[145] S. Hutzler, D. Weaire, Foam coarsening under forced drainage, Philosophical Magazine Letters, 80 (2000) 419-425.
[146] S. Hilgenfeldt, S.A. Koehler, H.A. Stone, Dynamics of Coarsening Foams: Accelerated and Self-Limiting Drainage, Physical Review Letters, 86 (2001) 4704-4707.
[147] A.E. Roth, C.D. Jones, D.J. Durian, Bubble statistics and coarsening dynamics for quasi-two-dimensional foams with increasing liquid content, PHYSICAL REVIEW E, 87 (2013) 042304.
[148] S.-J. Arnaud, L. Dominique, Time evolution of aqueous foams: drainage and coarsening, Journal of Physics: Condensed Matter, 14 (2002) 9397.
[149] V. Carrier, A. Colin, Coalescence in Draining Foams, Langmuir, 19 (2003) 4535-4538.
[150] G. Maurdev, A. Saint-Jalmes, D. Langevin, Bubble motion measurements during foam drainage and coarsening, Journal of Colloid and Interface Science, 300 (2006) 735-743.
[151] I.B. Ivanov, D.S. Dimitrov, Hydrodynamics of thin liquid films, Colloid & Polymer Sci, 252 (1974) 982-990.
[152] E. Manev, A. Scheludko, D. Exerowa, Effect of surfactant concentration on the critical thicknesses of liquid films, Colloid & Polymer Sci, 252 (1974) 586-593.
[153] A. Sharma, E. Ruckenstein, Critical thickness and lifetimes of foams and emulsions: Role of surface wave-induced thinning, Journal of Colloid and Interface Science, 119 (1987) 14-29.
[154] A. Vrij, J.T.G. Overbeek, Rupture of thin liquid films due to spontaneous fluctuations in thickness, Journal of the American Chemical Society, 90 (1968) 3074-3078.
[155] L. Wang, R.-H. Yoon, Role of hydrophobic force in the thinning of foam films containing a nonionic surfactant, Colloids and Surfaces A: Physicochemical and Engineering Aspects, 282–283 (2006) 84-91.
[156] D. Weaire, S. Hutzler, G. Verbist, E. Peters, A Review of Foam Drainage, Advances in Chemical Physics, John Wiley & Sons, Inc.2007, pp. 315-374.
[157] S.A. Koehler, S. Hilgenfeldt, H.A. Stone, Foam drainage on the microscale: I. Modeling flow through single Plateau borders, Journal of Colloid and Interface Science, 276 (2004) 420-438.
[158] V. Carrier, S. Destouesse, A. Colin, Foam drainage: A film contribution?, PHYSICAL REVIEW E, 65 (2002) 061404.
[159] R.A. Leonard, R. Lemlich, A study of interstitial liquid flow in foam. Part I. Theoretical model and application to foam fractionation, AIChE Journal, 11 (1965) 18-25.

[160] R.A. Leonard, R. Lemlich, A study of interstitial liquid flow in foam. Part II. Experimental verification and observations, AIChE Journal, 11 (1965) 25-29.
[161] G. Verbist, D. Weaire, A.M. Kraynik, The foam drainage equation, Journal of Physics: Condensed Matter, 8 (1996) 3715.
[162] V. Goldshtein, I. Goldfarb, I. Shreiber, Drainage waves structure in gas-liquid foam, International Journal of Multiphase Flow, 22 (1996) 991-1003.
[163] A.V. Nguyen, Liquid Drainage in Single Plateau Borders of Foam, Journal of Colloid and Interface Science, 249 (2002) 194-199.
[164] L. Randriamanjatosoa, M. Zanin, S. Grano, Use of the foam drainage equation to model water flow in flotation froth, CHEMECA, Engineering Australia, Melbourne, Australia, 2007, pp. 300-306.
[165] E. Lorenceau, N. Louvet, F. Rouyer, O. Pitois, Permeability of aqueous foams, THE EUROPEAN PHYSICAL JOURNAL E, 28 (2009) 293-304.
[166] A. Saint-Jalmes, Y. Zhang, D. Langevin, Quantitative description of foam drainage: Transitions with surface mobility, THE EUROPEAN PHYSICAL JOURNAL E, 15 (2004) 53-60.
[167] S.J. Neethling, J.J. Cilliers, Solids motion in flowing froths, Chemical Engineering Science, 57 (2002) 607-615.
[168] H.T. Lee, S.J. Neethling, J.J. Cilliers, Particle and liquid dispersion in foams, Colloids and Surfaces A: Physicochemical and Engineering Aspects, 263 (2005) 320-329.
[169] P. Stevenson, S. Ata, G.M. Evans, Convective–dispersive gangue transport in flotation froth, Chemical Engineering Science, 62 (2007) 5736-5744.
[170] N.A. Bennani, A. Fujiwara, S. Takagi, Y. Matsumoto, Coarse particles sedimentation within a quasi two-dimensional rising foam, Colloids and Surfaces A: Physicochemical and Engineering Aspects, 309 (2007) 7-12.
[171] F. Rouyer, N. Louvet, C. Fritz, O. Pitois, Transport of coarse particles in liquid foams: coupling of confinement and buoyancy effects, Soft Matter, 7 (2011) 4812-4820.
[172] F. Rouyer, C. Fritz, O. Pitois, The sedimentation of fine particles in liquid foams, Soft Matter, 6 (2010) 3863-3869.
[173] N. Louvet, R. Höhler, O. Pitois, Capture of particles in soft porous media, PHYSICAL REVIEW E, 82 (2010) 041405.
[174] B.P. Binks, Particles as surfactants—similarities and differences, Current Opinion in Colloid & Interface Science, 7 (2002) 21-41.
[175] M. Abkarian, A.B. Subramaniam, S.-H. Kim, R.J. Larsen, S.-M. Yang, H.A. Stone, Dissolution Arrest and Stability of Particle-Covered Bubbles, Physical Review Letters, 99 (2007) 188301.
[176] A. Cervantes Martinez, E. Rio, G. Delon, A. Saint-Jalmes, D. Langevin, B.P. Binks, On the origin of the remarkable stability of aqueous foams stabilised by nanoparticles: link with microscopic surface properties, Soft Matter, 4 (2008) 1531-1535.
[177] O. Pitois, M. Buisson, X. Chateau, On the collapse pressure of armored bubbles and drops, THE EUROPEAN PHYSICAL JOURNAL E, 38 (2015) 1-7.
[178] A. Britan, M. Liverts, G. Ben-Dor, S.A. Koehler, N. Bennani, The effect of fine particles on the drainage and coarsening of foam, Colloids and Surfaces A: Physicochemical and Engineering Aspects, 344 (2009) 15-23.
[179] R.M. Guillermic, A. Salonen, J. Emile, A. Saint-Jalmes, Surfactant foams doped with laponite: unusual behaviors induced by aging and confinement, Soft Matter, 5 (2009) 4975-4982.
[180] F. Carn, A. Colin, O. Pitois, M. Vignes-Adler, R. Backov, Foam Drainage in the Presence of Nanoparticle-Surfactant Mixtures, Langmuir, 25 (2009) 7847-7856.
[181] S. Guignot, S. Faure, M. Vignes-Adler, O. Pitois, Liquid and particles retention in foamed suspensions, Chemical Engineering Science, 65 (2010) 2579-2585.
[182] F. Carn, A. Colin, O. Pitois, R. Backov, Foam drainage study during plateau border mineralisation, Soft Matter, 8 (2012) 61-65.

[183] Y. Khidas, B. Haffner, O. Pitois, Capture-induced transition in foamy suspensions, Soft Matter, 10 (2014) 4137-4141.
[184] B. Haffner, Y. Khidas, O. Pitois, Flow and jamming of granular suspensions in foams, Soft Matter, 10 (2014) 3277-3283.
[185] F. Rouyer, B. Haffner, N. Louvet, Y. Khidas, O. Pitois, Foam clogging, Soft Matter, 10 (2014) 6990-6998.
[186] M. Durand, G. Martinoty, D. Langevin, Liquid flow through aqueous foams: From the plateau border-dominated regime to the node-dominated regime, Phys. Rev. E: Stat. Phys., Plasmas, Fluids, Relat. Interdiscip. Top., 60 (1999) R6307-R6308.
[187] A.V. Nguyen, H.J. Schulze, Colloidal Science of Flotation, Surfactant Science Series, Marcel Dekker, Inc, 2004.

Chapter 3: Foam Column Kinetics – Analogy to Reaction Kinetics

Jianlong Wang[1], Anh V Nguyen[1*] and Saeed Farrokhpay[2]
[1]School of Chemical Engineering, University of Queensland, Brisbane, Queensland 4072, Australia
[2]JKMRC, University of Queensland, Brisbane, Queensland 4072, Australia

[*]Correspondence: anh.nguyen@eng.uq.edu.au

Highlights:

- A model is proposed to relate foam column kinetics with reaction kinetics to interrelate the growth, drainage and collapse of foams.
- The growth and collapse of the foams and the transport of the gas and liquid within the growing foams are simulated.
- Two methods to calculate the foam collapse constant k_2^{2nd} are proposed and discussed.

Graphical abstract:

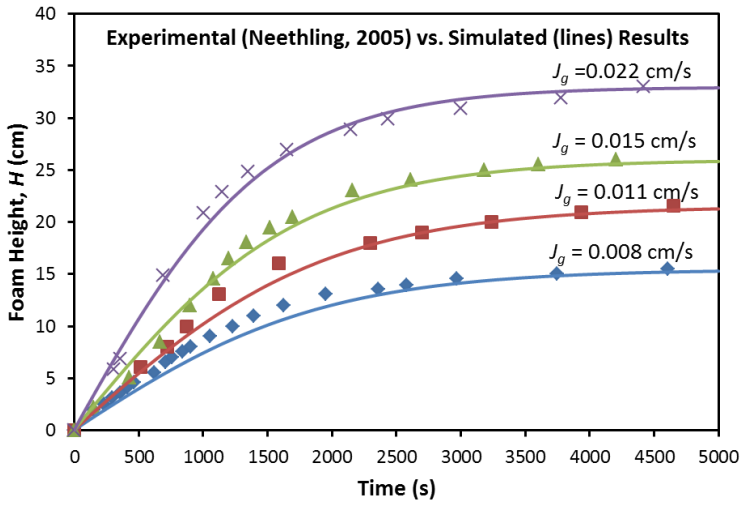

Abstract

This chapter presents a novel kinetic model that interrelates the growth, drainage and collapse of foams to simulate the evolution of foam height, liquid fraction, transport of liquid and gas in growing foams and foam collapse by analogy with reaction kinetics. The model assumes that the foam growth rate is determined by the competition between foam formation and collapse. The foam column kinetics is categorized as zeroth, first and second order, according to the dependence of the foam collapse rate on the foam volume or height. The model predictions of foam growth and collapse show good agreement with the experimental results. The predictions also show that the average liquid fraction decreases with increasing gas velocity, despite the increase in the overall liquid content in the foam. At relatively low gas velocity, the foam collapse rate predicted for growing foams is very close to the rate for standing foams. The discrepancy of the collapse rates obtained from growing and collapsing foams at higher gas velocity is caused by the higher reflux of surfactants in the growing foams relative to the reflux in standing foams, which leads to increased surfactant accumulation on the top of rising foams and, in turn, a lower foam collapse rate. This chapter illustrates the complexity of the behavior of growing foams, which is determined by a combination of mechanisms.

Keywords: foams, modeling, growth, drainage, collapse, kinetics

1. Introduction

In textbooks [2, 3], studies on foams are categorized according to the foam structure, birth (foamability), life (foam stability) and death (drainage, coarsening, rupture and coalescence) of foams and foam rheology. Although it is reasonable to isolate each category for convenience, the interrelation between the different categories of foam properties should never be ignored. For example, foam drainage and coarsening have been found to be interrelated [4-8]. Foam column kinetics describes the transient behaviors of foams, including growth, drainage and collapse. Foam column kinetics is crucially important for many industrial applications. For example, the precise control of the froth phase becomes particularly important in froth flotation because of the strong dependence of flotation performance on froth stability. Foam column kinetics has been used to predict the froth rising velocity and to calculate the fraction of bubbles bursting on the top surface of the froth, which is a key parameter in froth modeling and plant operations [9-12]. Foam column kinetics has also been applied in glass-melting furnaces [13-16]. Growing foams have been simulated based on the foam drainage equation and the bursting of bubbles on the top surface

of the foam [17, 18]. In these simulations, the foam collapse was modeled by assuming that the liquid films will rupture when the critical pressure they experience is reached. Although the fundamental physics governing the foam collapse process have been elucidated, a significant discrepancy between the simulated and experimental foam height values remains [17]. This discrepancy has been described as follows: "In a real foam, the films are unlikely to burst at a single exerted pressure, but rather are likely to exhibit a distribution in the bursting probabilities. … This distribution in the film stabilities probably accounts for the more gentle transition from not bursting to bursting seen in the experiments."

In this paper, instead of assuming that foam films begin to burst at a critical exerted pressure, we assume that the collapse of a foam follows reaction kinetics, which relates the foam collapse rate to the foam height. This correlation also corresponds to the explanation of the distribution of the film stabilities in [17]. For the first time, we derive a model for a growing foam that includes the effect of foam collapse on the foam growth by analogy with reaction kinetics. Then, we categorize the 'foam collapse reaction' as zeroth, first, and second order to reconcile the existing models for growing foams with our modeling framework. Together with the hydrodynamic theory of rising foams [19], we then interrelate the growth, drainage and collapse of foams using a series of mass balance equations for the foam growth, the evolution of the liquid fraction with time and the transport of liquid and gas in growing foams. Finally, we present the simulation results and make comparisons with the foam growth and collapse data reported in [17].

2. Modeling

2.1. Foam growth

We presume that the foam growth kinetics is controlled by two simultaneous processes: (1) foam formation and (2) foam collapse. It should be noted that no foam overflows from the foam column. The conservation balance for the gas phase gives:

$$G = G_1 + G_2 + G_3 \tag{1}$$

where G , G_1, G_2 and G_3 are the amounts of gas entering the foam column during agitation, gas of the bubbles in the pulp phase, gas of the bubbles in the foam and gas of the bursting bubbles leaving the foam, respectively. Here, we first assume the following: (1) the gas in the

pulp phase instantly attains a steady state, i.e., $[G_1] = const$, where the brackets represent the volume quantity. Likewise, the conservation balance for the liquid is described by:

$$L = L_1 + L_2 + L_3 \tag{2}$$

where L, L_1, L_2 and L_3 are the total amount of liquid in the system, the liquid in the pulp phase, the liquid between the un-burst bubbles in the foam and the liquid from the bursting bubbles, respectively. The second assumption is as follows: (2) the amounts of liquid among the un-burst bubbles and from the bursting bubbles are infinitesimally small relative to the amount of liquid in the pulp phase, i.e., $[L_1] = const$.

Foam growth kinetics can be described schematically and analogously as two series-parallel "reactions" as follows:

$$L_1 + G_1 \xrightarrow{k_1} F \tag{3}$$

$$F \xrightarrow{k_2} L_3 + G_3 \tag{4}$$

where $F = L_2 + G_2$ is the foam, and k_1 and k_2 are foam formation and foam collapse constants, respectively. Eq. (3) is related to the foam formation process, whereas Eq. (4) is related to the foam collapse process. Consider the 'foam formation reaction' illustrated in Eq. (3): the foam formation in the foam column can be described by analogy to a chemical reaction [20]. Because $[L_1]$ remains approximately constant, it can be included in the rate constant k_1 to obtain a pseudo-α-order foam formation rate equation:

$$\frac{d[F]}{dt} = k_1 [G_1]^{\alpha} \tag{5}$$

We assume that the rate of bubbles bursting on the top of the foam layer and inside the foam is insignificant relative to the rate of bubbles entering the foam from the liquid phase. Therefore, we have the following approximation:

$$\frac{d[F]}{dt} = k_1 [G_1]^{\alpha} = \frac{v_g}{1-\varepsilon} \tag{6}$$

where ε is the liquid fraction of the foam. The 'foam collapse reaction' in Eq. (4) must be considered during foam growth when bubbles burst. Therefore, the foam growth rate in Eq. (6) can be developed as:

$$\frac{d[F]}{dt} = \frac{v_g}{1-\varepsilon} - k_2[F]^{\beta} \tag{7}$$

where β is the order of the 'foam collapse reaction'.

2.1.1 Zeroth-order 'foam collapse reaction'

In a zeroth-order foam collapse reaction, the collapse rate is independent of foam volume or height. Therefore, the second term on the right-hand side of Eq. (7) is replaced by a constant, k :

$$\frac{d[F]}{dt} = \frac{v_g}{1-\varepsilon} - k \tag{8}$$

A zeroth-order reaction applies to the foam growth regime in which the equilibrium foam volume or height cannot be attained. For the stable foams that neither experience internal coalescence nor burst at the top surface, the foam growth rate equals $v_g/(1-\varepsilon)$ [13, 17]. Another case in this regime occurs when the bubbles begin to burst once the Plateau border size at the top of the foam reaches the critical value, but the foam continues to grow because of a sufficiently high gas flow rate, resulting in a foam growth rate that is smaller than the one in the former case [17]:

$$\frac{d[F]}{dt} = v_g - \lambda_1 A_{crit} \tag{9}$$

$$\lambda_1 = \frac{\rho g}{3C_{PB}\mu} \tag{10}$$

where A_{crit}, ρ, g and μ are the critical Plateau border area, the interstitial liquid density, the acceleration due to gravity and the interstitial liquid dynamic viscosity, respectively. C_{PB} is the Plateau border drag coefficient, which is 50 for the immobile interface and decreases with increasing interfacial mobility. Please note that the liquid content of foams is negligible in Eq. (9).

2.1.2 First-order ‘foam collapse reaction’

In the first-order foam collapse reaction, the foam collapse rate is proportional to the foam volume or height such that the following foam growth rate is obtained:

$$\frac{d[F]}{dt} = \frac{v_g}{1-\varepsilon} - k_2^{1st}[F] \tag{11}$$

In the foam growth regime in which the foam will reach the equilibrium volume or height, the foam growth rate will equal zero when the steady state is attained, making the maximum foam volume or height equal to:

$$[F]_{\max} = \frac{v_g}{(1-\varepsilon)k_2^{1st}} \tag{12}$$

where ε is the average liquid fraction of the foam layer in the steady state. Integrating Eq. (11) with the low liquid content assumption ($\varepsilon \approx 0$) gives the first-order foam growth kinetics:

$$[F] = [F]_{\max}(1-e^{-k_2^{1st}t}) \tag{13}$$

Furthermore, Eq. (13) can be recast as:

$$[F] = [F]_{\max}(1-e^{-t/\tau}) \tag{14}$$

where $\tau = 1/k_2$ is the dynamic stability factor of the foam defined by Bikerman [21]. Actually, Eq. (14) is the empirical equation used to describe the froth growth of froth flotation in the literature [9-11, 22]. For the first time, we give a fundamental basis for this empirical equation. That is, the foam growth rate is controlled by the competition between foam formation and foam collapse.

2.1.3 Second-order ‘foam collapse reaction’

In the second-order foam collapse reaction, the foam collapse rate is proportional to the foam volume or height squared, which gives the following foam growth rate:

$$\frac{d[F]}{dt} = \frac{v_g}{1-\varepsilon} - k_2^{2nd}[F]^2 \tag{15}$$

Again, the foam growth rate equals zero when the steady state is attained, and the maximum equilibrium foam volume or height is expressed as:

$$[F]_{\max} = \left[\frac{v_g}{(1-\varepsilon)k_2^{2nd}} \right]^{\frac{1}{2}} \tag{16}$$

2.2. Liquid and gas transport in growing foams

In this section, we combine the foam collapse reaction and hydrodynamic theory of rising foam [23] to simulate the liquid and gas transport in growing foams. Please note that the simulation in this study only applies to the foam system that can attain an equilibrium volume or height.

2.2.1 Assumptions and definitions

Understanding the practical growth of foams is challenging because they are complex systems with interrelated processes such as bubble coalescence within and on top of the foam and foam drainage. Thus, to proceed with the simulation, the following assumptions are made: (1) no bubble coalescence occurs within the foams, and thus, the bubble size remains constant; (2) the foam is one dimensional; (3) the second-order 'foam collapse reaction' applies; (4) all physical-chemical constants are considered to be fixed; and (5) the gas bubbles in the liquid phase instantly achieve steady state, i.e., $[G_1] = const$. Figure 1 shows the schematic diagram of growing foams coupled with foam collapse.

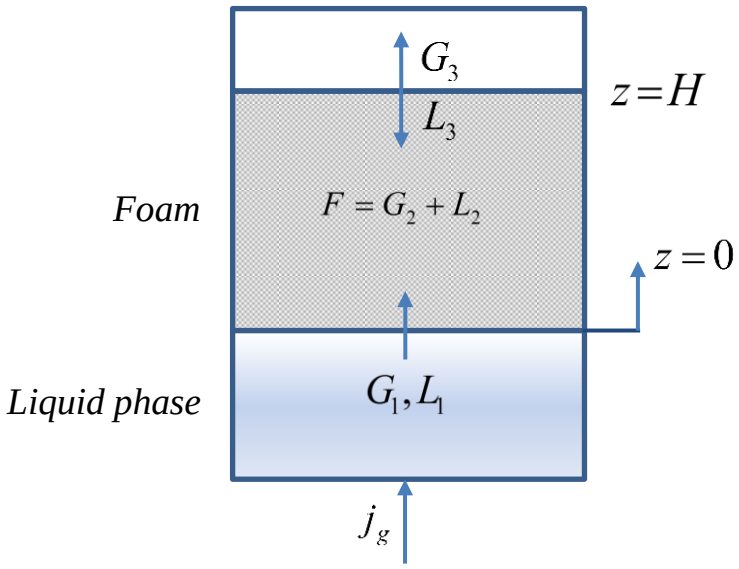

Figure 1. Schematic diagram of a pneumatic foam being generated by bubbling coupled with foam collapse

2.2.2 Mass balance

By referring to Figure 1 and applying the second-order 'foam collapse reaction', we can express the foam height growth rate as follows:

$$\frac{dH}{dt} = \frac{j_g}{1-\varepsilon} - k_2^{2nd} H^2 \tag{17}$$

where H is the foam height at time t. The rate constant k_2^{2nd} in Eq. (15) is expressed as:

$$k_2^{2nd} = \frac{j_g}{H_{\max}{}^2 (1-\varepsilon)} \tag{18}$$

It is widely accepted that the liquid fraction in the foam is spatially variant and decreases to an asymptote within a few centimeters up the foam column [17]. Therefore, the average liquid fraction in the foam also changes with time. By applying the chain rule with the expression of the liquid profile in the foam in [19], the change in the average liquid fraction with time is obtained:

$$\frac{d\varepsilon}{dt} = \frac{d\varepsilon}{dH}\frac{dH}{dt} = \left\{ \frac{p\rho g r_b \varepsilon^{1+q}}{q\sigma} \left[\left(\frac{\varepsilon j_g}{1-\varepsilon} - j_f \right) \frac{\mu}{\rho g r_b{}^2 m \varepsilon^n} - 1 \right] \right\} \times \left[\frac{j_g}{1-\varepsilon} - k_2^{2nd} H^2 \right] \tag{19}$$

The derivation of $\frac{d\varepsilon}{dH}$ is shown in Appendix A.

The following differential equations can be obtained by applying mass balance to the liquid among un-burst bubbles in the foam, L_2, the gas of bubbles in the foam, G_2, the liquid from the bursting bubbles in the foam, L_3, and the gas of bursting bubbles leaving the foam, G_3:

$$\frac{dL_2}{dt} = \varepsilon \frac{dH}{dt} A = \varepsilon \left[\frac{j_g}{1-\varepsilon} - k_2^{2nd} H^2 \right] A \tag{20}$$

$$\frac{dG_2}{dt} = (1-\varepsilon) \frac{dH}{dt} A = (1-\varepsilon) \left[\frac{j_g}{1-\varepsilon} - k_2^{2nd} H^2 \right] A \tag{21}$$

$$\frac{dL_3}{dt} = \varepsilon k_2^{2nd} H^2 A \tag{22}$$

$$\frac{dG_3}{dt} = (1-\varepsilon) k_2^{2nd} H^2 A \tag{23}$$

where A is the cross section of the foam column, which is equal to $7\times10^{-4}\ m^2$, as reported in [17]. Please note that an equation of the mass balance for the bubbling gas is given in [1], which combines Eqs. (21) and (23).

2.2.3 Boundary conditions

At time zero, the following properties equal zero:

$$H = L_2 = G_2 = L_3 = G_3 = 0 \tag{24}$$

The maximum possible liquid fraction defined in [19] is used as the boundary condition:

$$\varepsilon^* = \frac{n-1}{n+1} \tag{25}$$

Please note that the liquid fraction of the foam at the foam-liquid interface was also considered to be 0.26 for the foams with close-packed and mono-dispersed bubbles, and the liquid fraction of the foam at the foam-liquid interface was set as 0.36 for the foams with random and mono-dispersed bubbles [24].

2.3. Foam collapse in standing foam column

The equation for the simulation of foam collapse can be obtained using Eq. (17), with the gas flow rate, j_g, set to zero. Because there is no liquid flux into the standing foam column, the low liquid content assumption, $\varepsilon = 0$, applies. Finally, we arrive at:

$$\left(\frac{dH}{dt}\right)_{burst} = -k_2^{2nd} H^2 \tag{26}$$

Integrating Eq. (26), the equation for foam height vs. time during foam collapse is obtained:

$$\frac{1}{H} = \frac{1}{H_{\max}} + k_2^{2nd} t \tag{27}$$

The half-life of the collapsing foam is:

$$t_{1/2} = \frac{1}{k_2^{2nd} H_{\max}} \tag{28}$$

It should be noted that the foam collapse rate has been expressed as [25]:

$$\frac{dH}{dt} = -k / t \tag{29}$$

Therefore, the foam collapse process can be expressed as:

$$H / H_{\max} = -\alpha \ln\left(t / t_{1/2}\right) + 0.5 \tag{30}$$

where $t_{1/2}$ is the half foam decay time and α is a constant. $t_{1/2}$ can be obtained by fitting the foam or froth collapse data [12, 26]. Here, we note that Eqs. (29) and (30) are simply empirical equations and that there is no fundamental basis for their development. Instead, we propose Eqs. (27) and (28) on the basis of foam collapse kinetics. The half foam decay time, $t_{1/2}$, can also be calculated by Eq. (28).

3. Results and discussion

In this section, we show the interrelation of foam drainage, growth and collapse. The data of forced drainage experiments and the growth and collapse of foams stabilized by 4 ml/l Teepol solution in [17] are used to proceed with the simulation.

3.1. Forced drainage experiments

The liquid superficial drainage rate from a foam, j_d, can be expressed as a Stokes-type number, Sk, as a power-law function of the liquid volumetric fraction, ε [23]:

$$Sk = m\varepsilon^n \tag{31}$$

where m and n are two dimensionless adjustable constants that are dependent on the surfactant type and concentration and can be measured by forced drainage experiments. Sk is expressed as:

$$Sk = \frac{\mu j_d}{\rho g r_b^{\,2}} \tag{32}$$

To obtain the foam drainage parameters m and n, the forced drainage data for a 4 ml/l Teepol solution in [17] were re-plotted in Figure 2 to express the Stokes-type number, Sk, as a power-law function of the liquid volumetric fraction, ε [23].

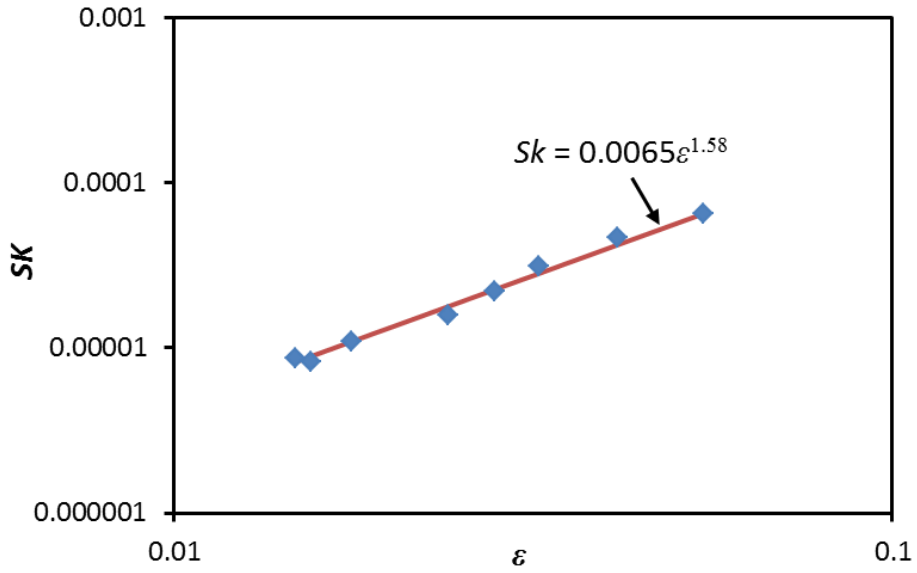

Figure 2. Sk vs. ε re-plotted from a forced drainage experiment on a foam created from a 4 ml/l Teepol solution [17], where $\mu = 1\ cP$, $\rho = 1000\ kg\ m^{-3}$, and $r_b = 1\ mm$, with $Sk = 0.0065\varepsilon^{1.58}$ superimposed on the plot.

The superficial liquid velocity up the column, j_f, can be expressed as [19]:

$$j_f = \frac{\varepsilon j_g}{1-\varepsilon} - j_d = \frac{\varepsilon j_g}{1-\varepsilon} - \frac{\rho g r_b^{\,2}}{\mu} m\varepsilon^n \tag{33}$$

At equilibrium, the following relationships can be established [19]:

$$\frac{dj_f}{d\varepsilon} = 0 \tag{34}$$

$$\frac{\mu j_g}{mn\rho g r_b^{\,2}} = \varepsilon^{n-1}(1-\varepsilon)^2 \tag{35}$$

j_f can be readily solved using Eq. (33) together with Eq. (34), giving $j_f = 1.33\times10^{-10}$, 3.16×10^{-10}, 7.35×10^{-10} and $2.09\times10^{-9} m/s$ at the superficial gas velocities of 8×10^{-5}, 1.1×10^{-4}, 1.5×10^{-4} and $2.2\times10^{-4}\ m/s$, respectively.

3.2. Simulation results

3.2.1 Foam growth

The change in the foam height with time can be simulated by solving Eqs. (17)–(19). Please note that the maximum equilibrium foam height, $H_{\max}$, is required to calculate the rate constant of foam collapse, k_2^{2nd}. The last experimental point in each series of published foam growth data is considered to be $H_{\max}$, giving $H_{\max}$ = 15.46, 21.53, 25.99 and 32.98 cm, at the superficial gas velocities of 8×10^{-5}, 1.1×10^{-4}, 1.5×10^{-4} and $2.2\times10^{-4}\ m/s$, respectively. Please note that the gas velocities we have chosen for this study are well below the transition velocity ($3.8\times10^{-4}\ m/s$) reported in [17]; at this point, the transition from reaching an equilibrium height to indefinite, continuous growth occurs. It should be noted that an expression for the steady-state foam height generated by bubbling nitrogen through high-viscosity solutions has been developed using three dimensionless parameters [16]. Recently, a more general expression for $H_{\max}$ based on the thermo-physical properties of the liquid and gas phases and the operating conditions was given in [27]. Although we did not use those methods to predict the equilibrium foam height $H_{\max}$ in this study, they do provide a possible way to predict the foam column kinetics without previous knowledge of $H_{\max}$.

Figure 3 shows the comparison between the experimental and simulated foam heights of growing foams as a function of time. The good agreement between the experimental data and the simulation results confirms the assumption that the foam collapse rate is proportional to the foam height squared. The bursting bubbles on the top of the foam layer will release the surfactant to the layer immediately below, leading to the accumulation of the surfactant on the top foam layer and a stabilization of the foam as a whole [28]. Therefore, the foam collapse rate is reduced as the foam height decreases. The foam collapse will be discussed in Section 3.2.3.

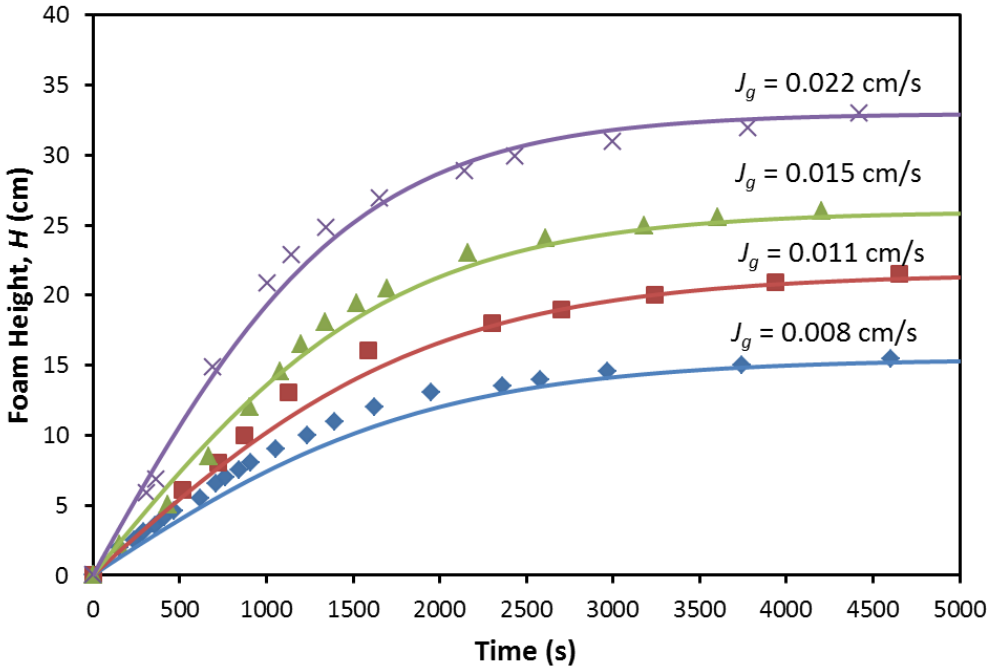

Figure 3. Comparison between experimental (points) and simulated (lines) foam height vs. time for foams created from a 4 ml/l Teepol solution at various gas velocities for $\mu = 1\ cP$, $\rho = 1000\ kg\ m^{-3}$, $r_b = 1\ mm$, $\sigma = 0.031\ N\ m^{-1}$ [29], $g = 9.81\ m\ s^{-2}$, $m = 0.065$, $n = 1.58$, $p = 1.28$, and $q = 0.46$. The experimental points are re-plotted from [17].

3.2.2 Liquid and gas transport in growing foams

Figure 4 shows the simulation results of the average liquid fraction in growing foams by solving Eqs. (17)–(19). Higher gas velocities can be seen to lead to a smaller average liquid content in the foam at a given time, which causes the average liquid fraction to more quickly decrease to its equilibrium value. Because the liquid fraction will decrease to an asymptote within a few centimeters up the foam column [17], foams generated with a higher gas velocity will generate more foam, leading to a smaller average liquid fraction and less time to reach the steady state.

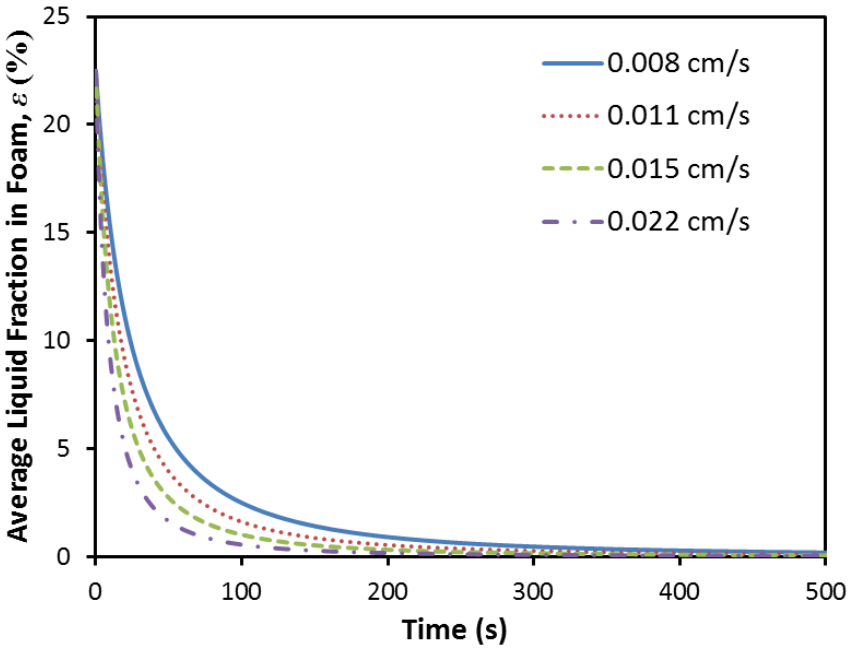

Figure 4. Average liquid fraction, ε, for foams created from a 4 ml/l Teepol solution as a function of time at various gas velocities.

Figures 5 and 6 illustrate the simulation results of liquid volume, L_2, and gas volume, G_2, for the growth foams by solving Eqs. (17)–(21). Although the average liquid fraction decreases as the gas velocity increases, the superficial liquid velocity up the column, j_f, increases with j_g (please see Section 3.1), which increases the liquid volume in the growing foams. The evolution of the gas volume in the growing foams shows the same trend for foam height as in Figure 3.

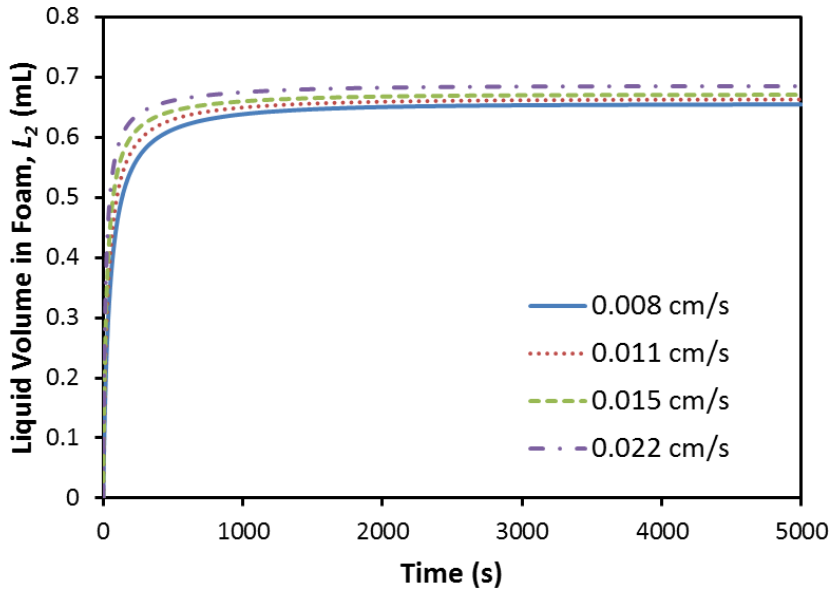

Figure 5. Liquid volume, L_2, in foams created from a 4 ml/l Teepol solution as a function of time at various gas velocities.

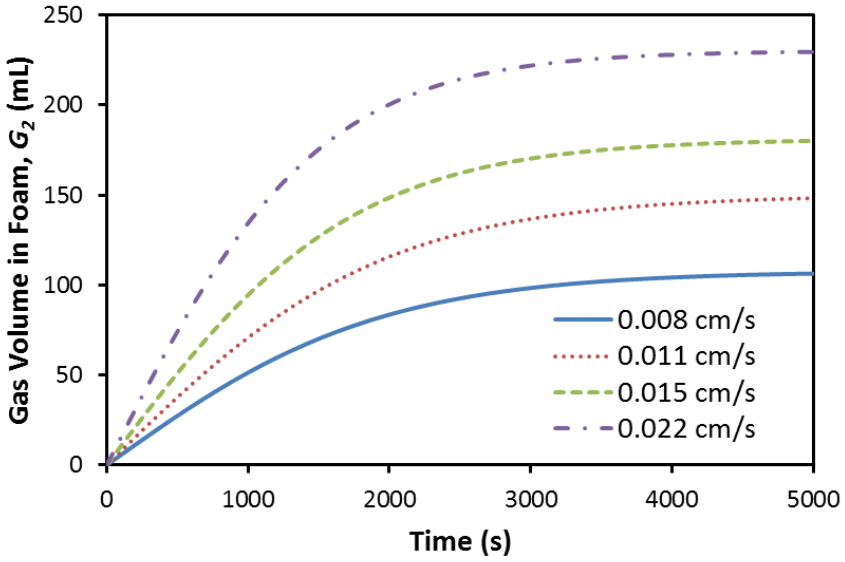

Figure 6. Gas volume, G_2, in foams created from a 4 ml/l Teepol solution as a function of time at various gas velocities.

The simulation results of the volumes of liquid, L_3, and gas, G_3, from bursting bubbles are shown in Figures 7 and 8 by solving Eqs. (17)–(19) and Eqs. (22)–(23), respectively. Unlike the liquid volume in the growing foams, which shows a certain pattern relative to gas velocity, the volume of liquid from bursting bubbles, L_3, does not show any trend as the gas velocity is increased. Based on Eq. (22), we can see that the flow rate of the liquid from bursting bubbles is proportional to the average liquid fraction, ε, and the foam height squared, H^2. Although the average liquid fraction decreases with gas velocity (Figure 4), the foam height increases (Figure 3), which leads to the complex variation of L_3 with gas velocity in Figure 7. Figure 8 shows the volume of gas from bursting bubbles, G_3, as a function of time at various gas velocities. When the foam height reaches the equilibrium value, the slope of each curve in Figure 8 equals the corresponding gas velocity.

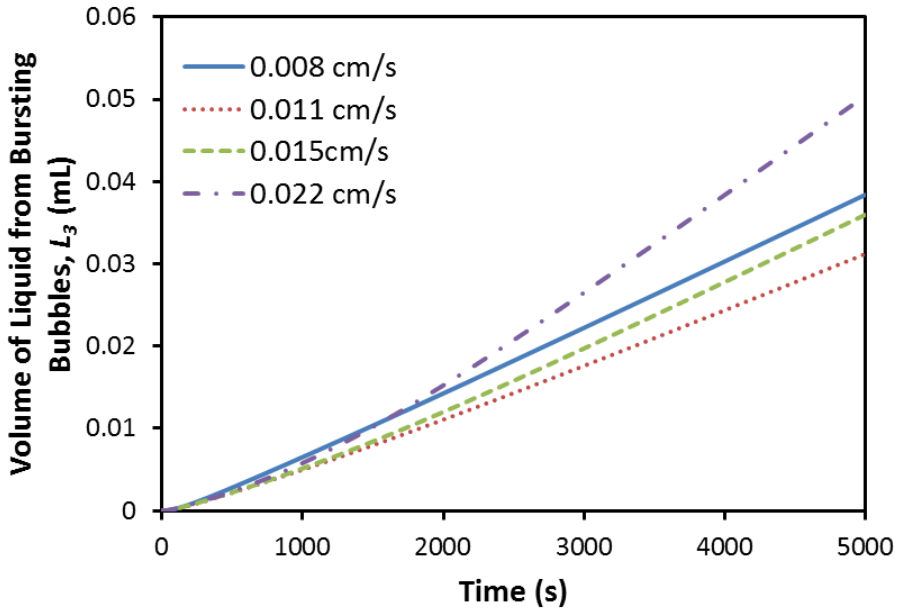

Figure 7. Volume of liquid from bursting bubbles, L_3, of foams created from a 4 ml/l Teepol solution as a function of time at various gas velocities.

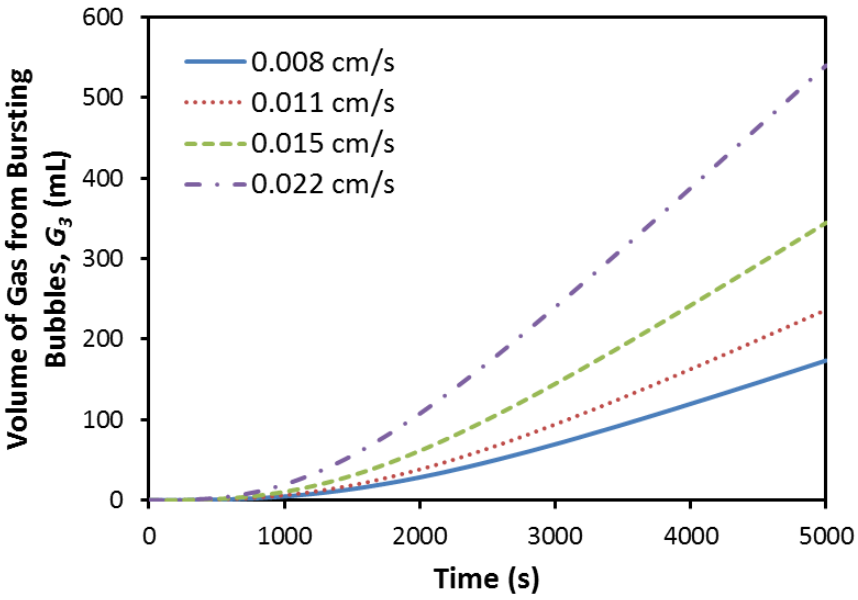

Figure 8. Volume of gas from bursting bubbles, G_3, of foams created from a 4 ml/l Teepol solution as a function of time at various gas velocities.

3.2.3 Foam collapse

Figure 9 shows a comparison between the experimental and simulated foam collapse according to Eq. (27) with the rate constant of foam collapse, k_2^{2nd}, as a fitting parameter. The good agreement between the experimental and simulated results confirms the assumption that the foam collapse rate is proportional to the foam height squared in the development of Eq. (17). Because k_2^{2nd} can be calculated either by Eq. (18) with the assumption of zero liquid fraction or by fitting the foam collapse data using Eq. (27), for comparison, we plot two series of k_2^{2nd} calculated using each method in Figure 10. The difference between the two methods is that Eq. (18) applies to growing foams, whereas Eq. (27) is applicable to standing foams. Figure 10 shows that the value of k_2^{2nd} obtained for growing foams decreases with the gas velocity, whereas the value of k_2^{2nd} calculated by fitting the collapse curves of standing foams remains almost constant (varying between 0.0035–0.0038 $m^{-1}s^{-1}$). The values of k_2^{2nd} calculated from growing foams are smaller than the ones from standing foams. Specifically, the values of k_2^{2nd} calculated by both methods are very close to each other for the foams generated at relatively low gas velocities (e.g., 0.008 cm/s). However, the gap widens as the gas velocity increases. Compared to the standing foams, more growing foams

collapse. Therefore, more surfactant molecules are released from collapsed foams and accumulate on the top of growing foams [28], leading to a relatively stable foam column (i.e., a smaller value of k_2^{2nd}). For this reason, the values of k_2^{2nd} calculated for growing foams are smaller than the ones calculated for standing foams. Higher gas velocities lead to more foam collapse (Figure 8), resulting in a smaller value of k_2^{2nd}, as shown in Figure 10. Finally, smaller gas velocities indicate that the foam collapse behavior (i.e., the value of k_2^{2nd}) is more similar to the behavior in standing foams.

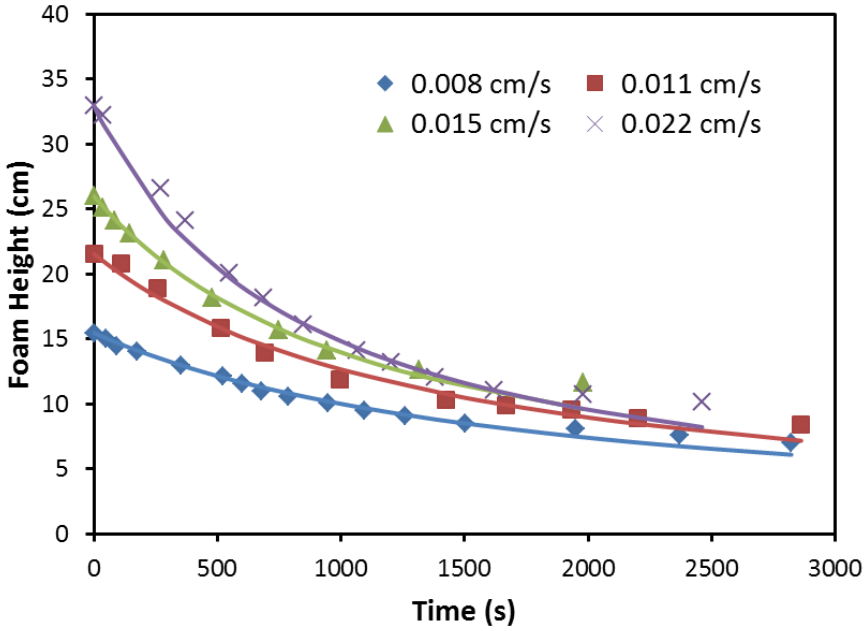

Figure 9. Comparison of experimental (points) and simulated (lines) foam height vs. time according to Eq. (27) for collapsing foams created from a 4 ml/l Teepol solution at various gas velocities. The experimental points are re-plotted from [17].

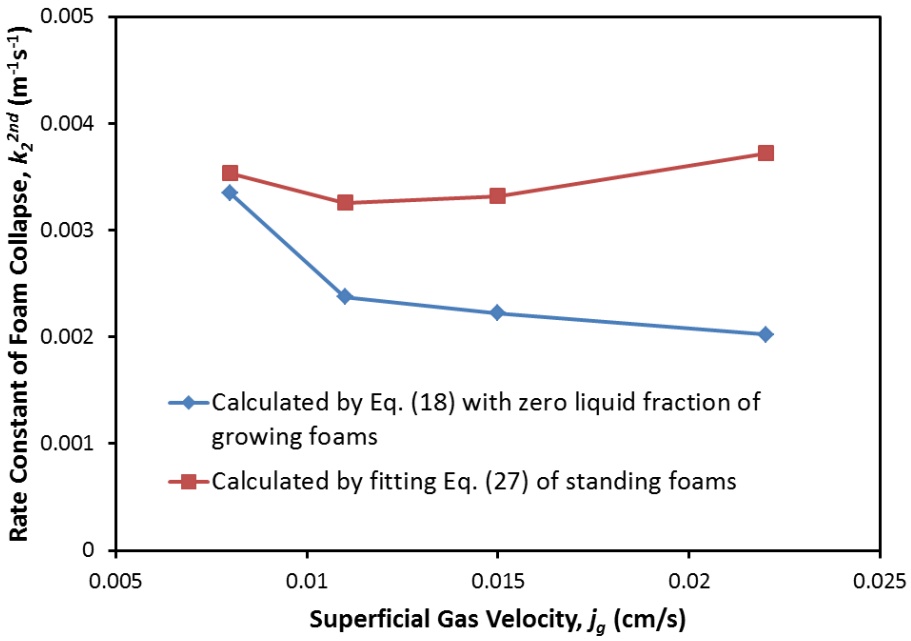

Figure 10. Comparison of the rate constant of foam collapse, k_2^{2nd}, calculated by Eq. (18) with the zero liquid fraction assumption of growing foams and by fitting with Eq. (27) for standing foams at various gas velocities.

4. Conclusions

This chapter has described a model for the foam column kinetics by analogy with reaction kinetics that interrelates the growth, drainage and collapse of foams with a series of mass balance equations (Eqs. (17)–(23)). The growth and collapse of foams and the transport of liquid and gas within the growing foams are predicted. The good agreement between the experimental and simulated results for foam growth and collapse verifies the assumption that the foam collapse follows reaction kinetics. The simulation results show that the average liquid fraction declines with the gas velocity despite an increase in the overall liquid content in the growing foams. The foam collapse constant, k_2^{2nd}, is determined for both growing foams and standing foams. Because of the higher surfactant reflux from the growing foams, the k_2^{2nd} of growing foams is generally smaller than that of standing foams. Finally, higher gas velocities increase the discrepancy between the values of k_2^{2nd} determined for each foam (Figure 10).

Acknowledgements

The authors gratefully acknowledge the China Scholarship Council (CSC) of the Chinese Government and The University of Queensland (UQ) for the CSC-UQ scholarship for JW.

Appendix A

When the liquid fraction is not constant with height, the capillary forces must be considered. Eq. (31) should be modified as [23]:

$$Sk = m\varepsilon^{n}(1+\Pi) \tag{A1}$$

where:

$$\Pi = \frac{q\sigma}{pr_b\rho g\varepsilon^{1+q}}\frac{\partial\varepsilon}{\partial H} \tag{A2}$$

and where σ is the equilibrium surface tension; r_b is the mean bubble diameter; ρ is the interstitial liquid density; g is the acceleration due to gravity; p and q are the dimensional number and index in the equation where the radius of curvature of the Plateau border walls, respectively; and r is expressed as a function of the liquid fraction and bubble radius: $r/r_b = p\varepsilon^{q} = 1.28\varepsilon^{0.46}$. A discussion of the values of p and q can be found in [23]. By modifying Eq. (33) with Eq. (A1), an expression for $d\varepsilon/dH$ is obtained:

$$\frac{d\varepsilon}{dH} = \frac{p\rho g r_b\varepsilon^{1+q}}{q\sigma}\left[\left(\frac{\varepsilon j_g}{1-\varepsilon} - j_f\right)\frac{\mu}{\rho g r_b^{2} m\varepsilon^{n}} - 1\right] \tag{A3}$$

References

[1] A. Bhakta, E. Ruckenstein, Decay of standing foams: drainage, coalescence and collapse, Advances in Colloid and Interface Science, 70 (1997) 1-124.

[2] I. Cantat, S. Cohen-Addad, F. Elias, F. Graner, R. Hohler, O. Pitois, F. Rouyer, A. Saint-jalmes, Foams: Structure and Dynamics, CPI Group (UK) Ltd, Croydon, 2013.

[3] D. Weaire, S. Hutzler, The Physics of Foams, Clarendon Press, Oxford, 1999.

[4] S. Hutzler, D. Weaire, S. Shah, Bubble sorting in a foam under forced drainage, Philosophical Magazine Letters, 80 (2000) 41-48.

[5] S. Hutzler, D. Weaire, Foam coarsening under forced drainage, Philosophical Magazine Letters, 80 (2000) 419-425.

[6] S. Hilgenfeldt, S.A. Koehler, H.A. Stone, Dynamics of Coarsening Foams: Accelerated and Self-Limiting Drainage, Physical Review Letters, 86 (2001) 4704-4707.

[7] A.E. Roth, C.D. Jones, D.J. Durian, Bubble statistics and coarsening dynamics for quasi-two-dimensional foams with increasing liquid content, PHYSICAL REVIEW E, 87 (2013) 042304.

[8] S.-J. Arnaud, L. Dominique, Time evolution of aqueous foams: drainage and coarsening, Journal of Physics: Condensed Matter, 14 (2002) 9397.

[9] N. Barbian, E. Ventura-Medina, J.J. Cilliers, Dynamic froth stability in froth flotation, Minerals Engineering, 16 (2003) 1111-1116.

[10] N. Barbian, K. Hadler, E. Ventura-Medina, J.J. Cilliers, The froth stability column: linking froth stability and flotation performance, Minerals Engineering, 18 (2005) 317-324.

[11] N. Barbian, K. Hadler, J.J. Cilliers, The froth stability column: Measuring froth stability at an industrial scale, Minerals Engineering, 19 (2006) 713-718.

[12] M. Zanin, E. Wightman, S.R. Grano, J.P. Franzidis, Quantifying contributions to froth stability in porphyry copper plants, International Journal of Mineral Processing, 91 (2009) 19-27.

[13] L. Pilon, A. G. Fedorov, R. Viskanta, Analysis of transient thickness of pneumatic foams, Chemical Engineering Science, 57 (2002) 977-990.

[14] P. Hrma, Model for a steady state foam blanket, Journal of Colloid and Interface Science, 134 (1990) 161-168.

[15] J. van der Schaaf, R.G.C. Beerkens, A model for foam formation, stability, and breakdown in glass-melting furnaces, Journal of Colloid and Interface Science, 295 (2006) 218-229.

[16] L. Pilon, A.G. Fedorov, R. Viskanta, Steady-State Thickness of Liquid–Gas Foams, Journal of Colloid and Interface Science, 242 (2001) 425-436.

[17] S.J. Neethling, H.T. Lee, P. Grassia, The growth, drainage and breakdown of foams, Colloids and Surfaces A: Physicochemical and Engineering Aspects, 263 (2005) 184-196.

[18] P. Grassia, S.J. Neethling, C. Cervantes, H.T. Lee, The growth, drainage and bursting of foams, Colloids and Surfaces A: Physicochemical and Engineering Aspects, 274 (2006) 110-124.

[19] P. Stevenson, Hydrodynamic theory of rising foam, Minerals Engineering, 20 (2007) 282-289.

[20] O. Levenspiel, Chemical Reaction Engineering, Industrial & Engineering Chemistry Research, 38 (1999) 4140-4143.

[21] J.J. Bikerman, Foam, Springer-Verlag, New York, 1973.

[22] Z. Aktas, J.J. Cilliers, A.W. Banford, Dynamic froth stability: Particle size, airflow rate and conditioning time effects, International Journal of Mineral Processing, 87 (2008) 65-71.

[23] P. Stevenson, Dimensional analysis of foam drainage, Chemical Engineering Science, 61 (2006) 4503-4510.

[24] S.J. Neethling, H.T. Lee, J.J. Cilliers, The recovery of liquid from flowing foams, Journal of Physics: Condensed Matter, 15 (2003) 1563.

[25] E. Iglesias, J. Anderez, A. Forgiarini, J.-L. Salager, A new method to estimate the stability of short-life foams, Colloids and Surfaces A: Physicochemical and Engineering Aspects, 98 (1995) 167-174.

[26] A. Bhakta, E. Ruckenstein, Modeling of the Generation and Collapse of Aqueous Foams, Langmuir, 12 (1996) 3089-3099.
[27] J.A. Attia, S. Kholi, L. Pilon, Scaling laws in steady-state aqueous foams including Ostwald ripening, Colloids and Surfaces A: Physicochemical and Engineering Aspects, 436 (2013) 1000-1006.
[28] S.S. Dukhin, V.I. Kovalchuk, E.V. Aksenenko, R. Miller, Surfactant accumulation within the top foam layer due to rupture of external foam films, Advances in Colloid and Interface Science, 137 (2008) 45-56.
[29] F. Confer, N. Fulcher, D. Charles, K. Ruschak, M. Antoniades, S. Weinstein, A cylindrical weir for the application of surfactants to coating process, International Coating Science and Technology Symposium, Atlanta, Georgia, 2012.

Chapter 4: Foamability of Sodium Dodecyl Sulfate Solutions: Anomalous Effect of Dodecanol Unexplained by Conventional Theories

Jianlong Wang[1], Anh V Nguyen[1*] and Saeed Farrokhpay[2]
[1]School of Chemical Engineering, University of Queensland, Brisbane, Queensland 4072, Australia
[2]JKMRC, University of Queensland, Brisbane, Queensland 4072, Australia

[*]Correspondence: anh.nguyen@eng.uq.edu.au

Highlights:

- Dual effects of DOH on foam stabilization and depression of pre-CMC SDS-DOH solutions were found.
- Decreased bubble surface potential and antifoam efficacy of DOH explain the decreased foamability of pre-CMC SDS-DOH solutions.
- A kinetic model was developed to simulate foam growth.

Graphical abstract:

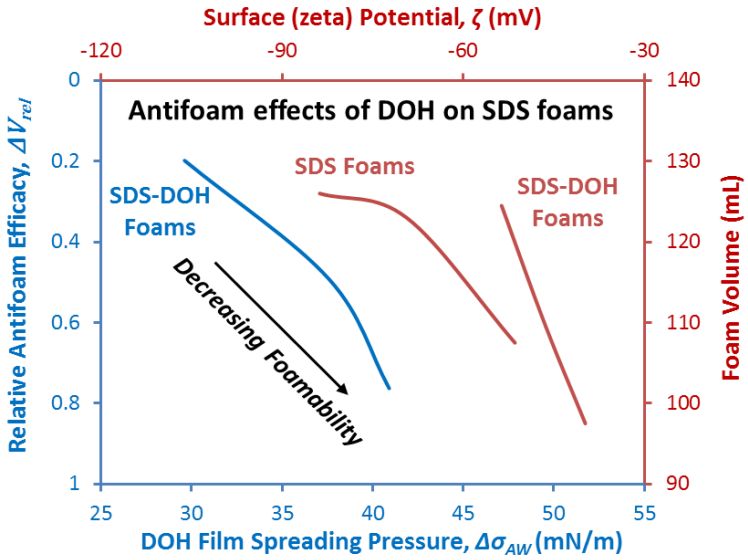

Abstract

Conventional theories indicate that surfactant solutions with low equilibrium surface tension, fast adsorption kinetics and high interfacial viscoelasticity increase foamability. These theories are applicable to single surfactants of pre-CMC. Here, we examine whether these theories are applicable for surfactant mixtures. Specifically, we investigated the foamability of sodium dodecyl sulfate (SDS)-dodecanol (DOH) solutions. We found that the foamability of SDS-DOH solutions exhibited 'anomalies' that were unexplained by conventional theories. The remarkable decrease in the foamability of SDS solutions caused by the addition of DOH could not be easily explained by the theories of surface tension and surface viscoelasticity. Instead, we proposed alternative mechanisms to resolve these unexpected results. Below the DOH solubility limit, the displacement of SDS molecules by DOH molecules at the air-water interface results in a reduced surface potential, leading to a lower foamability. The antifoam effects of DOH droplets can account for the reduced foamability above this limit. We also developed a foam growth kinetic model to simulate the experimental results and interpret the antifoam effects of DOH. This chapter highlights the complexity of the foamability of surfactant blends.

Keywords: foam, foamability, SDS, dynamic surface tension, surface viscoelasticity, antifoam

1. Introduction

Foamability and foam stability are two of the most common types of foam properties. The foamability of a solution is a measure of its capacity to produce a foam [1], whereas the foam stability is the lifetime of a foam. To generate foams, surfactant must be present in the solution. The addition of surfactants increases the liquid (foam) film stability and alters the interfacial properties of the air-liquid interface, such as the static surface tension, dynamic surface tension and surface viscoelasticity, which are crucially important for foamability. Unlike surfactants, antifoams prevent foam formation. As a rule of thumb, solutions with low equilibrium surface tension, fast adsorption dynamics and high surface viscoelasticity are considered to be good foaming solutions [2-4]. However, foam properties are determined by many interrelated factors that can interact and produce synergistic or antagonistic effects. Therefore, a single interfacial property is often inadequate to dominate foam properties, particularly for complex foaming systems such as surfactant mixtures.

As an example, we chose anionic (SDS) and non-ionic (DOH) surfactant mixtures. It is to note that DOH is the most frequent contaminant of SDS and it is very difficult to remove

DOH from SDS due to the hydrolysis of SDS in aqueous solution [5-9]. When the SDS is studied, attention should also be paid to the criteria of purity of SDS solutions and the concept of 'surface chemical purity' [10-13]. It should be noted that the effect of DOH on the micellar stability of SDS solutions has been studied and correlated with foam properties [14]. The decreased foamability of SDS (25 to 200 mM) micellar solutions is attributed to the greater stability of SDS-DOH micelles relative to SDS micelles, which reduce the rate of micelle collapse and consequently decreases the rate of SDS molecules being transported to the air-water interface. Although the mechanisms controlling the foamability of SDS-DOH mixtures at SDS concentrations above the CMC has been well explained, we can ask the following question: What mechanisms are active below the CMC?

In this chapter, we study the foam properties of SDS-DOH surfactant mixtures (with SDS concentrations ranging from 0.5 to 2.0 mM, which are clearly below the CMC of 8.0 mM) and correlate them with interfacial properties. First, we introduce the existing theories relating to the foam properties of surfactant solutions. Then, we develop a kinetic model to simulate the foam growth process. Subsequently, we measure the foam properties and relevant interfacial properties and uncover some 'anomalies' to illustrate the limitations of conventional theories. We also apply the model to simulate the foam growth data. Finally, we propose two mechanisms to rationalize the unexpected foam properties of surfactant mixtures.

2. Theory

2.1 Interfacial properties and foamability

2.1.1 Equilibrium surface tension

Equilibrium (static) surface tension determines the foamability through two factors: surface energy and bubble breakup. The surface energy of the foam system, E, is defined as:

$$E = \sigma A \tag{1}$$

where σ is the surface tension and A is the interfacial area of the foam. The surface energy increases as the foam creation increases. Therefore, if E is constant, a lower value of σ will give a larger value of A, which indicates relatively high foamability. Bubble breakup is the very first step of foam generation. Based on the theory of bubble or drop breakup in turbulent flows [15-17], the dimensionless number known as the Weber number is established:

$$We = \frac{\rho u^2 d}{\sigma} \tag{2}$$

where ρ is the density of the foaming solution and u^2 is the mean square velocity difference over a distance d, which is the bubble diameter. This value reflects the balance between the viscous forces that tend to deform the bubbles and the interfacial forces that tend to maintain their spherical shape. The Weber number indicates that bubble breakup is determined by both process parameters, such as rotational speed, and interfacial properties, such as surface tension. If an equilibrium is established between bubble coalescence and breakup, then the critical Weber number, We_c, is reached. In this case, lower values of σ give smaller bubble sizes, d, again indicating relatively high foamability.

2.1.2 Dynamics of adsorption

The surface tension term appears in both Eqs. (1) and (2), which describe surface energy and bubble breakup, respectively. However, it is not well defined or theoretically justified [15-17]. The following question, then, must be raised: What type of surface tension should be applied in these equations? To answer this question, we must first note that the equilibrium surface tension is not reached instantaneously. The evolution of the surface tension value is controlled by two processes: (i) the diffusion of surfactant molecules to the surface and (ii) the adsorption of surfactant molecules on the interface, which must overcome an associated energy barrier. Either of these processes may become the rate-determining step. Second, although we do not know the exact value, a rational choice of an adsorption reference time is the average lifetime of the bubbles at the solution/air interface during foam generation [18]. Therefore, if the adsorption dynamics is sufficiently fast, we can apply the equilibrium surface tension. Otherwise, the dynamic surface tension that is relevant to the time scale of foam generation should be used.

2.1.3 Surface viscoelasticity

The adsorption of surfactants on the air-water interface forms an adsorbed layer, which gives rise to interfacial viscoelasticity. Two types of interfacial rheology have been observed—interfacial shear rheology and dilational rheology—which characterize the response of the surface to shear stress and to extensional stress, respectively. In this study, we only focus on the effects of dilational viscoelasticity on foamability [19]. The surface

dilational modulus, ε, is defined as the ratio of the surface tension change, $d\gamma$, to the area change, dA/A, under dilational deformation:

$$\varepsilon = \frac{d\sigma}{d\ln A} \tag{3}$$

In practice, the surface dilational modulus is expressed as two parts: (i) the surface dilational elasticity, ε', which measures the capacity of the air-water interface to resist a dilational deformation, and (ii) surface dilational viscosity, ε'', which measures the speed of the relaxation processes restoring the equilibrium after the disturbance. During a harmonic deformation, if the change in the surface area is sufficiently small, then the induced surface tension oscillations will be sinusoidal and the surface viscoelastic modulus, ε, can be expressed as a complex number [19]:

$$\varepsilon = |\varepsilon| e^{i\phi} = A_0 \frac{\Delta\sigma}{\Delta A}\cos\phi + iA_0 \frac{\Delta\sigma}{\Delta A}\sin\phi \tag{4}$$

where ϕ, $|\varepsilon|$, A_0, $\Delta\sigma$ and ΔA are the phase shift between the surface tension and area oscillations, the surface dilational modulus, the mean area, and the amplitudes of the surface tension and the surface area variation, respectively (Figure 1). It should be noted that the phase shift between the surface tension and area is caused by the diffusion of surfactant molecules from the bulk or air-water interface to the stretched area. We can calculate the surface dilational elasticity by $\varepsilon' = A_0 \frac{\Delta\sigma}{\Delta A}\cos\phi$ and the surface dilational viscosity by $\varepsilon'' = \frac{A_0}{\omega}\frac{\Delta\sigma}{\Delta A}\sin\phi$, where ω is the angular frequency of oscillation.

The total harmonic distortion (THD), which estimates the deviation from linear behavior, is used as an estimation of measurement accuracy. It is defined as the ratio of the higher harmonics amplitude to the amplitude at the measured basic frequency [19]:

$$THD = \frac{\sqrt{\sum_{k=2}^{n} a_k^{\,2}}}{a_1} \tag{5}$$

where a_1 is the amplitude value of the basic frequency and a_2, a_3, …, a_n are amplitudes of the higher harmonics. In this work, the THD values are below 10% in most cases.

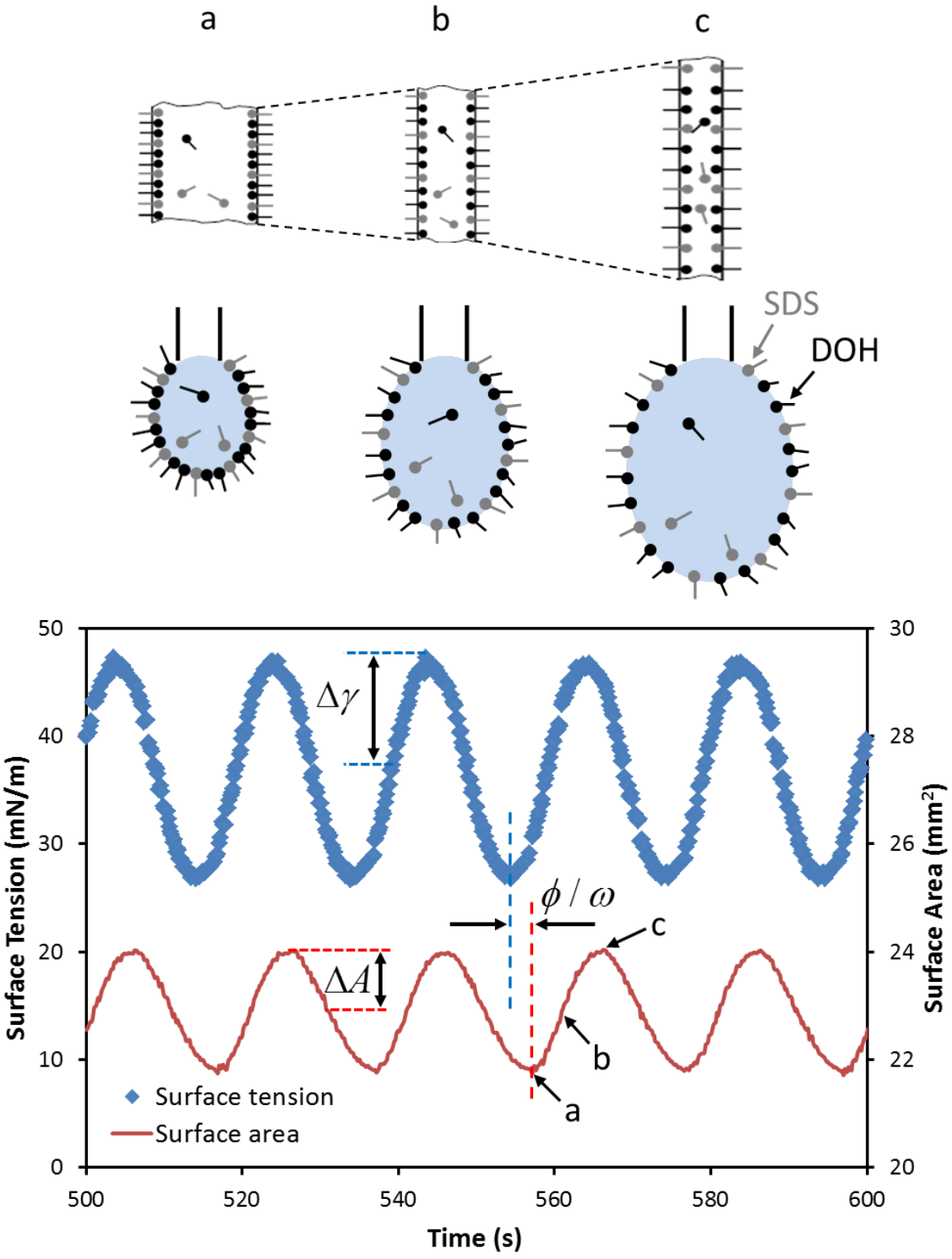

Figure 1. Schematic presentation of the thinning of a liquid film by stretching (top, reproduced from [20]). Expansion of a droplet in our experiments to simulate liquid film thinning (middle). Experimental results for a transient change in the surface tension and surface area of a SDS (0.5 mM)-DOH (5 mg/L) droplet oscillated at the frequency of 0.05 Hz (bottom). Amplitudes of surface tension and area, with a clear phase shift between the surface tension and surface area changes.

Oscillatory area experiments were conducted to simulate liquid film thinning (Figure 1). Assuming that the surface area of the film elements increases while its volume and the total amount of the surfactants remain constant and that the diffusion of surfactant molecules can be ignored, the surface concentration of surfactant molecules decreases during liquid film thinning. The reduction in the surface concentration induces a local increase in surface tension, which in turn resists the stretching of the liquid film and foam film drainage; consequently, the bubble coalescence rate decreases. High values of surface viscoelasticity can potentially lead to the suppression of marginal regeneration and a reduced rate of foam film drainage, which enhance foam stability and foamability.

2.2 Surface forces and foamability

When two bubbles meet, surface forces act on the two interfaces separated by the thickness of the liquid. The disjoining pressure, Π_d , was defined to characterize the forces per unit area between these two interfaces. Figure 2 illustrates the electrostatic, van der Waals, and steric contributions to the disjoining pressure in a film:

$$\Pi_d = \Pi_{dl} + \Pi_{van} + \Pi_{steric} \tag{6}$$

To enable the existence of a stable film, repulsive forces, such as the electrostatic force, must act between the interfaces. In this case, a positive disjoining pressure is induced in the film to counterbalance the attractive interactions that tend to rupture the liquid film. Therefore, a strong repulsive interaction between the interfaces in a liquid film enhances foam stability and foamability.

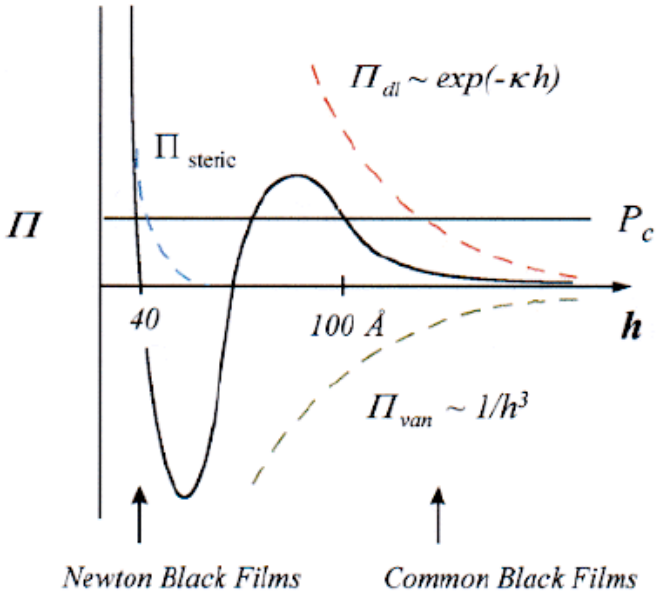

Figure 2. Schematic representation of a disjoining pressure isotherm that includes contributions from Π_{dl}, Π_{van} and Π_{steric}, reprinted from [21].

2.3 Antifoam and foamability

The entry of antifoams to the liquid film is required to destroy a liquid film or a foam layer. The entry barrier is defined as the critical pressure that leads to rupture of the asymmetric oil-water-air film and entry of the drop at the water-air interface [22]. Antifoams with low entry barriers completely collapse the foam in seconds, whereas antifoams with high entry barriers require hours to destroy the foam. The entry barrier has been found to increase with the surfactant concentration [22]. Once entering the foam film, antifoams destabilize the liquid film either by spreading the solution/gas interface or by bridging the two interfaces of the film, depending on the sign of the spreading coefficient, S_r, which is defined as follows [23]:

$$S_r = \sigma_{sg} - \sigma_{sa} - \sigma_{ga} \tag{7}$$

where σ_{sg}, σ_{sa} and σ_{ga} are the surface tension of the gas/antifoam interface, the solution/antifoam interface and the solution/gas interface, respectively. The conditions for spreading and bridging are $S_r > 0$ and $S_r < 0$, respectively [24]. The spreading pressure, $\Delta\sigma_{AW}$, is defined as the reduction in the equilibrium surface tension of the air-water interface caused by the addition of antifoam to the aqueous surface [25]:

$$\Delta\sigma_{AW} = \sigma^i - \sigma^f \tag{8}$$

where σ^f and σ^i are equilibrium surface tensions of surfactant solutions with and without antifoams, respectively. A positive value of $\Delta\sigma_{AW}$ indicates that it is thermodynamically favorable for antifoams to spread on the surface of the surfactant solution. For duplex antifoam films, the spreading pressure, $\Delta\sigma_{AW}$, equals the spreading coefficient, S_r [25, 26]:

$$\Delta\sigma_{AW} = \sigma^i - \sigma^f = \sigma_{sg} - (\sigma_{sa} + \sigma_{ga}) = S_r \tag{9}$$

In this study, the antifoam effect of DOH droplets is correlated with the spreading pressure, $\Delta\sigma_{AW}$, which is applied in more general situations.

3. Foam growth kinetics

Figure 3 shows a schematic diagram of foam growth process in a foam column. We assume that the foam growth kinetics is controlled by two simultaneous processes: (1) foam formation and (2) foam collapse. It should be noted that no foam overflows the foam column.

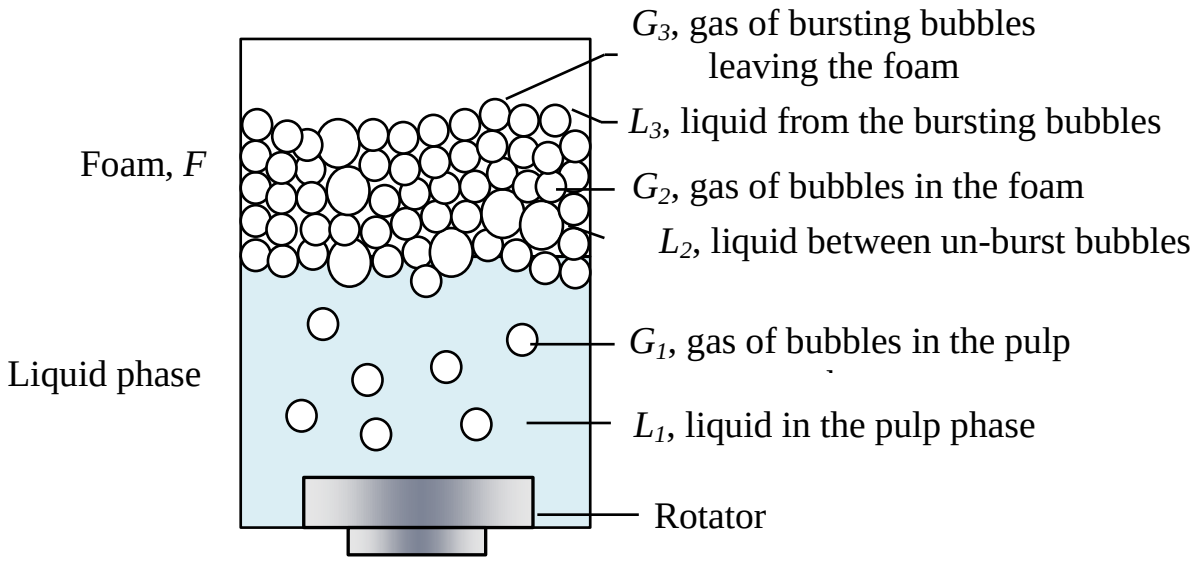

Figure 3. Schematic diagram of the foam growth process

The conservation balance for the gas phase gives:

$$G = G_1 + G_2 + G_3 \tag{10}$$

where G , G_1, G_2 and G_3 are the amounts of gas entering the foam column during agitating, gas of the bubbles in the pulp phase, gas of the bubbles in the foam and gas of the bursting bubbles leaving the foam, respectively. Here, the first assumption we make is as follows: (1) the gas in the pulp phase instantly attains the steady state, i.e., $[G_1] = const$, where the brackets indicate the volume quantity. Likewise, the conservation balance for the liquid is described by:

$$L = L_1 + L_2 + L_3 \tag{11}$$

where L , L_1, L_2 and L_3 are the total amount of liquid in the system, the liquid in the pulp phase, the liquid between un-burst bubbles in the foam and the liquid from the bursting bubbles, respectively. The second assumption is as follows: (2) the amounts of liquid between the un-burst bubbles and from the bursting bubbles are infinitesimally small relative to the amount of liquid in the pulp phase, i.e., $[L_1] = const$.

Foam growth kinetics can be described schematically and analogously as two series-parallel first-order “reactions” as follows:

$$L_1 + G_1 \xrightarrow{k_1} F \tag{12}$$

$$F \xrightarrow{k_2} L_3 + G_3 \tag{13}$$

where $F = L_2 + G_2$ is the foam and k_1 and k_2 are the foam formation and foam decay constants, respectively. Eq. (12) is relevant to the foam formation process, whereas Eq. (13) relates to the foam decay process. By applying the conservation balances in the foam volume and considering the two aforementioned assumptions, the foam kinetics in the foam column can be described analogously to a first-order chemical reactions as follows [27]:

$$\frac{d[F]}{dt} = k_1[L_1][G_1] - k_2[F] \tag{14}$$

Integrating Eq. (14) gives:

$$[F] = V_{\max}(1 - e^{-k_2 t}) \tag{15}$$

where $V_{max} = k_1[L_1][G_1]/k_2$ is the largest value of the foam volume that can be obtained under the experimental conditions. Furthermore, Eq. (15) can be recast as follows:

$$[F] = V_{max}(1 - e^{-t/\tau}) \quad (16)$$

where $\tau = 1/k_2$ is the dynamic stability factor of the foam defined by Bikerman [28]. Actually, Eq. (16) is the empirical equation used to simulate the froth growth process in the literature [29-32]. However, for the first time, we give a fundamental basis to this empirical equation. That is, the foam growth rate is controlled by the competition between the foam formation and foam decay, which are quantitatively described by k_1 and k_2, respectively (Eq. (14)).

4. Experimental

4.1. Materials

Both sodium dodecyl sulfate (SDS) and 1-dodecanol (DOH) were purchased from Sigma-Aldrich (Castle Hill, NSW, Australia) with purities of 99% and 98%, respectively. All chemicals were used as received. The solubility of DOH in water at 29.5°C is 0.04 wt% (4 mg/L), and the freezing point is 24°C [33]. All solutions were prepared using Milli-Q water (surface tension: 71.97 mN/m at 25°C; resistivity: 18.2 MΩcm at 25°C) [34]. A 10 mg/L DOH stock solution was prepared by ultrasonication in an ultrasonic bath for 15 min at a controlled temperature of 25°C. SDS-DOH mixtures were prepared by diluting the stock solution to the desired concentrations. The SDS-DOH solutions displayed a reduced surface activity over time because of the separation and consequent evaporation of DOH [35]. Therefore, only freshly prepared solutions were used in this study.

4.2. Foaming experiments

The foam tester device shown in Figure 4 was used to determine the foamability of the solutions. The device consists of (1) a 1.5 L glass cylinder used to hold the solution and the created foam, (2) a standard Rushton turbine agitator with baffles for creating foam by stirring the solution at a constant rotational speed, and (3) a sensor system with vertically mounted needle electrodes (Foam Tester R-2000, SITA Messtechnik, Germany) that can automatically move up and down to detect the foam surface. The sensor needles were obtained from SITA Messtechnik and permit accurate measurements of the foam volume with uneven foam surfaces in the presence of foam bubbles. The sensor system is connected

to a computer and controlled by a software program developed by SITA Messtechnik. The software also calculates the foam volume from the sensor positions. The device can reproducibly generate foams by stirring the solution at a constant rotational speed and stirring time and can automatically measure the foam volume at different times during foam generation. The sample volume was kept constant at 300 mL. Foams were generated by stirring the solution at 500 rpm and stopping every 10 seconds so that the sensor unit could measure the foam volume, which required approximately 9 seconds. For each solution, the experiments were repeated, and averaged results were obtained. The room temperature was kept constant at 25°C. The relative humidity of the room was also kept constant (50–60%).

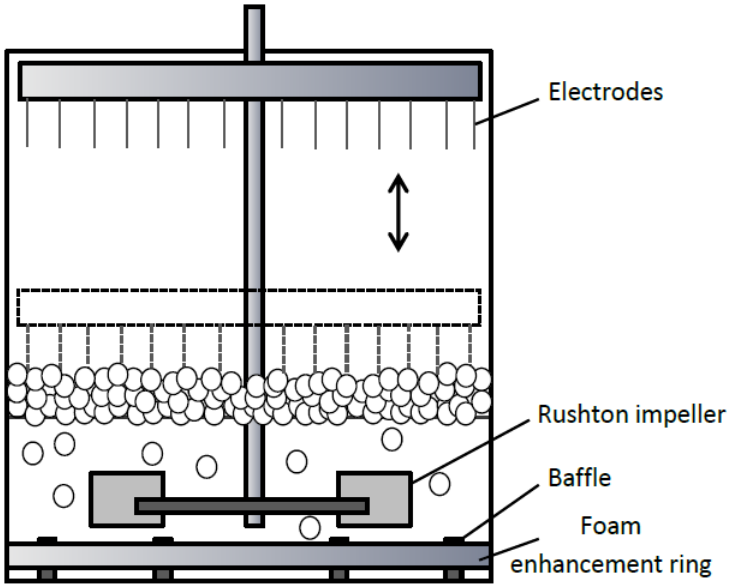

Figure 4. Schematic diagram of the experimental setup used to create the foam by stirring using Ruston impellers with baffles and to measure the transient foam volume from the transient electrical contact between the top foam surface and a SITA Messtechnik sensor system with vertically mounted needle electrodes, which can automatically move up and down to detect the foam surface.

4.3. Measurements of static (equilibrium) surface tension

The surface tension of SDS-DOH solutions was measured by the Wilhelmy plate method [36] using a platinum rectangular thin plate. The plate was connected to a sensitive force balance. All measurements were conducted at a temperature of 25°C. The surface tension of deionized water at the temperature reported in the literature was used to calibrate the surface tension measurements.

4.4. Measurements of dynamic surface tension and surface viscoelasticity

Measurements of dynamic surface tension and surface viscoelasticity were performed by a drop profile analysis tensiometer (PAT-1, SINTERFACE Technologies, Germany). The surface tension is determined from the shape of the pendant drop, and the active control loop of this instrument allows long-duration experiments with a constant drop volume or area. The solution drop was subjected to harmonic oscillations at a frequency of 0.05 Hz with oscillation amplitudes of 5–6% to measure the surface viscoelasticity. The room temperature was kept constant at 25°C. We used a drop formed at a steel capillary with a tip diameter of 1 mm by supplying the solution through an external tube. The drop shape was recorded at different times and fitted with the Young-Laplace equation to obtain the dynamic surface tension and surface elasticity and viscosity. The principles of this methodology are described in detail in the literature [37, 38].

4.5. Measurements of surface (zeta) potential of air bubbles in surfactant solutions

The zeta potential of micro air bubbles was measured by a Microelectrophoresis Apparatus Mk II (Rank Brothers Ltd, Cambridge, England). The equipment configuration and measurement procedures are described in detail elsewhere [39]. In each solution, more than 40 microbubbles were measured to obtain mean values of the bubble zeta potential and standard error. The room temperature was kept constant at 25°C.

5. Results and discussion

5.1. Foam growth

Figure 5 shows a comparison between the experimental foam growth data and the simulated data. At relatively low SDS concentrations (e.g., 0.5 mM), the effect of DOH on the foam growth of SDS foams is prominent: foam growth slows as the DOH concentration increases. However, the effect of DOH becomes weaker as the SDS concentration increased, and this weakening was especially obvious at the highest SDS concentration (i.e., 2.0 mM), for which the addition of DOH has essentially no impact on the foam growth. Although the addition of DOH reduces the foam growth of SDS solutions, the maximum equilibrium foam volume is higher for SDS solutions containing 10 mg/L of DOH than for the solutions containing no DOH.

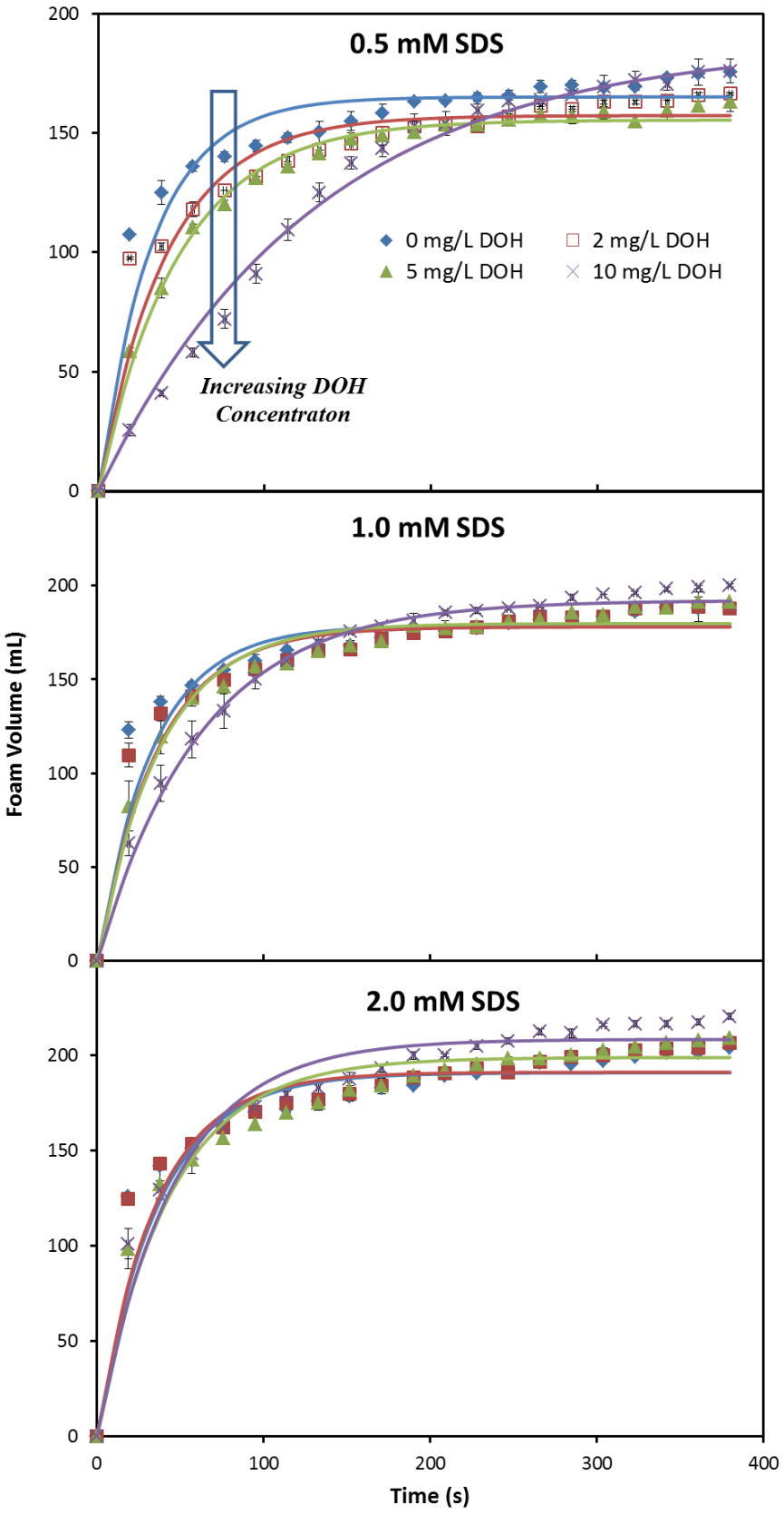

Figure 5. Experimental (points) and theoretical (lines) foam growth data of SDS-DOH solutions simulated by Eq. (16). The error bars show the standard errors of the mean.

The dynamic stability factor, τ , in Eq. (16), which corresponds to the simulated results in Figure 5, is presented in Figure 6. This figure shows that the dynamic stability factor increases as the DOH concentration increases. Notably, τ decreases as the SDS concentration increases at the highest DOH concentration (10 mg/L), which contradicts the observation that foam stability is usually proportional to the surfactant concentration below the CMC. Figure 7 shows the changes in the initial foam volume with various surfactant concentrations. The initial foam volume decreases as the DOH concentration increases but rises as the SDS concentration increases. The foam growth results demonstrate to the curious effect of DOH on SDS foam behaviors, which suggest that DOH acts as both a foam stabilizer and a foam depressant.

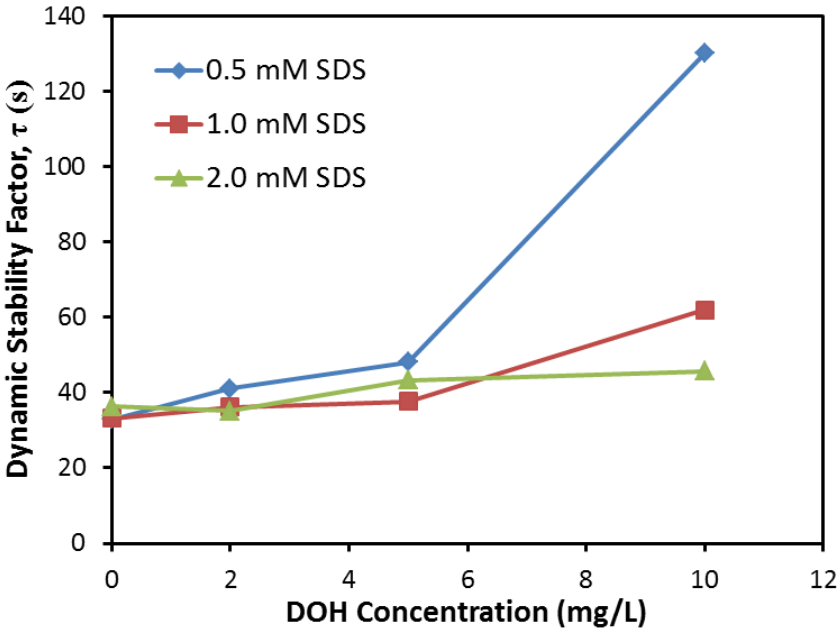

Figure 6. Dynamic stability factor, τ , as a function of reagent concentration. The lines are intended to act solely as visual guides.

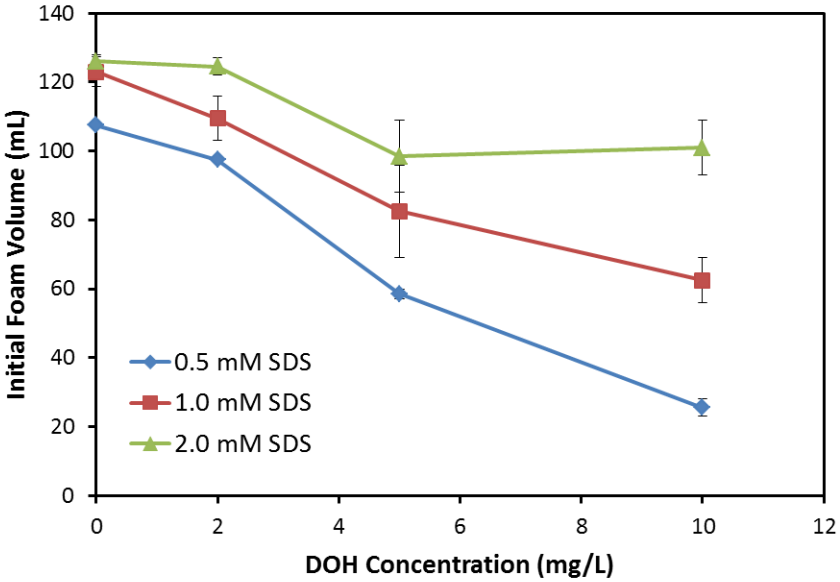

Figure 7. Initial foam volume (second experimental point in each curve in Figure 5) as a function of surfactant concentration. The lines are intended to act solely as visual guides.

5.2. Adsorption dynamics and surface viscoelasticity

As mentioned in Section 2.1.2, a rational choice of an adsorption reference time is the average lifetime of the bubbles at the solution/air interface during foam generation [18]. Usually, the characteristic surface ages during foam generation are in the range of 0.1–1 s [40]. Figure 8 presents the dynamic surface tension data of a 1.0 mM SDS-10 mg/L (5.3×10^{-5} mol/L) DOH solution from 0.1 s to 1500 s by combining the data from [41] with the data collected in our study. This figure shows that the adsorption of SDS attains equilibrium before the adsorption of DOH begins, indicating that SDS and DOH adsorb in different time domains [41]. It should be noted that DOH has been reported to increase the dynamic surface tension of SDS solutions at concentrations (e.g., 15 mM) above the CMC (i.e., 8 mM) within the lifetime of a bubble smaller than 0.15 s because the SDS-DOH micelles are stable compared with the SDS micelles; this effect decreases the rate of transport of the SDS molecules to the air-water interface [14]. Therefore, DOH acts as a foam booster when gentle foam generation methods, such as bubbling, are used but can also act as a foam depressant when more intense methods, such as shaking and agitating, are applied, depending on the rate of foam generation [14]. The dynamic surface tension results shown in Figure 8, however, reveal that the decreased foamability of SDS-DOH mixtures at SDS concentrations below the CMC (i.e., 0.5–2.0 mM) compared with the SDS alone cannot be explained by the increased dynamic surface tension at low surface age (0.1-1 s). Therefore, the mechanisms

that control the foamability of SDS-DOH mixtures at the SDS concentration above and below the CMC are entirely different.

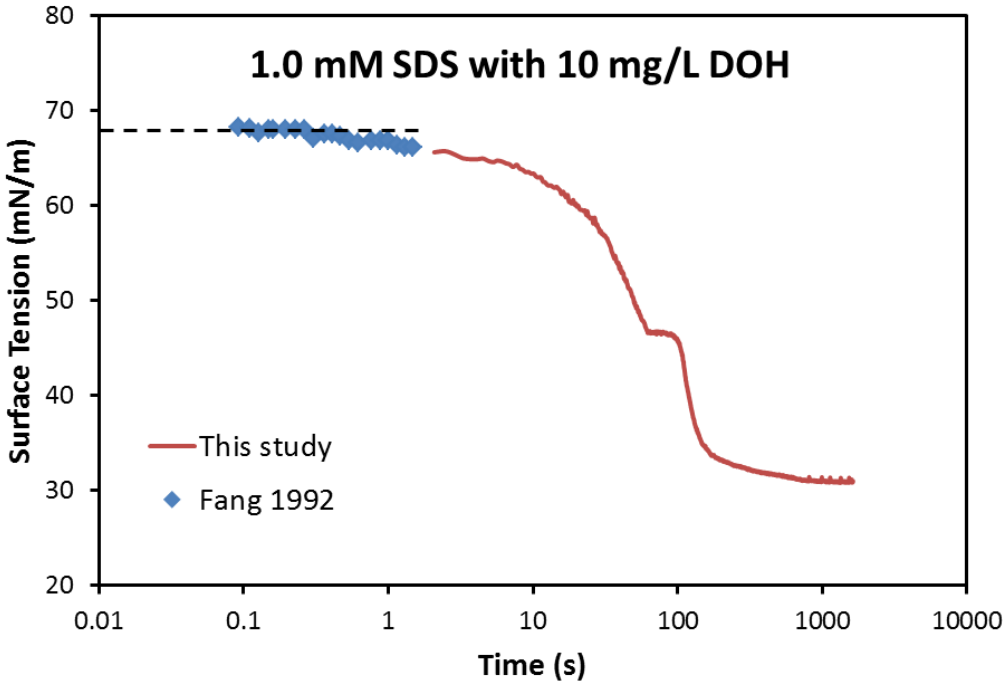

Figure 8. Dynamic surface tension of a 1.0 mM SDS-10 mg/L (5.3×10^{-5} mol/L) DOH solution measured by the inclined plate method (diamond), replotted from [41], and the pendant drop method (solid line). The dashed line indicates the equilibrium surface of 1.0 mM SDS solutions, $\sigma_{eq}^{SDS} = 68.0$ mN/m [41].

Figure 9 compares the dynamic surface pressure with the dynamic surface viscoelasticity (0.05 Hz) of SDS-DOH solutions to determine the transition of the adsorption layer from a liquid-like layer to a solid-like layer with surface age. It should be noted that the surface viscoelasticity was measured at a relatively low frequency (i.e., 0.05 Hz). Therefore, the measurements do not accurately represent the surface viscoelasticity relevant to foam generation when the surface age is 0.1–1 s. The surface viscoelasticity measurements of SDS-DOH mixtures at high frequency (e.g., 1–500 Hz) have been reported [42] and show that the addition of DOH also dramatically increases the surface viscoelasticity of SDS solutions at relatively high frequencies. Nevertheless, our results at low frequency can be correlated with the foam stability quantified according to the dynamic stability factor in Figure 6. Foam stability is controlled by foam drainage, followed by film rupture (coalescence) and Ostwald ripening (coarsening). Film rupture occurs very rapidly and is controlled by the surface

viscoelasticity at high frequency. However, coarsening is slow [43]; therefore, the measurements at low frequency in our study are relevant. Surface pressure graphs in Figure 9 show that the value of the surface pressure remains constant with the addition of DOH for the first few seconds and subsequently begins to increase gradually because of the different time scales of SDS and DOH adsorption. Surface elasticity and viscosity graphs indicate that the addition of DOH strongly increases the rheological properties of the air-water interface of SDS solutions. If we compare the surface pressure graphs to the surface viscoelasticity graphs, we can divide the adsorption process into three stages relative to the phase transition. Before the phase transition, the air-water interface is liquid-like, and the surface pressure and viscoelasticity increase with the adsorption of surfactant molecules. At the phase transition stage, the adsorption layer passes the region where the liquid and solid phases coexist, and the surface pressure remains constant, resulting in the disappearance of surface viscoelasticity. This phase transition phenomenon, which is induced by the adsorption of DOH, has been observed by direct methods, such as Brewster angle microscopy (BAM) [44-47] and grazing incidence X-ray diffraction (GIXD) [46, 47]. Beyond the phase transition, the air-water interface becomes solid-like, and the surface pressure continues to increase to a plateau. Correspondingly, the surface viscoelasticity increases dramatically until reaching its equilibrium values. It should be noted that solutions with higher DOH concentrations but lower SDS concentrations exhibit higher surface rheological properties. This result can be correlated with the dynamic stability factor in Figure 6, where foams stabilized by solutions with higher DOH concentrations but lower SDS concentrations are relatively stable.

According to the dynamic surface pressure and surface viscoelasticity results, the SDS-DOH solutions appear to exhibit satisfactory foamability. SDS is relatively soluble in water but is less surface active, whereas DOH is less soluble but more surface active [45, 46]. Therefore, in mixed solutions, SDS molecules adsorb quickly and increase the bubble breakup process, whereas DOH molecules adsorb later and prevent bubble coalescence by increasing the surface viscoelasticity of the air-water interface. Similar sequential adsorptions were also reported in a surfactant-protein system [48]. In addition, the high values of surface viscoelasticity caused by the presence of DOH in SDS solutions can potentially lead to the suppression of marginal regeneration and a reduced rate of foam film drainage [49-51]. Therefore, the high values of surface viscoelasticity can not only enhance the foam stability but also increase the foamability if the increased surface viscoelasticity is developed on bubble surfaces during foam generation with a surface age of 0.1–1 s. The enhanced surface viscoelasticity in this time scale has been reported [42] with a frequency range of 1–500 Hz.

However, as shown in Figures 5 and 7, the foamability of SDS solutions decreases with the addition of DOH. Therefore, we must consider other contributions, such as the surface forces between interfaces in the liquid film and the antifoam effects of DOH droplets [52].

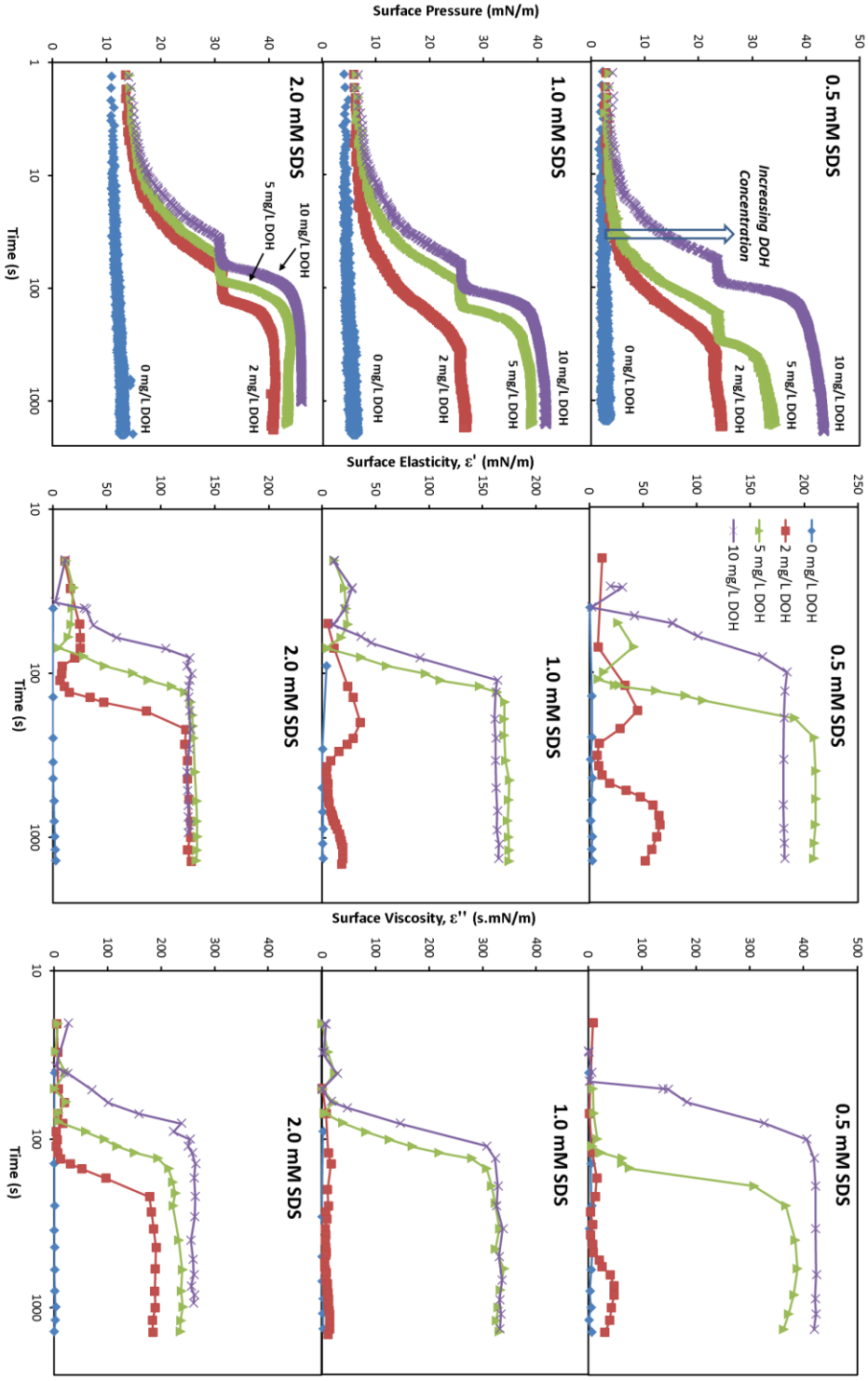

Figure 9. Dynamic surface pressure, surface elasticity, ε', and surface viscosity, ε'', as a function of SDS and DOH concentrations, where the surface viscoelasticity was measured at a frequency of 0.05 Hz. The lines are intended to act solely as visual guides.

5.3. Surface potential

Figure 10 shows the surface (zeta) potential data of air bubbles in SDS solutions with and without 2 mg/L of DOH. The concentration of DOH is reasonably below its solubility limit (4 mg/L at 29.5°C, as shown in Section 3.1). The displacement of SDS molecules by DOH molecules, which is caused by the considerably higher surface activity of DOH relative to SDS, results in a significant decrease in the surface potential. As a result, the liquid film becomes less stable because of the decreased electrostatic repulsion between the interfaces. Figure 10 also shows the surface potential increases with SDS concentration, indicating the increased electrostatic interactions that favor liquid film stability. The surface potential results are consistent with the foamability results in Figure 7, in which the initial foam volume decreases with increased DOH concentration but increases with increased SDS concentration.

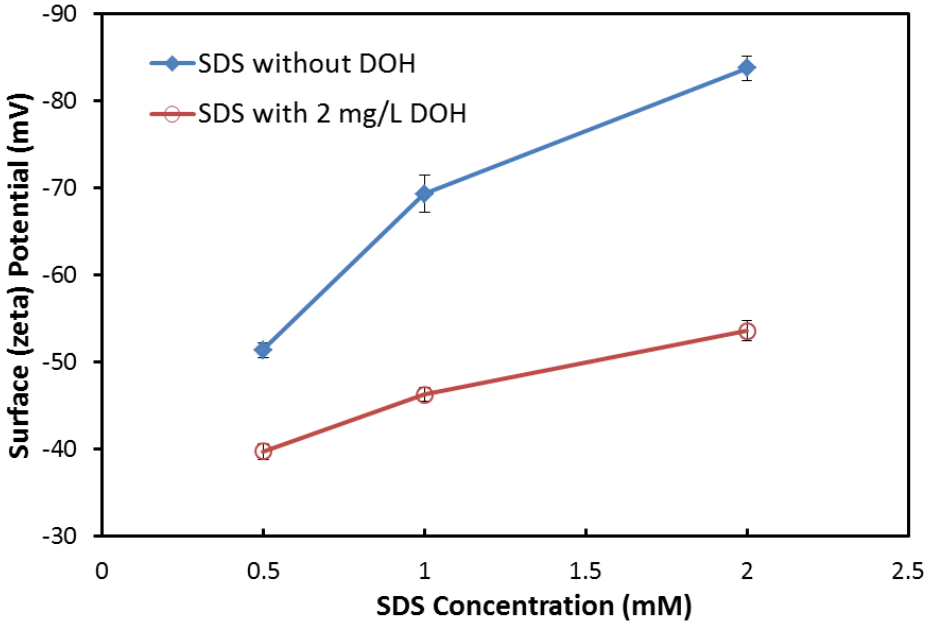

Figure 10. Comparison of the surface (zeta) potential of air bubbles in SDS solutions with and without 2 mg/L of DOH. The lines are intended to act solely as visual guides.

5.4. Antifoam effects

Table 1 shows the equilibrium surface tension values of SDS solutions with and without 10 mg/L of DOH and the corresponding spreading pressure. The equilibrium surface tension of SDS solutions without DOH decreases with SDS concentration, which confirms the fact that lower equilibrium surface tension results in higher foamability. However, this phenomenon is not observed in SDS-DOH solutions. In such solutions, the DOH concentration is far beyond its solubility limit, indicating that DOH exists in the form of a

droplet. Therefore, we hypothesize that DOH droplets act as antifoams in SDS solutions. Figure 11 shows a convincing correlation between the relative antifoam efficacy, ΔV_{rel}, and the spreading pressure, $\Delta\sigma_{AW}$, that supports our hypothesis. The antifoam efficacy, ΔV_{rel}, is calculated as the change in the initial foam volume upon the addition of DOH and is expressed as a fraction relative to the volume without DOH [26]:

$$\Delta V = V_0 - V_a \tag{17}$$

$$\Delta V_{rel} = \Delta V / V_0 \tag{18}$$

where V_0 and V_a are the initial foam volumes in the absence and the presence of DOH, respectively. As shown in Figure 11, because the entry barrier of DOH droplets increases with SDS concentration, which diminishes the antifoam effect, the relative antifoam efficacy, ΔV_{rel}, decreases with the SDS concentration. The increase of the entry barrier as the SDS concentration increases also explains the observation that the antifoam effect of DOH weakens as the SDS concentration increases (Figure 5). A similar correlation between the relative antifoam efficacy, ΔV_{rel}, and the spreading pressure, $\Delta\sigma_{AW}$, has been reported to demonstrate the antifoam effects of polydimethylsiloxane [26].

Table 1. DOH film spreading data of SDS solutions with 10 mg/L of DOH

SDS concentration (mM)	**Equilibrium surface tension of SDS without DOH, σ^i (mN/m)**	**Equilibrium surface tension of SDS with DOH, σ^f (mN/m)**	**Spreading pressure, σ_{AW} (mN/m)**
0.5	69.18±0.065	28.26±0.055	40.91
1.0	65.89±0.28	28.31±0.040	37.58
2.0	57.64±0.40	28.02±0.18	29.61

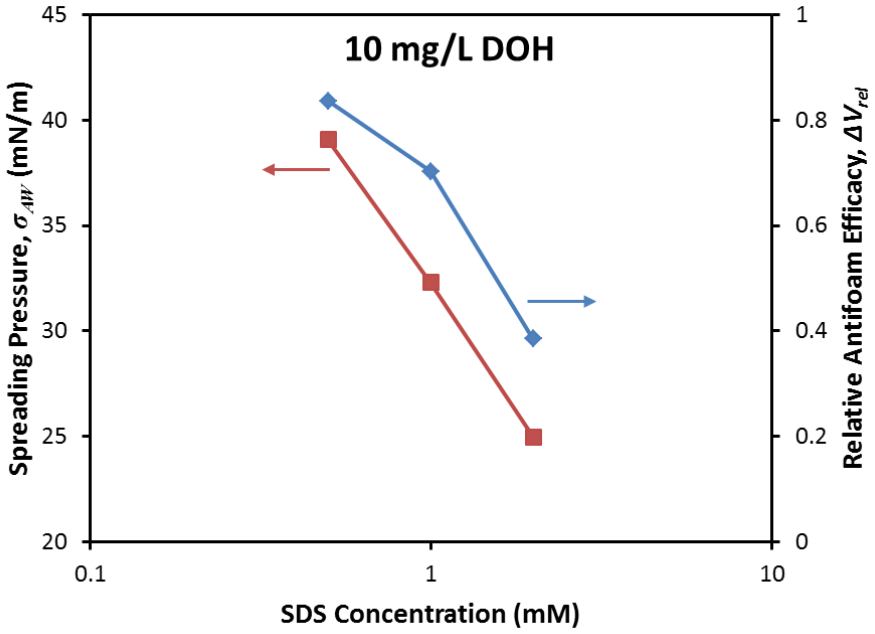

Figure 11. Correlation between the relative antifoam efficacy, ΔV_{rel}, and the spreading pressure, $\Delta\sigma_{AW}$, of SDS solutions with 10 mg/L of DOH. The lines are intended to act solely as visual guides.

6. Conclusions

Herein, we examined the foamability of SDS-DOH mixtures at SDS concentrations below the CMC and attempted to correlate this property with interfacial properties, such as the equilibrium and dynamic surface tension, dynamic surface viscoelasticity, surface potential and DOH droplet spreading on the liquid film. We also developed a foam growth kinetic model to simulate the foam growth data and interpret the experimental results. In mixed solutions, SDS molecules adsorb quickly and increase the bubble breakup process, while DOH molecules adsorb later, preventing bubble coalescence by increasing the surface viscoelasticity of the air-water interface. These foam growth results exhibited unexpected effects of DOH on SDS foam behaviors. Collectively, the results suggest that DOH acts as both a foam stabilizer and a foam depressant. The unexpected decrease in the foamability is explained by the displacement of SDS molecules by DOH molecules at the air-water interface below the DOH solubility limit and by the antifoam effects of DOH droplets above the limit. Our study reveals the complex foam behavior of surfactant mixtures.

Acknowledgements

The authors gratefully acknowledge the China Scholarship Council (CSC) of the Chinese Government and The University of Queensland (UQ) for the CSC-UQ scholarship for JW.

References

[1] I. Cantat, S. Cohen-Addad, F. Elias, F. Graner, R. Hohler, O. Pitois, F. Rouyer, A. Saint-jalmes, Foams: Structure and Dynamics, CPI Group (UK) Ltd, Croydon, 2013.
[2] K. Małysa, R. Miller, K. Lunkenheimer, Relationship between foam stability and surface elasticity forces: Fatty acid solutions, Colloids and Surfaces, 53 (1991) 47-62.
[3] C. Stubenrauch, L.K. Shrestha, D. Varade, I. Johansson, G. Olanya, K. Aramaki, P. Claesson, Aqueous foams stabilized by n-dodecyl-β-d-maltoside, hexaethyleneglycol monododecyl ether, and their 1 : 1 mixture, Soft Matter, 5 (2009) 3070-3080.
[4] A. Salonen, M. In, J. Emile, A. Saint-Jalmes, Solutions of surfactant oligomers: a model system for tuning foam stability by the surfactant structure, Soft Matter, 6 (2010) 2271-2281.
[5] P.D.T. Huibers, V.S. Lobanov, A.R. Katritzky, D.O. Shah, M. Karelson, Prediction of Critical Micelle Concentration Using a Quantitative Structure–Property Relationship Approach, Journal of Colloid and Interface Science, 187 (1997) 113-120.
[6] J.L. Kurz, EFFECTS OF MICELLIZATION ON THE KINETICS OF THE HYDROLYSIS OF MONOALKYL SULFATES, The Journal of Physical Chemistry, 66 (1962) 2239-2246.
[7] V.A. Motsavage, H.B. Kostenbauder, The influence of the state of aggregation on the specific acid-catalyzed hydrolysis of sodium dodecyl sulfate, Journal of Colloid Science, 18 (1963) 603-615.
[8] H. Nogami, S. Awazu, Y. Kanakubo, Studies on Decomposition and Stabilization of Drugs in Solution. XIII. On Sodium Lauryl Sulfate, CHEMICAL & PHARMACEUTICAL BULLETIN, 11 (1963) 13-18.
[9] C.J. Garnett, A.J. Lambie, W.H. Beck, M. Liler, Kinetics of the acid-catalysed hydrolysis of dodecylsulphate and dodecyldiethoxysulphate surfactants in concentrated micellar solutions. Part 1.-Effects of acid and surfactant concentrations and of the nature and concentration of counterions, Journal of the Chemical Society, Faraday Transactions 1: Physical Chemistry in Condensed Phases, 79 (1983) 953-964.
[10] K. Lunkenheimer, G. Wienskol, A.J. Prosser, Automated High-Performance Purification of Surfactant Solutions: Study of Convective-Enhanced Adsorption, Langmuir, 20 (2004) 5738-5744.
[11] R. Miller, K. Lunkenheimer, On the importance of the purity of surfactant solutions in determining their adsorption kinetics, Colloid & Polymer Sci, 260 (1982) 1148-1150.
[12] R. Miller, K. Lunkenheimer, A criterion for judging the purity of surfactant solutions based on diffusion controlled adsorption kinetics, Colloid & Polymer Sci, 264 (1986) 273-276.
[13] K. Lunkenheimer, R. Miller, A criterion for judging the purity of adsorbed surfactant layers, Journal of Colloid and Interface Science, 120 (1987) 176-183.
[14] A. Patist, T. Axelberd, D.O. Shah, Effect of Long Chain Alcohols on Micellar Relaxation Time and Foaming Properties of Sodium Dodecyl Sulfate Solutions, Journal of Colloid and Interface Science, 208 (1998) 259-265.
[15] A.N. Kolmogorov, On the breakage of drops in a turbulent flow, Dokl. Akad. Nauk. SSSR, 66 (1949) 825-828.
[16] J.O. Hinze, Fundamentals of the hydrodynamic mechanism of splitting in dispersion processes, AIChE Journal, 1 (1955) 289-295.

[17] A.V. Nguyen, H.J. Schulze, Colloidal science of flotation, Marcel Dekker, New York, 2004.
[18] K. Malysa, K. Lunkenheimer, Foams under dynamic conditions, Current Opinion in Colloid & Interface Science, 13 (2008) 150-162.
[19] R. Miller, L. Liggieri, Interfacial Rheology, Progress in Colloid and Interface Science Volume 1, Brill, Leiden and Boston, 2009.
[20] K.J. Mysels, K. Shinoda, S. Frankel, Soap films: studies of their thinning, Pergamon Press, London, New York, Pairs, Los Angeles, 1959.
[21] V. Bergeron, Forces and structure in thin liquid soap films, Journal of Physics: Condensed Matter, 11 (1999) R215-R238.
[22] A. Hadjiiski, S. Tcholakova, N.D. Denkov, P. Durbut, G. Broze, A. Mehreteab, Effect of Oily Additives on Foamability and Foam Stability. 2. Entry Barriers, Langmuir, 17 (2001) 7011-7021.
[23] P.R. Garrett, Defoaming: Theory and Industrial Applications New York, 1993.
[24] N.D. Denkov, Mechanisms of Foam Destruction by Oil-Based Antifoams, Langmuir, 20 (2004) 9463-9505.
[25] P.R. Garrett, The Science of Defoaming: Theory, Experiment and Applications, Surfactant science series volume, CRC Press Taylor&Francis Group, Boca Raton, 2013.
[26] B.K. Jha, S.P. Christiano, D.O. Shah, Silicone Antifoam Performance: Correlation with Spreading and Surfactant Monolayer Packing, Langmuir, 16 (2000) 9947-9954.
[27] O. Levenspiel, Chemical Reaction Engineering, Industrial & Engineering Chemistry Research, 38 (1999) 4140-4143.
[28] J.J. Bikerman, Foam, Springer-Verlag, New York, 1973.
[29] N. Barbian, E. Ventura-Medina, J.J. Cilliers, Dynamic froth stability in froth flotation, Minerals Engineering, 16 (2003) 1111-1116.
[30] N. Barbian, K. Hadler, E. Ventura-Medina, J.J. Cilliers, The froth stability column: linking froth stability and flotation performance, Minerals Engineering, 18 (2005) 317-324.
[31] N. Barbian, K. Hadler, J.J. Cilliers, The froth stability column: Measuring froth stability at an industrial scale, Minerals Engineering, 19 (2006) 713-718.
[32] Z. Aktas, J.J. Cilliers, A.W. Banford, Dynamic froth stability: Particle size, airflow rate and conditioning time effects, International Journal of Mineral Processing, 87 (2008) 65-71.
[33] R. Stephenson, J. Stuart, Mutual binary solubilities: water-alcohols and water-esters, Journal of Chemical & Engineering Data, 31 (1986) 56-70.
[34] J.A. Dean, Lange's Handbook of Chemistry, McGRAW-HILL, INC., New York, 1967.
[35] L. Liggieri, F. Ravera, M. Ferrari, Surface Rheology Investigation of the 2-D Phase Transition in n-Dodecanol Monolayers at the Water-Air Interface, Langmuir, 19 (2003) 10233-10240.
[36] A.W. Adamson, A.P. Gast, Physical Chemistry of Surface, 6th Edition, John Wiley & Sons, Inc., New York, 1997.
[37] D. Möbius, R. Miller, Novel methods to study interfacial layers, Elsevier, Amsterdam, 2001.
[38] S.A. Zholob, A.V. Makievski, R. Miller, V.B. Fainerman, Optimisation of calculation methods for determination of surface tensions by drop profile analysis tensiometry, Advances in Colloid and Interface Science, 134–135 (2007) 322-329.
[39] C. Yang, T. Dabros, D. Li, J. Czarnecki, J.H. Masliyah, Measurement of the Zeta Potential of Gas Bubbles in Aqueous Solutions by Microelectrophoresis Method, Journal of Colloid and Interface Science, 243 (2001) 128-135.
[40] N.D. Denkov, K.G. Marinova, S.S. Tcholakova, Mechanistic understanding of the modes of action of foam control agents, Advances in Colloid and Interface Science, 206 (2014) 57-67.
[41] J.P. Fang, P. Joos, The dynamic surface tension of SDS— dodecanol mixtures: 1. The submicellarsystems, Colloids and Surfaces, 65 (1992) 113-120.
[42] K.D. Wantke, H. Fruhner, J. Örtegren, Surface dilatational properties of mixed sodium dodecyl sulfate/dodecanol solutions, Colloids and Surfaces A: Physicochemical and Engineering Aspects, 221 (2003) 185-195.

[43] D. Georgieva, A. Cagna, D. Langevin, Link between surface elasticity and foam stability, Soft Matter, 5 (2009) 2063-2071.
[44] D. Vollhardt, G. Emrich, Coadsorption of sodium dodecyl sulfate and medium-chain alcohols at the air–water interface, Colloids and Surfaces A: Physicochemical and Engineering Aspects, 161 (2000) 173-182.
[45] V.B. Fainerman, D. Vollhardt, G. Emrich, Dynamics and Phase Transition in Adsorbed Monolayers of Sodium Dodecyl Sulfate/Dodecanol Mixtures, The Journal of Physical Chemistry B, 105 (2001) 4324-4330.
[46] D. Vollhardt, G. Brezesinski, S. Siegel, G. Emrich, Phase transition in adsorbed monolayers of sodium dodecyl sulfate/dodecanol mixtures, J. Phys. Chem. B, 105 (2001) 12061-12067.
[47] D. Vollhardt, V.B. Fainerman, Characterisation of phase transition in adsorbed monolayers at the air/water interface, Advances in Colloid and Interface Science, 154 (2010) 1-19.
[48] D. Vitasari, P. Grassia, P. Martin, Simulation of dynamics of adsorption of mixed protein–surfactant on a bubble surface, Colloids and Surfaces A: Physicochemical and Engineering Aspects, 438 (2013) 63-76.
[49] J.-L. Joye, G.J. Hirasaki, C.A. Miller, Asymmetric Drainage in Foam Films, Langmuir, 10 (1994) 3174-3179.
[50] J.L. Joye, G.J. Hirasaki, C.A. Miller, Dimple formation and behavior during axisymmetrical foam film drainage, Langmuir, 8 (1992) 3083-3092.
[51] D.O. Shah, N.F. Djabbarah, D.T. Wasan, A correlation of foam stability with surface shear viscosity and area per molecule in mixed surfactant systems, Colloid & Polymer Sci, 256 (1978) 1002-1008.
[52] L. Arnaudov, N.D. Denkov, I. Surcheva, P. Durbut, G. Broze, A. Mehreteab, Effect of Oily Additives on Foamability and Foam Stability. 1. Role of Interfacial Properties, Langmuir, 17 (2001) 6999-7010.

Chapter 5: Effects of the Nonpolar Collector on Foam Stability

Jianlong Wang[1], Anh V Nguyen[1*] and Saeed Farrokhpay[2]

[1]School of Chemical Engineering, University of Queensland, Brisbane, Queensland 4072, Australia,

[2]JKMRC, University of Queensland, Brisbane, Queensland 4072, Australia

[*]Correspondence: anh.nguyen@eng.uq.edu.au

Highlights

- Diesel oil was found to decrease the foam growth rate of MIBC solutions.
- A model was developed and applied to simulate foam growth kinetics.
- The antifoam efficacy of diesel was correlated with its spreading pressure.
- The antifoam effect was explained by oil-frother molecular interactions.

Graphical abstract

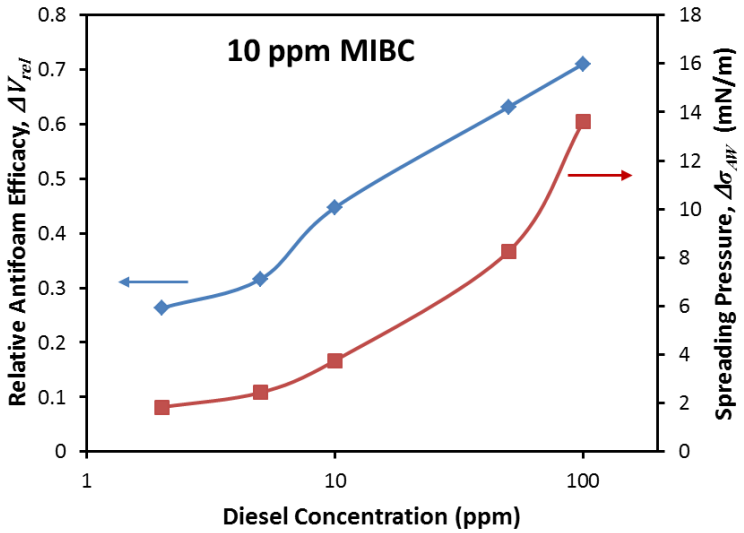

Abstract

Froth stability determines the quality of the final concentrate in flotation. However, understanding of the factors that control the froth stability remains limited. We hypothesize that the commonly used nonpolar collectors in the flotation of naturally hydrophobic minerals may have a significant impact on foam stability. As an example, we chose diesel oil as a nonpolar collector to study its effects on the foam properties of MIBC solutions. We developed a quantitative foam growth measurement using a non-overflowing flotation cell and imaging analysis of the foam system. We also developed a foam growth model with two parameters (i.e., foam formation and foam decay rate constants, k_1 and k_2) to simulate the behavior of the foam column kinetics. The results revealed that the presence of diesel oil, even in trace amounts (2 ppm), can effectively decrease the foam growth rate by accelerating the foam decay process. We proposed two mechanisms to explain the observed antifoam effects of diesel oil: (i) the spreading of diesel oil droplets at the liquid film interface, which is quantified by the spreading pressure, and (ii) the molecular interactions between the diesel oil and frother molecules. This study establishes a benchmark for investigating the effect of nonpolar collectors on three-phase froth stability.

Keywords: nonpolar collector, diesel, MIBC, antifoam

1. Introduction

Appropriately managing the froth phase can effectively improve the performance of froth flotation [1-6]. However, the froth phase is probably the most complex aspect of the froth flotation process. Although frothers are added to produce the froth phase, these ingredients alone do not control froth stability. For example, froth stability is also influenced by the size, shape and hydrophobicity of solid particles, the presence of other reagents (e.g., collectors and modifiers), the pH of the pulp phase, the process water chemistry and operational factors [1, 7-11]. Therefore, the production and maintenance of a satisfactory froth phase during the various stages of a flotation process is an art rather than a science and is often problematic for flotation operators.

Nonpolar collectors are used in the flotation of naturally hydrophobic particles, such as coal, graphite and molybdenite [12, 13]. Among these nonpolar collectors, diesel oil is most commonly used for coal and molybdenite flotation. The primary function of diesel oil is to increase the affinity of solid particles for the air bubbles by intermolecular van der Waals forces. However, oil droplets are also known to be antifoams [14-17]. Therefore, we can ask

the following question: Does diesel oil exert some additional “side effects” on froth stability? Here, for the sake of simplicity, we will initially only focus on foam stability. The aim of this work is to gain a better understanding of the effect of the nonpolar collector on foam stability for future reference and to serve as a benchmark for understanding the stability of three-phase flotation froth. First, we describe the experimental procedures and provide a new mathematical model for foam kinetics to simulate the foam growth process. Second, we analyze the experimental results and simulate the foam growth process using the proposed model. Finally, we discuss some possible antifoam mechanisms involving diesel oil.

2. Experimental

2.1. Materials

MIBC with a purity of +99% was purchased from Acros Organics (New Jersey, US). Diesel oil was purchased from CALTEX (QLD, Australia). All chemicals were used as received. All solutions were prepared using tap water (Brisbane, Queensland, Australia).

2.2. Foaming experiments

The foaming experiments were conducted in a 1.5 L JK Tech (Brisbane, Australia) Batch Flotation cell [13] by the addition of 0.8 L of water with an air flow rate of 3.3 L/min and an agitation speed of 1200 rpm. MIBC and diesel oil were added simultaneously to the bulk solution and conditioned for 1 minute prior to the foaming experiments. When the airflow was directed into the flotation cell, the foam height was recorded using a digital camera (Canon A650 IS). One minute was required to reach the equilibrium maximum foam height. The videos were processed using software (Launch ImageGrab v 5.0, Paul Glagla, France) to extract images at different foaming times. Foam volumes at various times were calculated based on these images. Overflow of the foam from the cell did not occur. All experiments were conducted at an ambient temperature of 22°C.

2.3. Surface tension measurements

Please refer to Section 4.3 in Chapter 4 for details.

3. Quantification of foam growth

Please refer to Section 3 in Chapter 4 for details.

4. Results and discussion

4.1. Experimental results

Figure 1 shows the variation of the foam volume versus time for solutions with different reagent concentrations. The maximum equilibrium foam volume decreases with the diesel oil concentration. As expected, the equilibrium foam volume increases with the MIBC concentration.

The antifoam efficacy, ΔV_{rel}, is calculated as the change in the equilibrium foam volume upon the addition of diesel oil and is expressed as a fraction relative to the volume without diesel oil (Please refer to Eq. 17 and Eq. 18 for the definition of ΔV_{rel}).

Figure 2 shows the dependence of the relative antifoam efficacy on the reagent concentrations. As expected, the relative antifoam efficacy increases with the diesel oil concentration but decreases with MIBC concentration. The most significant antifoam effect of diesel oil was observed in the solutions with the lowest MIBC concentration (10 ppm).

Fuel oil has been reported to decrease the froth stability in the presence of an anionic frother. However, this phenomenon does not occur with polyglycol (nonionic) frothers [10]. This anomaly is because of the higher adsorption capacity of the nonionic frother at the air-water interface relative to the ionic frother [18]. The stronger affinity of polyglycol for the air-liquid interface exceeds the effect of the fuel oil. Instead of using polyglycol as a nonionic frother, we used the relatively weak frother MIBC. For the first time, we confirm that fuel oil can also decrease foam stability in the presence of a nonionic frother.

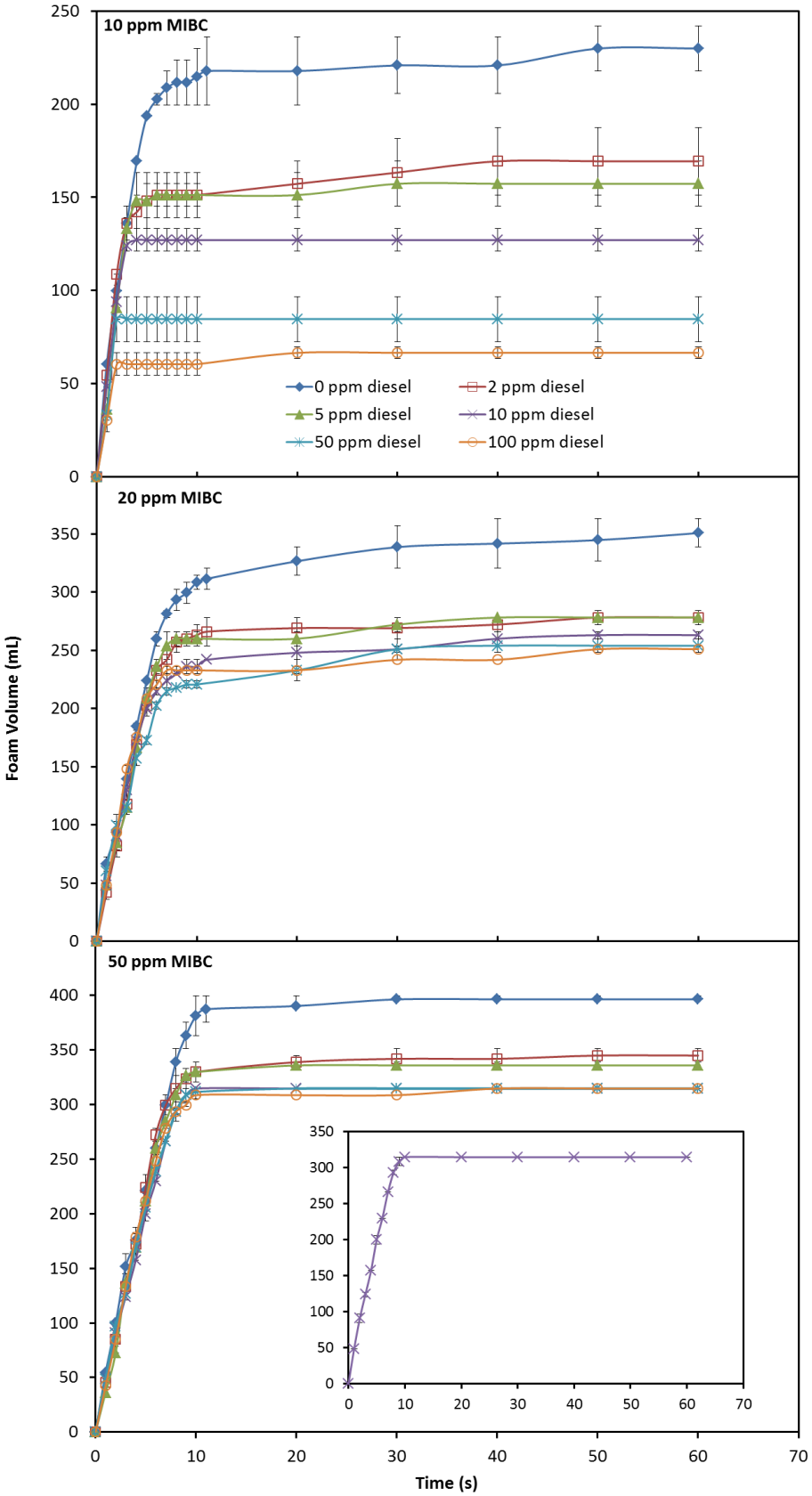

Figure 1. Variation of foam volume with time for MIBC-diesel solutions. The error bars indicate the standard errors of the mean.

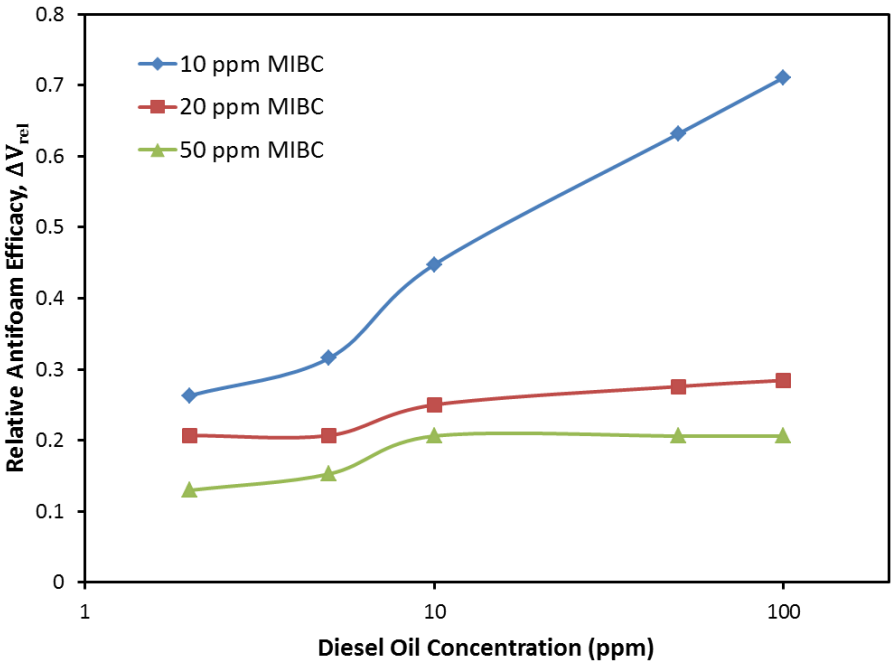

Figure 2. Dependence of ΔV_{rel} on the diesel oil and MIBC concentrations

4.2. Simulation of foam growth

In this section, we use the mathematical model developed previously to quantify and simulate the foam growth kinetics. First, the foam decay constant, k_2, is calculated by $k_2 = v_g / V_{\max}$, where v_g equals 55 mL/s (3.3 L/min) and $V_{\max}$ was measured as in the previous section. Then, the foam column kinetic behavior is simulated using Eq. 15 from Chapter 4.

Figure 3 shows the comparison between the experimental and simulated results. The difference between these results, especially for the highest MIBC concentration (50 ppm) in Figure 3, is caused by the presence of liquid in the foam, which makes the experimental foam growth more rapid than the simulated foam growth.

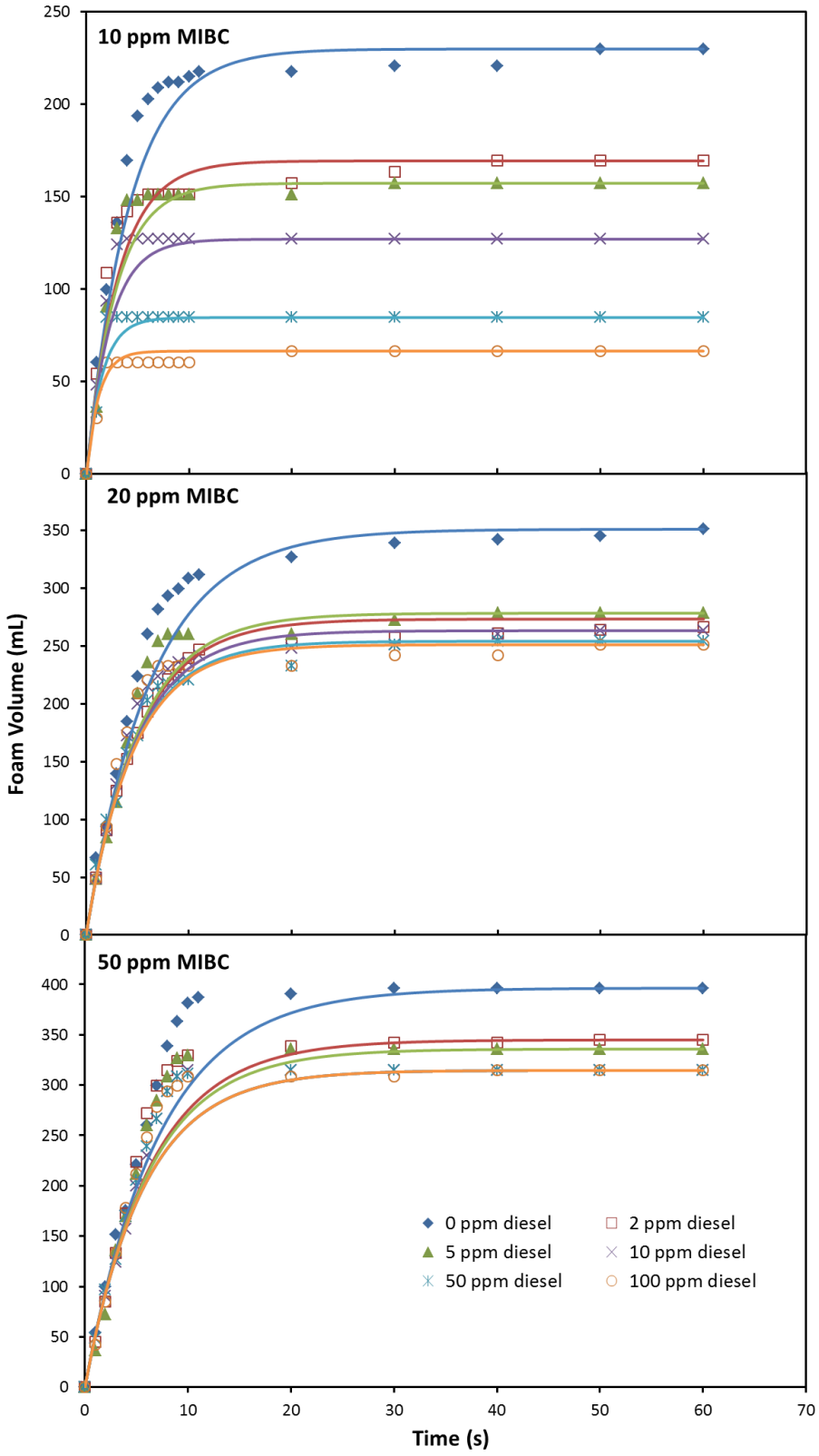

Figure 3. Experimental (points) and theoretical (lines) foam growth data of MIBC-diesel solutions (we use the same legends as in Figure 3) according to Eq. (15) in Chapter 4, where the gas flow rate is $v_g = 55$ mL/s

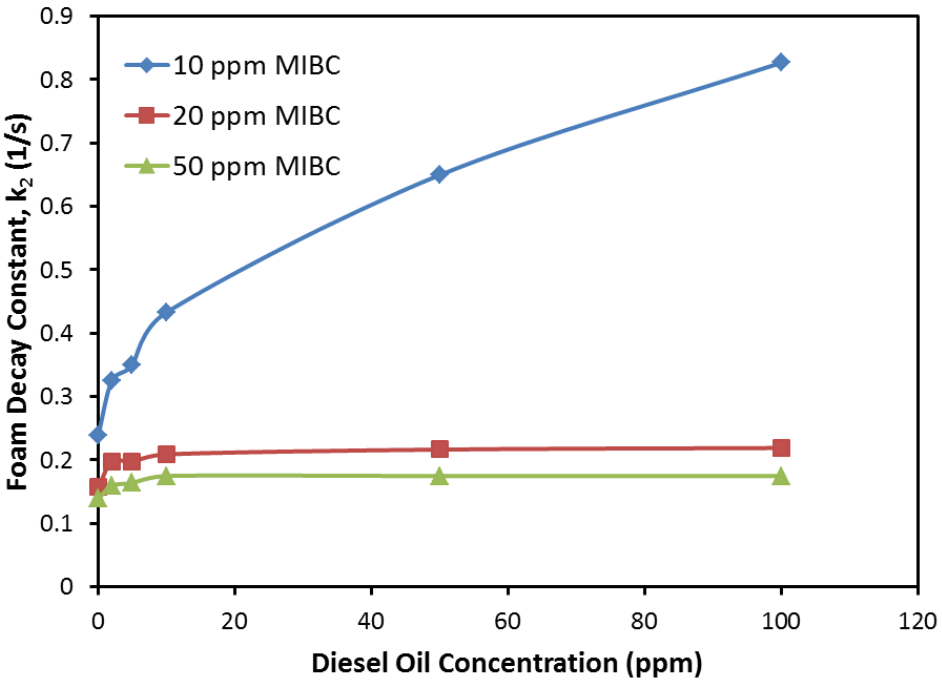

Figure 4. Foam decay constant, k_2, of MIBC-diesel solutions calculated by $k_2 = v_g / V_{\max}$

Figure 4 shows the foam decay constant, k_2, as a function of MIBC and diesel concentrations. We found that k_2 decreases with MIBC concentration. There are two reasons for the decreased k_2: (1) the presence of MIBC inhibits bubble coalescence [19-23] and (2) the presence of MIBC stabilizes the liquid films between the bubbles [24-27].

We also observed that k_2 increased with the diesel oil concentration. The increased foam decay rate is caused by the antifoam effect of the diesel oil droplets, which can destroy the foam [14, 15, 17, 28]. The antifoam effect of diesel oil is most significant in the solutions containing the lowest concentration of MIBC (10 ppm).

4.3. Antifoam mechanisms of diesel oil

4.3.1. Correlation between antifoam efficacy and spreading pressure

Please refer to Section 2.3 in Chapter 4 for details about the definition of $\Delta\sigma_{AW}$.

In this study, the antifoam effect of DOH droplets was correlated with the spreading pressure $\Delta\sigma_{AW}$, which is applied in more general situations. Table 1 shows the values of the surface tension and spreading pressure in 10 ppm MIBC containing different diesel oil concentrations. Figure 5 shows the correlation between the relative antifoam efficacy, ΔV_{rel},

and spreading pressure, $\Delta\sigma_{AW}$, which supports our hypothesis that diesel oil acts as an antifoam in MIBC solutions.

Table 1. Oil film spreading data of 10 ppm MIBC solutions

Diesel concentration (ppm)	Surface tension, σ (mN/m)	Spreading pressure, $\Delta\sigma_{AW}$ (mN/m)
0	72.32±0.10	0.00
2	70.48±0.44	1.84
5	69.88±0.01	2.44
10	68.56±0.22	3.76
50	64.06±1.04	8.26
100	58.72±0.12	13.60

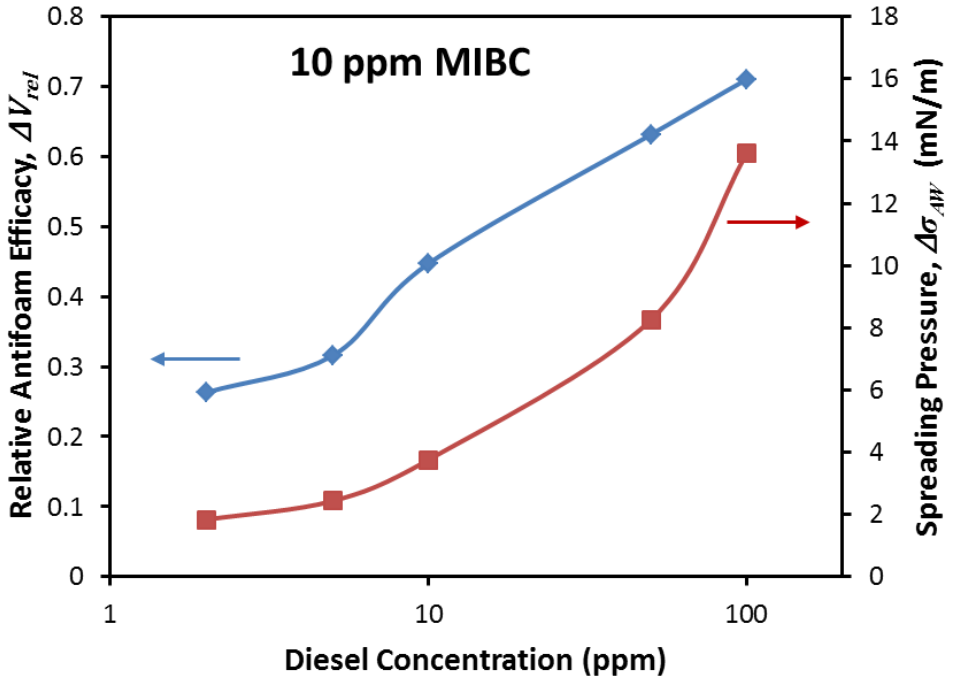

Figure 5. Correlation between the relative antifoam efficacy, ΔV_{rel}, and the spreading pressure, $\Delta\sigma_{AW}$, of 10 ppm MIBC solutions with different diesel oil concentrations.

4.3.2. Interactions between diesel oil and frother molecules

Figure 6 illustrates the molecular interactions between diesel oil droplets and MIBC molecules in the flotation cell. There are two consequences of this interaction: (i) the MIBC

molecules align themselves at the oil-water interface with the hydrophilic group in the water and the hydrophobic tail in the oil and (ii) the MIBC molecules act as an emulsifier to form a stable emulsion by reducing the oil-water interfacial tension. Both outcomes facilitate the foam decay process. The adsorption of MIBC molecules on the oil-water interface depletes the MIBC molecules in the water phase, resulting in a less stable foam layer. The adsorption of MIBC molecules on the oil-water interface can also increase the stability of the oil droplets that act as antifoams. Therefore, the foam decay constant, k_2, increases with the diesel oil concentration, as illustrated in Figure 5. The increase in k_2 is most evident for the solutions containing the lowest MIBC concentration (10 ppm).

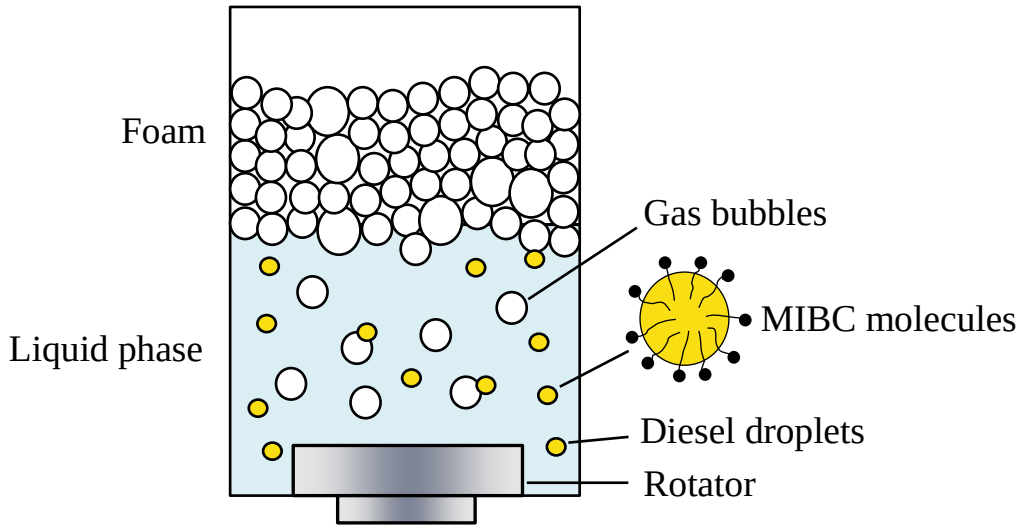

Figure 6. Schematic of the interactions between oil droplets and MIBC molecules in the flotation cell

5. Conclusions

We conducted experiments to examine the effects of a nonpolar collector on the foam growth kinetics of MIBC solutions. We found that diesel oil, which is a commonly used nonpolar collector in the flotation of naturally hydrophobic minerals, could decrease the foam growth rate by accelerating the foam decay process. We developed a kinetic model to quantify the foam growth process. The model describes the foam growth rate in terms of the competition between foam formation and foam decay. We found that the presence of diesel

oil increased the value of the foam decay constant, k_2, whereas the presence of MIBC decreased it. The antifoam effect of diesel oil was explained based on the entry barrier and spreading pressure. We also discussed the interactions between diesel oil and frother molecules to illustrate diesel oil's antifoam effects.

Acknowledgements

The authors gratefully acknowledge the China Scholarship Council (CSC) of the Chinese Government and The University of Queensland (UQ) for the CSC-UQ scholarship for JW. The authors thank Professor Jan Cilliers in the Department of Earth Science and Engineering, Imperial College London, for his comments on the foam growth model developed in Section 3 and his contribution to the development of Eq. (7).

References

[1] M.C. Fuerstenau, G. Jameson, R.-H. Yoon, Froth Flotation A Century of Innovation, SME, Colorado, 2007.
[2] A.V. Nguyen, H.J. Schulze, Colloidal science of flotation, Marcel Dekker, New York, 2004.
[3] S. Ata, Phenomena in the froth phase of flotation — A review, International Journal of Mineral Processing, 102–103 (2012) 1-12.
[4] S. Farrokhpay, The significance of froth stability in mineral flotation — A review, Advances in Colloid and Interface Science, 166 (2011) 1-7.
[5] K. Hadler, M. Greyling, N. Plint, J.J. Cilliers, The effect of froth depth on air recovery and flotation performance, Minerals Engineering, 36–38 (2012) 248-253.
[6] N. Barbian, K. Hadler, E. Ventura-Medina, J.J. Cilliers, The froth stability column: linking froth stability and flotation performance, Minerals Engineering, 18 (2005) 317-324.
[7] S.I. Karakashev, O. Ozdemir, M.A. Hampton, A.V. Nguyen, Formation and stability of foams stabilized by fine particles with similar size, contact angle and different shapes, Colloids and Surfaces A: Physicochemical and Engineering Aspects, 382 (2011) 132-138.
[8] Z. Aktas, J.J. Cilliers, A.W. Banford, Dynamic froth stability: Particle size, airflow rate and conditioning time effects, International Journal of Mineral Processing, 87 (2008) 65-71.
[9] S. Ata, Coalescence of Bubbles Covered by Particles, Langmuir, 24 (2008) 6085-6091.
[10] H. El-Shall, N.A. Abdel-Khalek, S. Svoronos, Collector–frother interaction in column flotation of Florida phosphate, International Journal of Mineral Processing, 58 (2000) 187-199.
[11] S. Farrokhpay, M. Zanin, An investigation into the effect of water quality on froth stability, Advanced Powder Technology, 23 (2012) 493-497.
[12] M. Zanin, I. Ametov, S. Grano, L. Zhou, W. Skinner, A study of mechanisms affecting molybdenite recovery in a bulk copper/molybdenum flotation circuit, International Journal of Mineral Processing, 93 (2009) 256-266.
[13] T. Wei, Y. Peng, S. Farrokhpay, Froth stability of coal flotation in saline water, Mineral Processing and Extractive Metallurgy (Trans. Inst. Min Metall. C), (2014).
[14] B.K. Jha, S.P. Christiano, D.O. Shah, Silicone Antifoam Performance: Correlation with Spreading and Surfactant Monolayer Packing, Langmuir, 16 (2000) 9947-9954.
[15] L. Arnaudov, N.D. Denkov, I. Surcheva, P. Durbut, G. Broze, A. Mehreteab, Effect of Oily Additives on Foamability and Foam Stability. 1. Role of Interfacial Properties, Langmuir, 17 (2001) 6999-7010.

[16] A. Hadjiiski, S. Tcholakova, N.D. Denkov, P. Durbut, G. Broze, A. Mehreteab, Effect of Oily Additives on Foamability and Foam Stability. 2. Entry Barriers, Langmuir, 17 (2001) 7011-7021.
[17] N.D. Denkov, Mechanisms of Foam Destruction by Oil-Based Antifoams, Langmuir, 20 (2004) 9463-9505.
[18] M.J. Rosen, Surfactants and Interfacial Phenomena, Wiley, New York, 1989.
[19] G. Bournival, R.J. Pugh, S. Ata, Examination of NaCl and MIBC as bubble coalescence inhibitor in relation to froth flotation, Minerals Engineering, 25 (2012) 47-53.
[20] W. Kracht, H. Rebolledo, Study of the local critical coalescence concentration (l-CCC) of alcohols and salts at bubble formation in two-phase systems, Minerals Engineering, 50–51 (2013) 77-82.
[21] S. Castro, C. Miranda, P. Toledo, J.S. Laskowski, Effect of frothers on bubble coalescence and foaming in electrolyte solutions and seawater, International Journal of Mineral Processing, 124 (2013) 8-14.
[22] Y.S. Cho, J.S. Laskowski, Effect of flotation frothers on bubble size and foam stability, International Journal of Mineral Processing, 64 (2002) 69-80.
[23] A. Srinivas, P. Ghosh, Coalescence of Bubbles in Aqueous Alcohol Solutions, Industrial & Engineering Chemistry Research, 51 (2011) 795-806.
[24] L. Wang, R.-H. Yoon, Effects of surface forces and film elasticity on foam stability, International Journal of Mineral Processing, 85 (2008) 101-110.
[25] S.I. Karakashev, D.S. Ivanova, Z.K. Angarska, E.D. Manev, R. Tsekov, B. Radoev, R. Slavchov, A.V. Nguyen, Comparative validation of the analytical models for the Marangoni effect on foam film drainage, Colloids and Surfaces A: Physicochemical and Engineering Aspects, 365 (2010) 122-136.
[26] X. Qu, L. Wang, S.I. Karakashev, A.V. Nguyen, Anomalous thickness variation of the foam films stabilized by weak non-ionic surfactants, Journal of Colloid and Interface Science, 337 (2009) 538-547.
[27] L. Wang, R.-H. Yoon, Role of hydrophobic force in the thinning of foam films containing a nonionic surfactant, Colloids and Surfaces A: Physicochemical and Engineering Aspects, 282–283 (2006) 84-91.
[28] P.R. Garrett, Defoaming: Theory and Industrial Applications New York, 1993.

Chapter 6: Effects of Surface Rheology and Surface Potential on Foam Stability

Jianlong Wang[1], Anh V Nguyen[1*] and Saeed Farrokhpay[2]
[1]School of Chemical Engineering, University of Queensland, Brisbane, Queensland 4072, Australia
[2]JKMRC, University of Queensland, Brisbane, Queensland 4072, Australia

[*]Correspondence: anh.nguyen@eng.uq.edu.au

Highlights:

- A model is proposed for foam collapse that was inspired by chemical kinetics.
- The stability of SDS-DOH foams is dominated by surface viscoelasticity, despite the decreased double-layer repulsion.
- The stability of SDS-NaCl foams is dominated by double-layer repulsion at the same surface concentration of SDS molecules.

Graphical abstract:

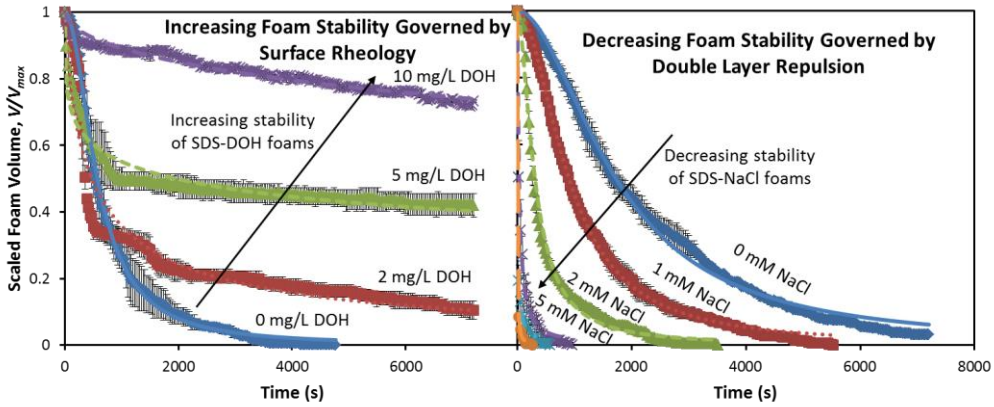

Abstract

Here, we examine the rupture of standing aqueous foams stabilized by the anionic surfactant SDS, using DOH and sodium chloride (NaCl) respectively to produce different surface viscoelasticities and surface potentials in order to elucidate the roles of surface rheology and intermolecular forces in foam stability. A model is proposed that is analogous to reaction kinetics, which is used to quantify the foam collapse process. The presence of DOH in the SDS solutions can significantly increase the surface viscoelasticity and foam stability, despite the decreased surface potential caused by the displacement of SDS molecules by DOH molecules at the air-water interface. The correlation between surface viscoelasticity and foam stability is explained by the decrease in foam drainage and the enhancement of liquid film stability. For SDS-NaCl mixtures with the same value of the mean ionic product (1 mM), an increased concentration of NaCl in the SDS solution reduces the surface potential and the Debye length because of the screening effect resulting from the binding of sodium counter ions to the sulfate head groups. The foam stability decreases because of the weakened repulsive interactions between the two interfaces of the liquid films, despite the presence of the same surface concentration of SDS molecules, as indicated by the same equilibrium surface tension. This chapter highlights two different mechanisms that dominate foam stability.

Keywords: foam, foam stability, surface rheology, surface potential

1. Introduction

Foam consists of a mixture of a large volume of gas with a much smaller amount of liquid. Because of its large surface area, a foam is thermodynamically unstable and irreversibly evolves and disappears with time [1]. The lifetime of a foam is known to depend on three interrelated mechanisms: the foam drainage caused by gravity, the coarsening caused by gas transfer between bubbles induced by capillary pressure differences, and the bubble coalescence caused by the rupture of liquid films between neighboring bubbles [2]. However, the mechanisms that determine foam collapse remain poorly understood. For example, although many research efforts have focused on the stability of liquid films, which constitute one of the elementary building blocks of foams (with the other being the Plateau borders) [4-6], the correlation between the stability of an isolated film and the stability of the entire foam layer is not fully understood [2, 7]. The rupture of a single liquid film in foams has been shown to depend on previous rupture events; in other words, rupture occurs in correlated bursts [8-11]. Further, it has been correctly noted that [12], "In a real foam, the film are

unlikely to burst at a single exerted pressure, but rather are likely to exhibit a distribution in the bursting probabilities." However, little is known with regard to this distribution of bursting. Similarly, the dependence of foam collapse on the interfacial properties is also not well understood [2].

In this chapter, we first review the theories regarding foam stability in terms of the interfacial properties and the surface forces in a single liquid film. Then, we propose a novel model inspired by chemical kinetics to describe the collapse of standing foams. Finally, we study the foam stability of SDS-DOH and SDS-NaCl foams to elucidate the effects of surface rheology and surface potential on foam stability.

2. Theory

2.1 Surface viscoelasticity and foam stability

Please refer to Section 2.1.3 in Chapter 4 for details.

2.2 Surface forces and foam stability

Please refer to Section 2.2 in Chapter 4 for details.

3. Modeling of foam column collapse

Foam collapse kinetics can be described schematically and analogously to a chemical reaction [13] as follows:

$$F \xrightarrow{k} L + G \tag{1}$$

where F is the foam, L is the liquid released from the collapsed foam, G is the gas leaving the burst bubbles and k is the foam collapse constant. Assuming a second-order foam collapse reaction, the foam collapse rate is proportional to the foam volume squared:

$$\frac{dV}{dt} = -kV^2 \tag{2}$$

where V is the foam volume and t is the foam collapse time. Integrating Eq. (2) with a scaled foam volume gives:

$$\int_1^{V/V_{\max}} \frac{dV}{V^2} = -k\int_0^t dt \tag{3}$$

$$\frac{V}{V_{\max}} = 1 - \frac{t}{\tau + t} \tag{4}$$

where $\tau = 1/k$ is the half lifetime of the foam. Please note that the unit of the foam collapse constant, k, changes from $ml^{-1}s^{-1}$ to s^{-1} after normalization of the foam volume. It should be noted that the fundamental physics of foam collapse are described by Eq. (4), which can be generalized as follows:

$$\frac{V}{V_{\max}} = 1 - \frac{t^n}{\tau^n + t^n} \tag{5}$$

By applying the first derivative of the scaled foam volume with respect to time and expressing the time as a function of the scaled foam volume, we can obtain the prefactor of the foam collapse rate, n/τ, as follows:

$$\frac{d\left(V/V_{\max}\right)}{dt} = -\frac{n\tau^n t^{n-1}}{\left(\tau^n + t^n\right)^2} \tag{6}$$

$$t = \tau\left(\frac{1 - V/V_{\max}}{V/V_{\max}}\right)^{1/n} \tag{7}$$

$$\frac{d\left(V/V_{\max}\right)}{dt} = -\frac{n}{\tau}\left(V/V_{\max}\right)^{(1+1/n)}\left(1 - V/V_{\max}\right)^{(1-1/n)} \tag{8}$$

4. Experimental

4.1. Materials

Both SDS and DOH were purchased from Sigma-Aldrich (US) with purities of 99% and 98%, respectively. NaCl was purchased from Univar (Australia) with a purity of 99%. All chemicals were used as received. The solubility of DOH in water at 29.5°C is 0.04 wt% (4 mg/L), and the freezing point is 24°C [14]. All solutions were prepared using Milli-Q water (surface tension: 71.97 mN/m at 25°C; resistivity: 18.2 MΩcm at 25°C) [15]. A 10 mg/L DOH stock solution was prepared by ultrasonication in an ultrasonic bath for 15 min at a controlled temperature of 25°C. SDS-DOH mixtures were prepared from the stock solution by dilution to the desired concentrations. The SDS-DOH solutions displayed a reduced

surface activity over time because of the separation and consequent evaporation of DOH [16]. Therefore, only freshly prepared solutions were used in this study.

4.2. Foam collapse measurements

Please refer to Section 4.2 in Chapter 4 for details about the foam tester.

During foam collapse, the foam volume was measured by the sensor unit every 30 seconds. For each solution, the experiments were repeated, and averaged results were obtained. The room temperature was kept constant at 25°C. The relative humidity of the room was also kept constant (50–60%).

4.3. Measurements of dynamic surface tension and surface viscoelasticity

Please refer to Section 4.4 in Chapter 4 for details.

4.4. Measurements of surface (zeta) potential of air bubbles in surfactant solutions

Please refer to Section 4.5 in Chapter 4 for details.

5. Results and discussion

5.1 Foam stability of SDS-DOH mixtures

5.1.1 Foam collapse for SDS-DOH foams

Figure 1 shows the foam collapse curves for SDS-DOH mixtures and the simulation results fitted by Eq. (5). The simulation results fit the experimental data very well, indicating the validity of the model developed in Section 3. The presence of DOH is found to significantly increase the foam stability of SDS foams, and its efficacy is proportional to the DOH concentration. To quantify the foam collapse process and make comparisons, the half foam lifetime, τ, in Eq. (5) and the prefactor of the foam collapse rate, n/τ, in Eq. (8) are plotted as a function of the DOH and SDS concentrations, as shown in Figure 2. The half foam lifetime, τ, increases with the SDS and DOH concentrations. Conversely, the prefactor of the foam collapse rate, n/τ, decreases with the SDS and DOH concentrations.

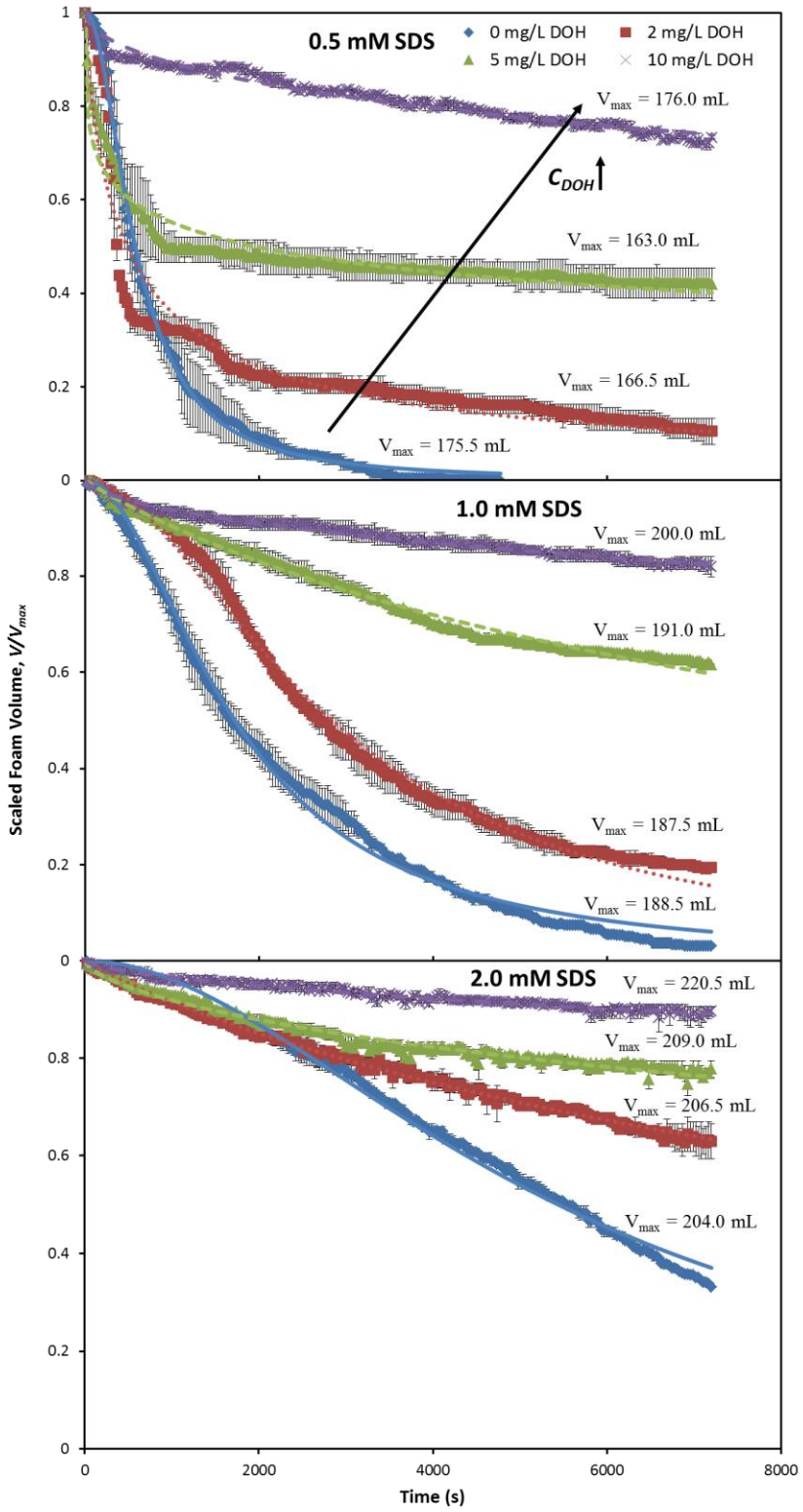

Figure 1. Scaled foam volume vs. time for collapsing SDS-DOH foams. Symbols and lines indicate the experimental data and simulation results fitted by Eq. (5), respectively. The error bars represent the standard errors of the mean. The value of $V_{\max}$ for each solution is indicated.

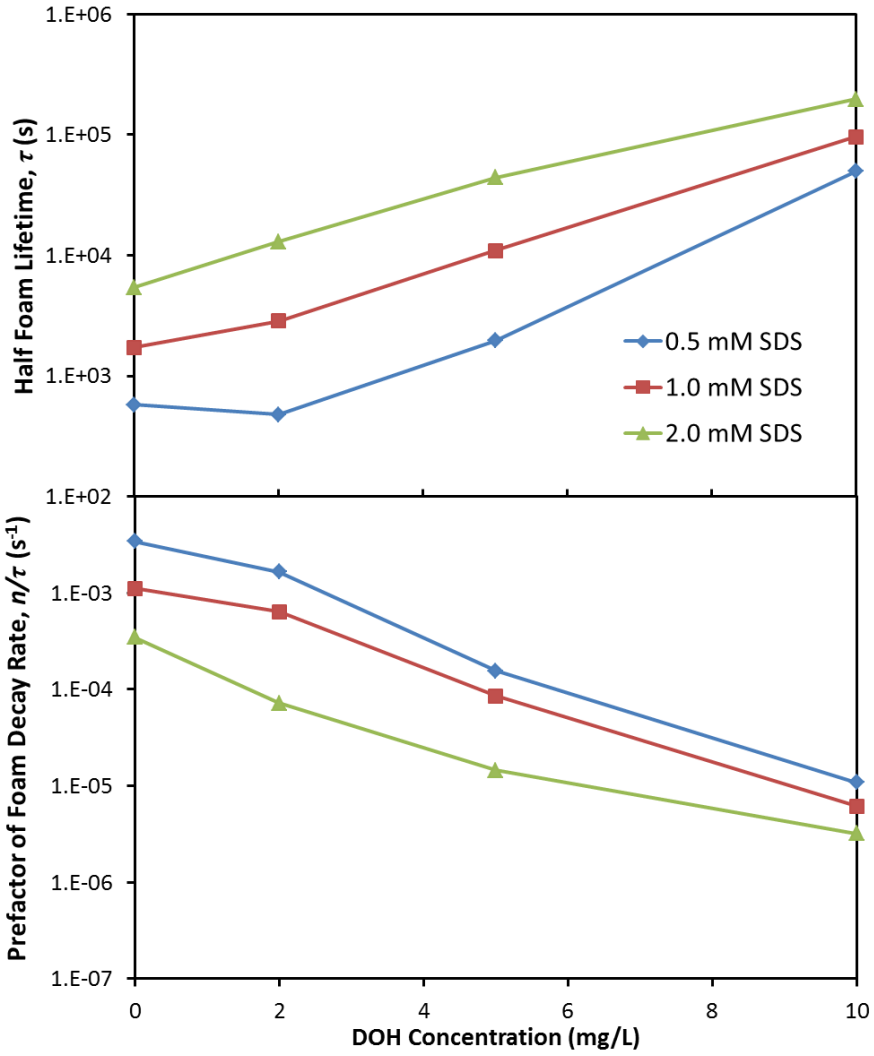

Figure 2. The half foam lifetime, τ, in Eq. (5) and the prefactor of foam decay, n/τ, in Eq. (8) for collapsing SDS-DOH foams.

5.1.2 Dynamic surface tension and surface viscoelasticity

Please refer to Section 5.2 in Chapter 4 for details.

5.1.3 Surface potential

Figure 3 (Figure 10 in Chapter 4) shows the surface (zeta) potential data of air bubbles in SDS solutions with and without 2 mg/L of DOH. The concentration of DOH is reasonably below its solubility limit, which is 4 mg/L at 29.5°C, as shown in Section 4.1. The displacement of SDS molecules by DOH molecules results in a substantial decrease in the surface potential, which is caused by the considerably higher surface activity of DOH relative to SDS. Similarly, the surface charge of TTAB solutions has been shown to be decreased by the addition of DOH because of the replacement of TTAB molecules by DOH molecules [17]. Despite the reduced double-layer repulsion, the presence of DOH increases the foam stability

of SDS foams because of the dominant effect of the surface viscoelasticity. The surface potential also increases with the SDS concentration, indicating increased electrostatic interactions that favor the liquid film and foam stability.

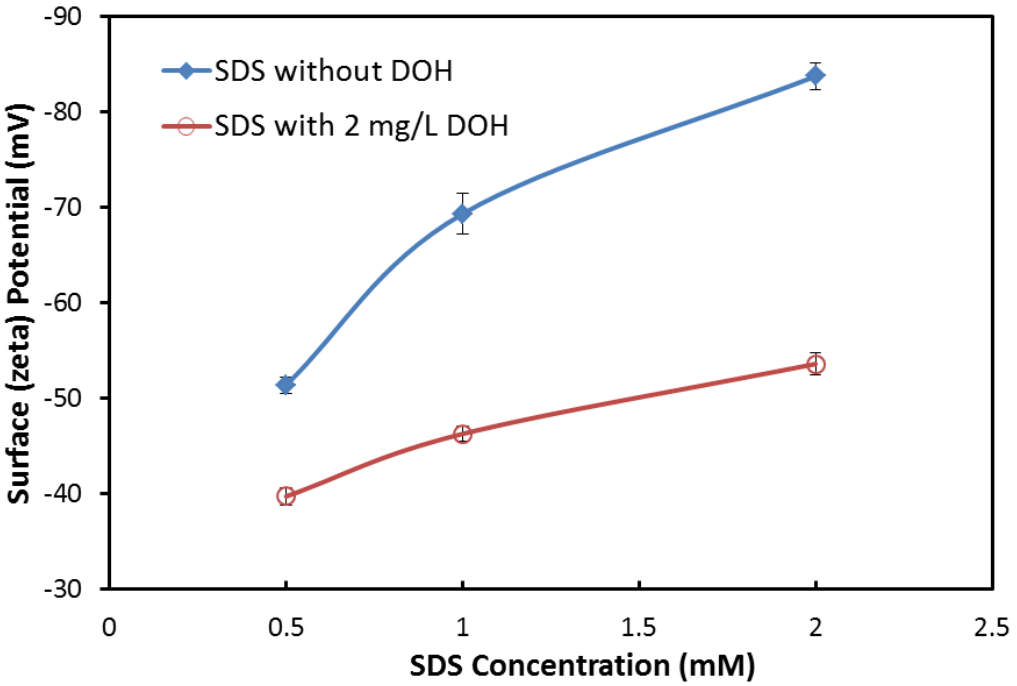

Figure 3. Comparison of the surface (zeta) potential of air bubbles in SDS solutions with and without 2 mg/L of DOH.

5.2 Foam stability of SDS-NaCl mixtures

5.2.1 Dependence of adsorption on the mean ionic product, c^*

The adsorption and surface tension have been shown to depend on the mean ionic activity rather than the surfactant concentration when an inorganic electrolyte, such as NaCl, is present [18-20]. To elucidate the effect of NaCl on the stability of SDS foams, we carefully selected the molar concentration ratio of SDS to NaCl to maintain a constant surface tension (Figure 4) by adjusting the mean ionic activity, $c^* = f_{\pm}(c_{SDS+NaCl} \times c_{SDS})^{1/2}$, to 1 mM. $f_{\pm}$ is the average activity coefficient of ions in the solution and is calculated using the Debye-Hückel equation as follows:

$$\log f_{\pm} = -\frac{0.5115 \times \sqrt{I}}{1+1.316 \times \sqrt{I}} + 0.055 \times I \qquad (9)$$

where I is the ionic strength in mol/l and the numerical constants correspond to 25°C [21].

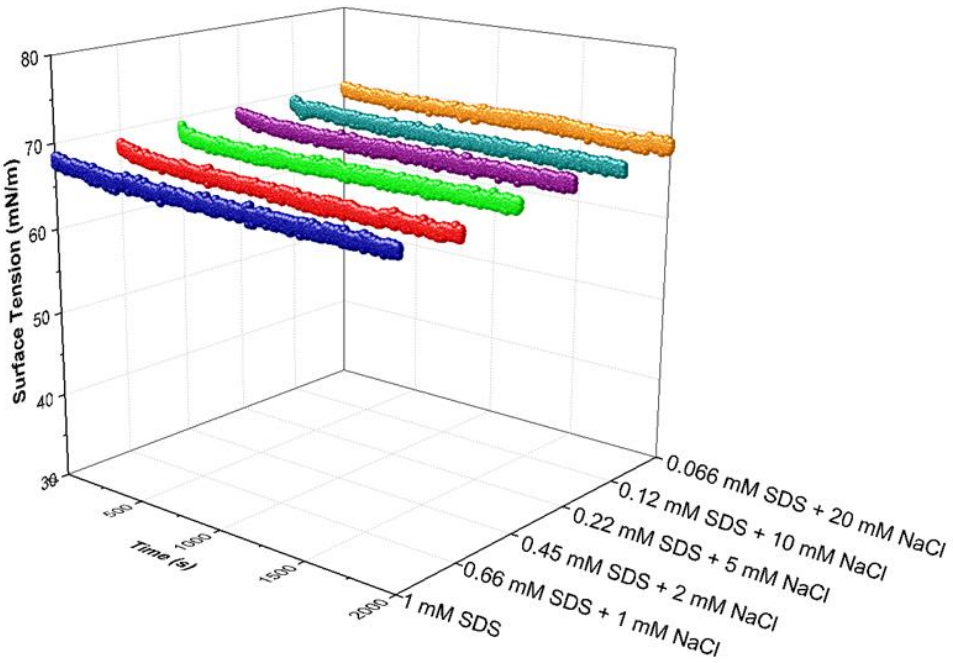

Figure 4. Dynamic surface tension of SDS-NaCl solutions with the same value of the mean ionic activity, $c^* = 1$ mM.

Figure 4 indicates that as a result of the reduced electrostatic double-layer repulsion, the presence of NaCl in SDS solutions promotes the adsorption of SDS molecules on the air-water interface, despite the relatively low concentration of SDS in the solution. The effect of NaCl on the foam stability of the solutions containing 0.1 mM of SDS was previously examined [6] by simple shaking tests [22]. An increased foam lifetime was recorded as the NaCl concentration was increased from 0 mM to 1 mM. However, when the NaCl concentration was increased further to 10 mM and 100 mM, the foam lifetime decreased. The increased foam lifetime was partially ascribed to the rapid decrease in the hydrophobic force in foam films, whereas the decreased foam stability was attributed to the decreased electrostatic repulsion in the foam films. We agree with the above conclusions. However, we wish to emphasize that the increased foam stability caused by increasing the NaCl concentration in SDS solutions with a constant SDS concentration (0.1 mM) shown in [6] was also caused by the enhanced adsorption of SDS molecules on the air-water interface resulting from the decreased double-layer repulsion.

5.2.2 Foam collapse for SDS-NaCl foams

Figure 5 shows the foam collapse curves for SDS-NaCl mixtures and the simulation results fitted by Eq. (5). The simulation results fit the experimental data very well, again

indicating the validity of the model developed in Section 3. The presence of NaCl is found to significantly reduce the foam lifetime of SDS foams, and the efficacy is proportional to the NaCl concentration. To quantify the foam collapse process and make comparisons, the half foam lifetime, τ, in Eq. (5) and the prefactor of the foam collapse rate, n/τ, in Eq. (8) are plotted as a function of NaCl concentration in Figure 6. The half foam lifetime, τ, decreases with the NaCl concentration in SDS solutions. Conversely, the prefactor of the foam collapse rate, n/τ, increases with the NaCl concentration.

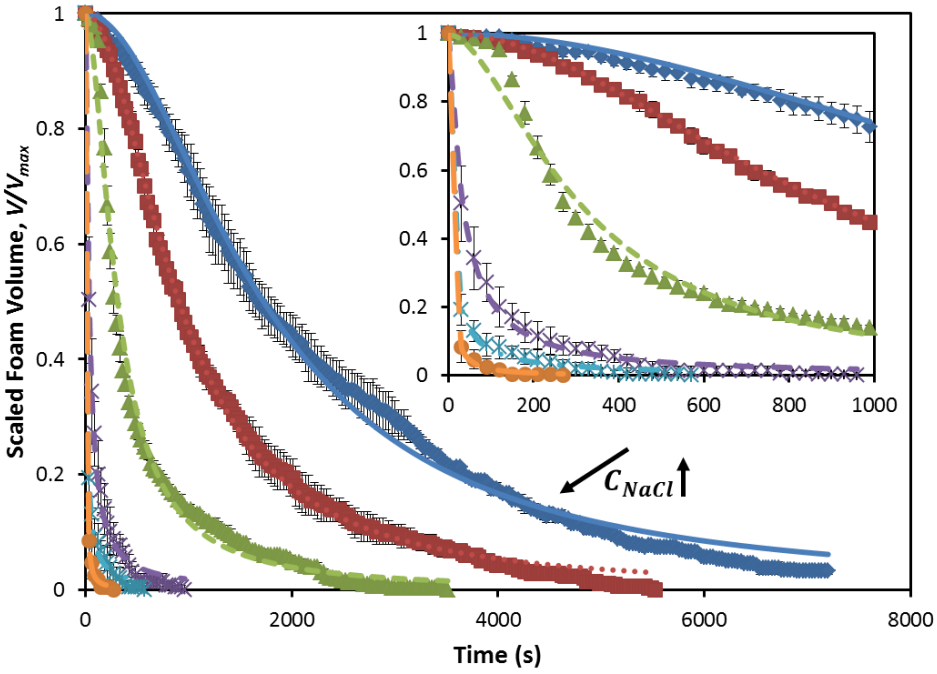

Figure 5. Scaled foam volume vs. time for collapsing SDS-NaCl foams with the same value of the mean ionic activity, $c^* = 1$ mM. Symbols and lines indicate the experimental data and simulation results fitted by Eq. (9), respectively. Arrows in the graph indicate the direction of the increase in the NaCl concentration from 0 mM to 20 mM. The values of V_{max} are 188.5 mL, 178.0 mL, 169.5 mL, 141.0 mL, 126.0 mL and 115.0 mL for SDS-NaCl solutions with NaCl concentrations of 0 mM, 1 mM, 2 mM, 5 mM, 10 mM and 20 mM, respectively.

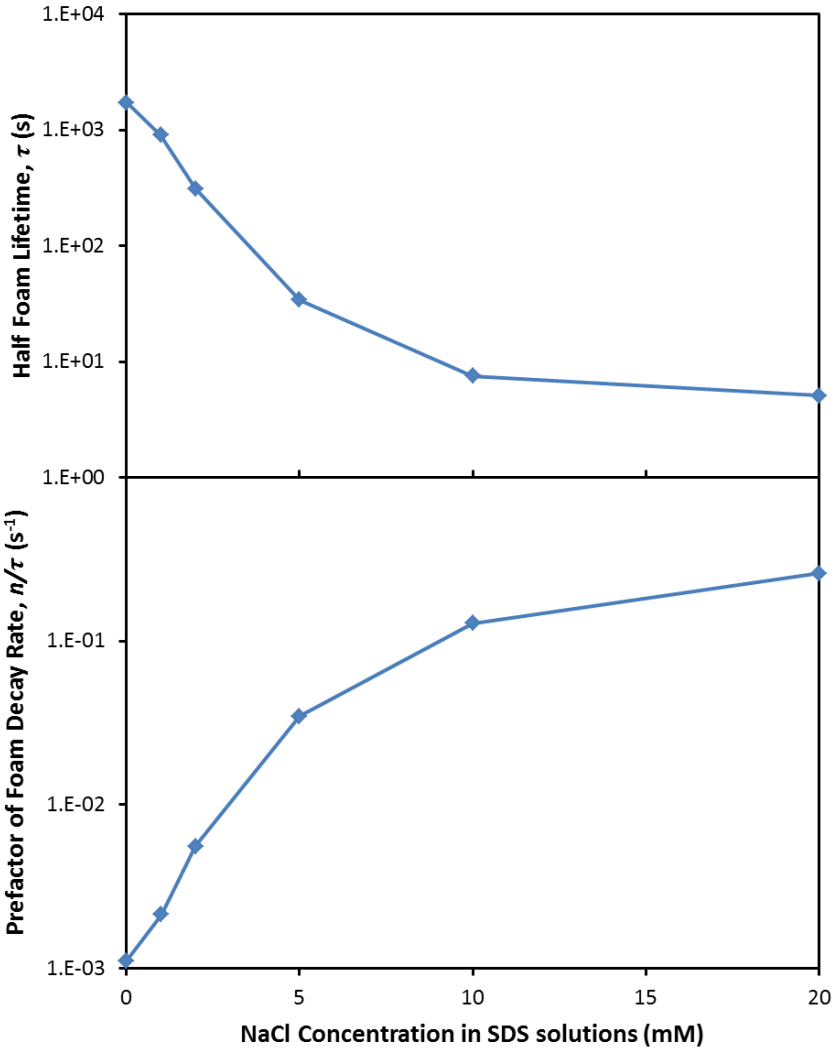

Figure 6. The half foam lifetime, τ, in Eq. (5) and the prefactor of foam decay, n/τ, in Eq. (8) for collapsing SDS-NaCl foams with the same value of the mean ionic activity, $c^* = 1$ mM.

5.2.3 Correlation between foam stability and surface (zeta) potential

To correlate the foam stability of SDS-NaCl mixtures with the surface (zeta) potential of air bubbles in the solution and the characteristic thickness of the electrical double-layer (EDL), we conducted measurements of the zeta potential of air bubbles in SDS-NaCl solutions and calculated the Debye length, κ^{-1}. For the monovalent electrolytes, κ^{-1} is mathematically described by [23]:

$$\kappa^{-1} = \sqrt{\frac{\varepsilon_r \varepsilon_0 k_B T}{2 N_A e^2 I}} \tag{10}$$

where ε_0 is the permittivity of vacuum, ε_r is the dielectric constant, k_B is Boltzmann's constant, T is the absolute temperature in Kelvin, N_A is Avogadro's number, e is the elementary charge and I is the ionic strength of the solution in mol/m^3. For a monovalent electrolyte at 25°C, the Debye length of aqueous solutions can be expressed as a function of ionic strength only [24]:

$$\kappa^{-1} = \frac{0.304}{\sqrt{I}} \tag{11}$$

where κ^{-1} is measured in nm and the ionic strength I is measured in mol/L. Please note that the magnitude of the Debye length depends only on the properties of the solution rather than on any property of the surface, such as its charge or potential.

Table 1 shows the zeta potential, ς, of air bubbles, the Debye length, κ^{-1}, and the half foam lifetime, τ, for SDS-NaCl solutions with the same value of the mean ionic activity, $c^* = 1$ mM but different values of the ionic strength I. For comparison, the zeta potential data of SDS micelles with different NaCl concentrations from [25] are also shown. Because of the screening effect caused by the binding of sodium counter ions to the sulfate head groups [26], the absolute value of the zeta potential, ς, decreases from 69.2 mV to 34.1 mV when the NaCl concentration increases from 0 mM to 20 mM in SDS solutions. The absolute value of the zeta potential for 1 mM SDS without NaCl (69.2 mV) is reasonably lower than the zeta potential of SDS micelles (87.0 mV). Similar to the effect of NaCl concentration on the zeta potential of SDS micelles [25], the presence of 1 mM NaCl significantly reduces the absolute value of the zeta potential for SDS solutions with $c^* = 1$ mM from 69.2 mV to 42.6 mV. However, when the NaCl concentration increases from 1 mM to 20 mM, the absolute value of the zeta potential for SDS solutions with $c^* = 1$ mM decreases from 42.6 mV to 34.1 mV. Because of the increased ionic strength in the solution, the Debye length decreases from 9.6 nm to 2.1 nm when the NaCl concentration increases from 0 mM to 20 mM for the SDS solutions with $c^* = 1$ mM, indicating that the presence of NaCl decreases the distance within which the electrostatic interactions between the two charged interfaces become significant. Because of the decreased repulsion and characteristic thickness of the electrical double layer, the half foam lifetime, τ, decreases from 1724.1 s to 5.1 s when the NaCl concentration

increases from 0 mM to 20 mM for the SDS solutions with $c^* = 1$ mM. Please note that the increased surface mobility of SDS foams in the presence of NaCl may also contribute to the decreased foam stability [27].

Table 1. Zeta potential, ς, of air bubbles, Debye length, κ^{-1}, and half foam lifetime, τ, for SDS-NaCl solutions with the same value of the mean ionic activity, $c^* = 1$ mM, and the zeta potential data of SDS micelles with different NaCl concentrations from [25] highlighted by gray shading.

C_{SDS} (mM)	C_{NaCl} (mM)	Mean ionic activity, c^* (mM)	Zeta potential, ς (mV)	Debye length, κ^{-1} (nm)	Half foam lifetime, τ (s)
1.00	0	1.0	-69.2±2.2	9.6	1724.1
0.66	1.0	1.0	-42.6±2.2	7.5	903.0
0.45	2.0	1.0	-41.9±2.4	6.1	309.8
0.22	5.0	1.0	-37.0±2.5	4.2	34.1
0.12	10.0	1.0	-36.0±1.3	3.0	7.6
0.066	20.0	1.0	-34.1±1.3	2.1	5.1
17.3	0	above CMC	-87.0	-	-
1.7	42.8	above CMC	-50.8	-	-
1.7	85.6	above CMC	-49.3	-	-
1.7	128.3	above CMC	-45.8	-	-
1.7	171.1	above CMC	-43.5	-	-

6. Conclusions

The foam stability of SDS-DOH and SDS-NaCl foams was studied to elucidate the mechanisms by which foams collapse. For SDS-DOH foams, the high surface viscoelasticity caused by the presence of DOH is responsible for the highly stable foams, despite the decreased double-layer repulsive forces between the interfaces of the liquid films caused by the replacement of SDS molecules by DOH molecules. In contrast, for SDS-NaCl foams, the deceased double-layer repulsion in the presence of NaCl caused by the binding of sodium counter ions to the sulfate head groups results in a significant decrease in the stability of the SDS foams, regardless of whether the same amount of SDS molecules is adsorbed on the

interface. Additionally, we proposed a novel model to describe the foam collapse that is inspired by chemical kinetics.

Acknowledgements

The authors gratefully acknowledge the China Scholarship Council (CSC) of the Chinese Government and The University of Queensland (UQ) for the CSC-UQ scholarship for JW.

References

[1] D. Weaire, S. Hutzler, The Physics of Foams, Clarendon Press, Oxford, 1999.
[2] I. Cantat, S. Cohen-Addad, F. Elias, F. Graner, R. Hohler, O. Pitois, F. Rouyer, A. Saint-jalmes, Foams: Structure and Dynamics, CPI Group (UK) Ltd, Croydon, 2013.
[3] A. Saint-Jalmes, Physical chemistry in foam drainage and coarsening, Soft Matter, 2 (2006) 836-849.
[4] S.I. Karakashev, A.V. Nguyen, Effect of sodium dodecyl sulphate and dodecanol mixtures on foam film drainage: Examining influence of surface rheology and intermolecular forces, Colloids and Surfaces A: Physicochemical and Engineering Aspects, 293 (2007) 229-240.
[5] S.I. Karakashev, E.D. Manev, A.V. Nguyen, Effect of double-layer repulsion on foam film drainage, Colloids and Surfaces A: Physicochemical and Engineering Aspects, 319 (2008) 34-42.
[6] L. Wang, R.-H. Yoon, Hydrophobic Forces in the Foam Films Stabilized by Sodium Dodecyl Sulfate: Effect of Electrolyte, Langmuir, 20 (2004) 11457-11464.
[7] D. Monin, A. Espert, A. Colin, A New Analysis of Foam Coalescence: From Isolated Films to Three-Dimensional Foams, Langmuir, 16 (2000) 3873-3883.
[8] W. Müller, J.M.d. Meglio, Avalanches in draining foams, Journal of Physics: Condensed Matter, 11 (1999) L209.
[9] N. Vandewalle, J.F. Lentz, S. Dorbolo, F. Brisbois, Avalanches of Popping Bubbles in Collapsing Foams, Physical Review Letters, 86 (2001) 179-182.
[10] N. Vandewalle, J.F. Lentz, Cascades of popping bubbles along air/foam interfaces, PHYSICAL REVIEW E, 64 (2001) 021507.
[11] N. Vandewalle, H. Caps, S. Dorbolo, Cascades of popping bubbles, Physica A: Statistical Mechanics and its Applications, 314 (2002) 320-324.
[12] S.J. Neethling, H.T. Lee, P. Grassia, The growth, drainage and breakdown of foams, Colloids and Surfaces A: Physicochemical and Engineering Aspects, 263 (2005) 184-196.
[13] O. Levenspiel, Chemical Reaction Engineering, Industrial & Engineering Chemistry Research, 38 (1999) 4140-4143.
[14] R. Stephenson, J. Stuart, Mutual binary solubilities: water-alcohols and water-esters, Journal of Chemical & Engineering Data, 31 (1986) 56-70.
[15] J.A. Dean, Lange's Handbook of Chemistry, McGRAW-HILL, INC., New York, 1967.
[16] L. Liggieri, F. Ravera, M. Ferrari, Surface Rheology Investigation of the 2-D Phase Transition in n-Dodecanol Monolayers at the Water-Air Interface, Langmuir, 19 (2003) 10233-10240.
[17] B. Oriane, M. Anne, S. Gilles, B. Anne-Laure, Surface conductivity measurements in nanometric to micrometric foam films, Journal of Physics: Condensed Matter, 27 (2015) 194118.
[18] V.B. Fainerman, E.H. Lucassen-Reynders, Adsorption of single and mixed ionic surfactants at fluid interfaces, Advances in Colloid and Interface Science, 96 (2002) 295-323.
[19] V.B. Fainerman, D. Mèobius, R. Miller, Surfactants: chemistry, interfacial properties, applications, Elsevier Science, Ltd, Amsterdam, 2001.
[20] V.B. Fainerman, S.V. Lylyk, E.V. Aksenenko, J.T. Petkov, J. Yorke, R. Miller, Surface tension isotherms, adsorption dynamics and dilational visco-elasticity of sodium dodecyl sulphate solutions, Colloids and Surfaces A: Physicochemical and Engineering Aspects, 354 (2010) 8-15.

[21] R.A. Robinson, R.H. Stokes, Electrolyte solutions: the measurement and interpretation of conductance, chemical potential and diffusion in solutions of simple electrolytes, Butterworths, London, 1965.
[22] Å. Waltermo, P.M. Claesson, S. Simonsson, E. Manev, I. Johansson, V. Bergeron, Foam and Thin-Liquid-Film Studies of Alkyl Glucoside Systems, Langmuir, 12 (1996) 5271-5278.
[23] W.B. Russel, D.A. Saville, W.R. Schowalter, Colloidal Dispersions, Cambridge University Press, 1989.
[24] J.N. Israelachvili, Intermolecular and Surface Forces, Elsevier, Sydney, 2011.
[25] Q. Xu, M. Nakajima, S. Ichikawa, N. Nakamura, P. Roy, H. Okadome, T. Shiina, Effects of surfactant and electrolyte concentrations on bubble formation and stabilization, Journal of Colloid and Interface Science, 332 (2009) 208-214.
[26] G.V. Hartland, F. Grieser, L.R. White, Surface potential measurements in pentanol-sodium dodecyl sulphate micelles, Journal of the Chemical Society, Faraday Transactions 1: Physical Chemistry in Condensed Phases, 83 (1987) 591-613.
[27] D.S.H. Sita Ram Sarma, K.C. Khilar, Comments on effects of electrolyte on the drainage of aqueous foams, Journal of Colloid and Interface Science, 137 (1990) 300-303.

Chapter 7: Foam Drainage in the Presence of Solid Particles

Jianlong Wang[1], Anh V Nguyen[1*] and Saeed Farrokhpay[2]
[1]School of Chemical Engineering, University of Queensland, Brisbane, Queensland 4072, Australia
[2]JKMRC, University of Queensland, Brisbane, Queensland 4072, Australia

[*]Correspondence: anh.nguyen@eng.uq.edu.au

Highlights:

- We conducted forced drainage experiments of CTAB foams with silica particles.
- The presence of solid particles induces a transition of the foam drainage regime.
- The presence of solid particles increases the rigidity of foam interfaces.

Graphical abstract:

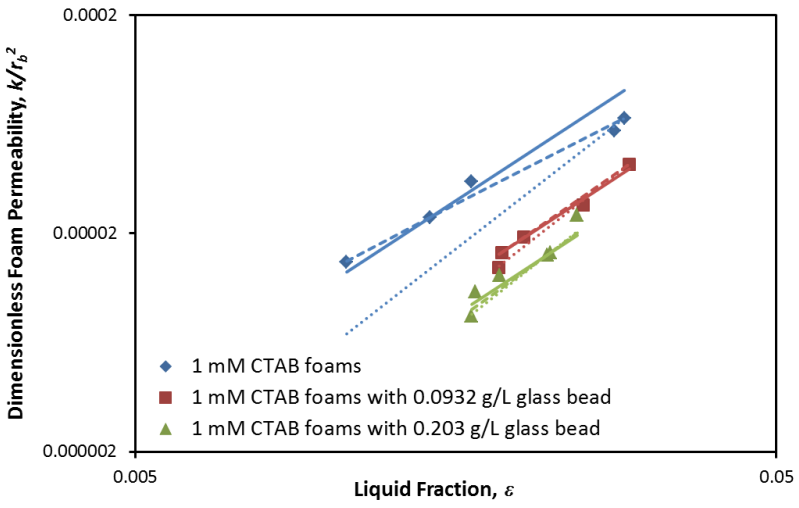

Abstract

We conducted forced drainage experiments to study the liquid flow within the foams stabilized by a cationic surfactant (CTAB) in the presence of partially hydrophobic glass beads with a floatable size ($d_{0.8} = 86.6\mu m$). The results show that the presence of solid particles, even when present in small amounts (0.093 g/L), can significantly decrease the foam permeability. The scaling behavior (power law) between the drainage velocity and the imposed flow rate indicates that the presence of solid particles in the foams triggers a transition of the foam drainage regime from a node-dominated regime to a Plateau border-dominated regime. We applied two foam drainage equations for aqueous foams to simulate the experimental data and interpret the transition. The simulation results show that the presence of solid particles in the foams increases the rigidity of the interfaces and the viscous losses in the channels (Plateau borders) of the foams, and decreases the foam permeability. This study explores the liquid drainage in the three-phase froth and is relevant to the field of froth flotation, in which the wash water is commonly applied to the froth layer to improve the product's grade.

Keywords: foam, foam drainage, froth flotation, solid particle

1. Introduction

Foams are widely applied in our daily lives and in industries because of their lightness and large specific surface area. A recent textbook summarized their applications, including food, cosmetics, cleaning, surface treatment, building materials, reducing pollution and the extraction of natural resources (e.g., froth flotation) [1]. Their immense practical and industrial importance has motivated fundamental studies of foams. The lifetime of a foam depends on three different mechanisms: the foam drainage caused by gravity, the coarsening caused by the gas transfer between bubbles induced by capillary pressure differences, and the bubble coalescence caused by the rupture of liquid films between neighboring bubbles [1]. Because foam drainage influences the liquid fraction of a foam, which determines both the coarsening and bubble coalescence [2-8], it is crucially important with regard to the lifetime of a foam. In the earliest work on modeling foam drainage [9], it was assumed that the viscous losses caused by the liquid flow occur only in the Plateau borders (i.e., the channels) with rigid walls. This assumption was applied by subsequent researchers [10, 11], and a Plateau border-dominated approach for the study of foam drainage was developed. This approach was challenged when the contributions of the nodes, where the channels meet, were

recognized and mobile Plateau border walls were assumed [12]. Since then, the standard foam drainage equation [9] has been modified [13] and foam drainage models that consider viscous losses from both the Plateau borders and nodes have been proposed [14, 15]. All of these foam drainage models have been applied only to two-phase aqueous foams. In practice, however, three-phase foams or froths in which solid particles are present are more common in industrial processes, such as froth flotation. In froth flotation, the wash water is commonly applied to the froth phase to flush the entrained gangue out of the froth and consequently increase the product's grade. Although froth washing has been widely applied in froth flotation, a complete understanding of the liquid flow in a three-phase froth is lacking.

Recently, foam drainage results in the presence of suspended particulate matter, such as coal fly ashes [16], clays [17], and particulate suspensions [18, 19], together with fundamental studies on the drainage behavior of liquid and hydrophilic particles in foams [20-26], have been reported. Nevertheless, few studies have focused on foam drainage in the presence of partially hydrophobic particles (i.e., hydrophobized by the adsorption of a surfactant to the particle surface) with sizes in the most floatable region (approximately 10 micron to 70 micron), which is of paramount interest for froth flotation. The partial hydrophobization of (and addition of a negative charge to) silica particles by cationic surfactants, such as hexadecyltrimethylammonium bromide (CTAB) [27] and dodecylamine acetate [28], with sizes of 10 μm and 45 μm, respectively, can increase the stability of foams and liquid films. Although the decreased drainage of liquid films by these partially hydrophobic particles with sizes larger than the average film thickness has been ascribed to the dispersion of surface waves [27], which is caused marginal regeneration [29], an understanding of the drainage behavior remains lacking. In the present study, we conducted forced drainage experiments to investigate the liquid flow within the foams stabilized by a cationic surfactant (i.e., CTAB) in the presence of partially hydrophobic glass beads. We also applied two existing foam drainage equations for two-phase aqueous foams to the experimental results for three-phase froths. This chapter attempts to address the following questions: How does the presence of solid particles affect foam drainage? Can the foam drainage equations for aqueous foams be applied to describe the foam drainage of three-phase foams? What are the effects of solid particles on the stress state of the gas-liquid interface of foams?

2. Theory

2.1. Foam permeability

The flow of liquid through a foam layer is analogous to the fluid flow through a porous medium. However, it must be recalled that there are two significant differences between liquid drainage through a foam and that through a porous medium [1]. First, in a foam, the size of the network (i.e., Plateau borders and nodes) through which the liquid flow is not fixed but is actually dependent on the flow itself. That is to say, the bubbles can move apart to allow liquid to pass and then move back. Second, the interfaces are not completely rigid but are instead partially mobile in a foam, depending on the interfacial properties, such as the surface shear viscosity. The classic Darcy's law that describes the fluid flow through a porous medium is also applicable to aqueous foams [8, 12, 30-32]. For a gravity-driven flow, we obtain [30]:

$$j_d = \frac{\kappa}{\mu}\rho g \tag{1}$$

where j_d is the superficial liquid velocity imposed on the top of the foam layer, κ is the foam permeability, μ is the liquid dynamic viscosity, ρ is the liquid density and g is the acceleration due to gravity. The permeability is usually scaled with the square of the bubble size to obtain a dimensionless foam permeability, κ / r_b^2 [30]. Here, we correlate the dimensionless foam permeability for the liquid fraction, ε, using two existing foam drainage equations [14, 33] for aqueous foams to study the effects of glass beads on foam permeability.

2.2. Foam drainage model I: Liquid flow through a single Plateau border

The velocity profile within a single Plateau border has been numerically calculated. The expression for the mean liquid velocity through a vertical Plateau border, u, has also been proposed [33]:

$$u = \frac{A}{\mu}\frac{dp}{dz}\left\{\frac{0.0655Bo^{-0.5}}{0.209 + Bo^{0.628}} + 0.02\right\} \tag{2}$$

where A is the cross-sectional area of the Plateau borders, dp/dz is the pressure gradient (positive downward), and the Boussinesq number is defined by $Bo = \mu_s / \mu r$, where μ_s is the surface shear viscosity and r is the radius of curvature of the Plateau border walls. If we

suppose that the angles between the liquid films that form the Plateau border are 120°, the area of the Plateau border cross-section is $A=\left(\sqrt{3}-\pi/2\right)r^2$ [1, 10], where r has been approximated to be a function of the liquid fraction, ε, and the bubble radius, r_b [34]: $r/r_b=1.28\varepsilon^{0.46}$, using the equation in [14], which was developed from geometrical arguments. Consider the random orientation of the Plateau borders in the foams: the average distance between two points along the Plateau borders is three times the straight line distance between the points [10, 14], i.e., $u=3j_d/\varepsilon$. Additionally, bearing in mind Eqs. (1) and (2), the dimensionless foam permeability, κ/r_b^2, can be expressed as a function of the liquid fraction, ε [32]:

$$\frac{\kappa}{r_b^2}=0.088\varepsilon^{1.92}\left\{\frac{0.0655Bo^{-0.5}}{0.209+Bo^{0.628}}+0.02\right\} \tag{3}$$

Please note that Eq. (3) assumes that all losses occur in the Plateau borders with a finite surface shear viscosity. If we assume that the walls of the Plateau borders are rigid (i.e., Bo is infinite), Eq. (3) can be re-written as $\kappa/r_b^2=0.0018\varepsilon^{1.92}$ [32]. The dimensionless foam permeability as a function of the liquid fraction can be calculated with Eq. (3) for $Bo=$ constant and $\mu_s=$ constant.

2.3. Foam drainage model II: Viscous losses contribution from nodes

The advantage of Eq. (3) is that the surface shear viscosity can be estimated if the relationship between κ/r_b^2 and ε can be obtained by forced drainage experiments. However, because the contribution of the viscous losses from the nodes is ignored, the applicability of Eq. (3) is limited, especially for the node-dominated foam drainage regime [12, 35]. Alternatively, a foam drainage equation that can account for the effects of both the Plateau borders and nodes has been proposed [14] and can be re-written as:

$$\frac{\kappa}{r_b^2}=\varepsilon\left[\frac{3C_{pb}}{\left(1.28\varepsilon^{0.46}\right)^2}+\frac{4.178\left(C_v-0.418C_{pb}\right)}{1.28\varepsilon^{0.46}}\left(1-\varepsilon\right)^{1/3}+6.806\left(C_v-1.588C_{pb}\right)\left(1-\varepsilon\right)^{2/3}\right]^{-1} \tag{4}$$

where C_{pb} is the Plateau border loss coefficient that equals 50 if the walls of the Plateau borders are rigid, and C_V is the vertex (node) loss coefficient.

3. Experimental

3.1. Materials

CTAB was purchased from Sigma-Aldrich with a purity $\geq 99\%$. The glass beads were obtained from the mining lab of The University of Queensland.

3.2. Forced drainage experiment

The forced drainage experimental method was first introduced in [36]. Briefly, foams were prepared within a transparent perspex column (internal diameter: 90 mm; length: 500 mm) filled with 450 mL of 1 mM CTAB solution containing different concentrations of glass beads (0, 1 and 2 wt%) while blowing bubbles of nitrogen through a sparger plate (sintered bronze) at the bottom of the column. The low solubility of nitrogen can effectively prevent the bubble coalescence within the foam column. Subsequently, the gas flow was stopped, and the foam column was left to drain under gravity for 15 minutes. Finally, an additional volume of 1 mM CTAB was introduced onto the top of the foam column using a burette with different volumetric flowrates, Q. The foam column was then divided by the wet front into the wet zone above the front and the dry zone below it. A power law relationship between the superficial velocity of the wet front, V_f, and the imposed liquid flowrate, Q, was reported [37]. For convenience, we use the superficial velocities in this study, and as a result, V_f is also proportional to a power of the superficial drainage velocity in the foams:

$$V_f \propto \left(\frac{Q}{A}\right)^{\alpha} = {j_d}^{\alpha} \tag{5}$$

It has been found that $\alpha = 1/2$ corresponds to a Poiseuille flow through rigid Plateau borders [38] or a Plateau border-dominated regime [35], whereas $\alpha = 1/3$ corresponds to a plug flow through a mobile gas-liquid interface or node (vertice)-dominated regime [12]. The volumetric liquid fraction, ε, of the foams in the wet zone can be calculated by:

$$\varepsilon = \frac{j_d}{V_f} \tag{6}$$

Therefore, the most striking advantage of the forced drainage experiment is that the liquid fraction can be readily controlled by altering the liquid flowrate imposed on the top of the foam column. The concentration of the glass beads within the foam column was estimated by

measuring the dry weight of the glass beads from the collected overflow foams and the volume of the overflow foams. The images of the foam layer captured by a digital camera were processed using an image processing software (ImageJ, NIH, US) to measure the bubble size. More than 100 bubbles were measured for each solution to obtain the Sauter mean diameter, d_{32}. Please note that the potential errors involved in this method of measuring the bubble size have been discussed previously [39]. The Sauter mean bubble diameter, d_{32}, for foams stabilized by 1 mM CTAB solutions with 0, 1 and 2 wt% glass beads are 0.92, 1.28 and 1.57 mm, respectively. The value of d_{32} for 0.8 mM CTAB foam is 1.07 mm.

3.3. Particle size measurement

Particle size measurements were conducted with a Mastersizer 2000 from Malvern Instruments using laser diffraction. The intensity of the light scattered as a laser beam passes through a dispersed particulate sample was measured. Then, the light intensity was analyzed to calculate the size of the particles that created the scattering pattern. The particle size distribution of the glass beads is shown in Figure 1. The 50% ($d_{0.5}$) and 80% ($d_{0.8}$) sizes of the glass bead sample are 59.4 μm and 86.6 μm, respectively.

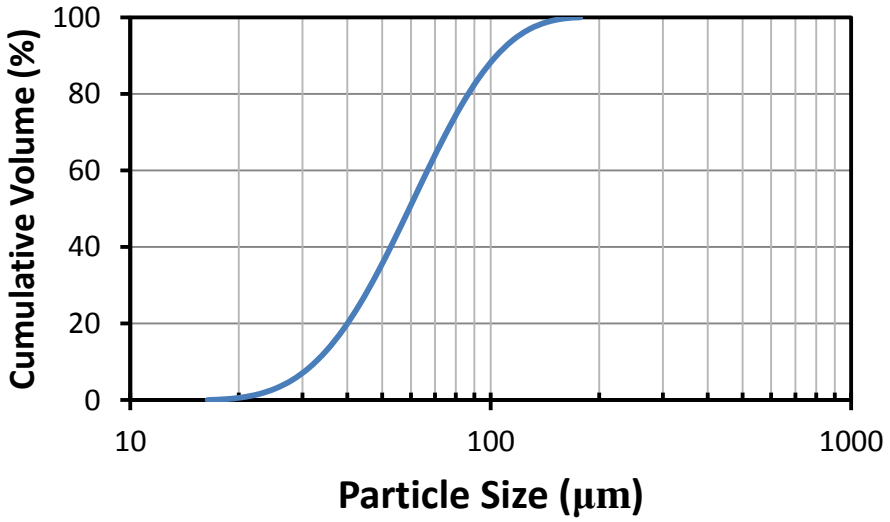

Figure 1. The cumulative size distribution of the glass bead sample.

3.4. Contact angle measurement

A glass bead was carefully attached to a bubble produced by a capillary to measure the contact angle. A capillary was connected to a hole with an internal diameter of 1 mm on the wall of a perspex container of dimensions $5 \times 5 \times 80$ mm that was filled with 1 mM CTAB solution. A glass bead was dropped into the hole, and a microsyringe and microsyringe pump system were used to produce one bubble attached to the glass bead. With the glass bead attached to the interface of the bubble, an image (Figure 2) was captured by a CCD camera (Potron, Japan). The edges of the bubble and the glass bead were digitalized, and the contact angle (33.8°) was calculated based on the image using Matlab software. The contact angle value indicates that the negatively charged surface of the glass bead is partially hydrophobized by the cationic surfactant CTAB. Although this contact angle is still low for flotation purposes, our study remains relevant to the froth phase in froth flotation where large amounts of hydrophobic particles attach to the air-water interface, resulting in changes in the interface mobility.

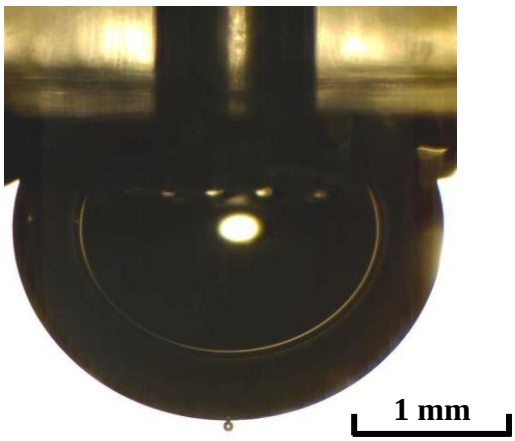

Figure 2. Image of the bubble with one glass bead attached to calculate the contact angle.

4. Results and discussion

4.1. Transition of foam drainage regime

Figure 3 summarizes the forced drainage data for CTAB foams with different glass bead concentrations. The CTAB foams without glass beads where $\alpha = 0.34$ for 1 mM CTAB (above the CMC of 0.92 mM) foams and $\alpha = 0.36$ for 0.8 mM CTAB foams exhibit a foam drainage regime similar to the node-dominated regime where $\alpha = 1/3$, and the flow in the Plateau borders is plug-like [12]. The similar α values indicate that the transition of the foam drainage regime is independent of the surfactant concentration. Notably, the power law

exponent increases from 0.34 for 1 mM CTAB foams without glass beads to 0.51 for the same foams with 0.0932 g/L glass beads and further increases to 0.64 for a higher glass bead concentration (0.203 g/L). We recall that a value of α close to $1/2$ indicates a Plateau border-dominated regime, where the flow in the Plateau borders is Poiseuille-like. Therefore, the presence of glass beads in the CTAB foams triggers a transition of the foam drainage regime from a node-dominated regime to a Plateau border-dominated regime. A similar transition has also been reported in foams stabilized by SiO_2 nanoparticle-cationic surfactant (TTAB) mixtures [18]. To investigate the effects of glass beads on the foam permeability and interfacial properties of CTAB foams, the two foam drainage equations in Section 2 are applied to interpret the experimental data.

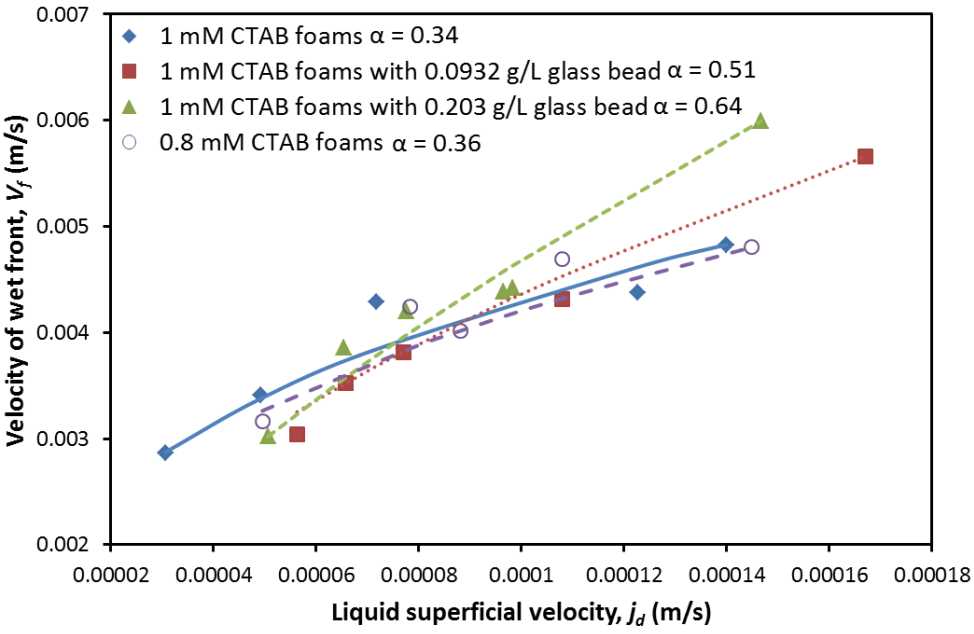

Figure 3. Forced drainage results for CTAB foams with different glass bead concentrations in foams. The different lines correspond to power law fits of experimental data.

4.2. Dimensionless foam permeability

Figure 4 shows the dimensionless foam permeability as a function of the liquid fraction for 1 mM CTAB foams with different glass bead concentrations. A decrease in dimensionless foam permeability has been observed as the glass bead concentration increases. The decrease in foam permeability caused by the presence of solid particles has previously been established in surfactant foams containing SiO_2 nanoparticles [18], clay particles [17] and

coal fly ash [16]. Please note that the effects of the size, shape and hydrophobicity of solid particles on the stability of foams and liquid films have been known for a long time [40-46]. Specifically, the maximum stability of the froth with quartz particles (26–44 μm) was observed at an intermediate degree of hydrophobicity, and the hydrophilic particles did not exert a noticeable influence on the froth stability [43]. This effect of the hydrophobicity of solid particles on froth stability indicates that the attached partially hydrophobic solid particles may alter the stress state of the interface and thereby affect the liquid drainage and the froth stability as a whole.

As expected, fits of the forced drainage data for 1 mM CTAB foams with Eq. (3) for both $Bo = \text{constant}$ and $\mu_s = \text{constant}$ are less ideal than those for the foams with glass beads because Eq. (3) only accounts for the viscous losses in the Plateau borders, whereas the liquid flow in 1 mM CTAB foams without glass beads is node dominated. In contrast, the foam drainage equation that accounts for the contribution of viscous losses from both the Plateau borders and the nodes fits the forced drainage data for CTAB foams both with and without glass beads fairly well. Table 1 summarizes the power law exponent, α, in Eq. (5), the constants Bo and μ_s in Eq. (3), and the constants C_{PB} and C_V in Eq. (4) for 1 mM CTAB foams with and without glass beads. As the glass bead concentration in CTAB foams increases, α also increases from 0.34 to 0.64, indicating a transition from the node-dominated regime to the Plateau border-dominated regime. Please note that a large power law index, such as $\alpha = 0.64$, exceeds the limit of the Plateau border-dominated regime, which is $\alpha = 0.5$. A similar phenomenon has been reported for surfactant foams with coal fly ash [16], for which the large permeability exponents and prefactors are attributed to the rheology of the powder suspension and clogging in the confined regions of the Plateau borders. Because the draining liquid used in this study is a surfactant solution rather than a powder suspension, we can assume that only the second mechanism applies. To verify this clogging effect, we calculated the confinement parameter [19, 21, 24-26], which compares the size of the particle with the maximum diameter of the circle inscribed in the Plateau border cross-section: $\lambda = d / d_{\lim}$, where $d_{\lim} = 2r\left(2/\sqrt{3} - 1\right)$. To find the maximum possible value of $d_{\lim}$ (i.e., the smallest value of λ), we applied the largest bubble radius ($r_b = 0.635\,\text{mm}$) observed for foams stabilized by 1 mM CTAB with 2 wt% glass beads with a liquid fraction of $\varepsilon = 5\%$ (i.e., well above the experimental values shown in Figure 4) to calculate the radius of

curvature of the Plateau border walls: $r/r_b = 1.28\varepsilon^{0.46}$. Finally, we obtain the value of $d_{\lim} \approx 62\mu m$. By applying $d_{0.8} = 86.6\mu m$, we obtain the smallest possible value of $\lambda \approx 1.4$. It has been reported that for $\lambda > 1$, particles are trapped in the foams, and the resulting drainage velocity is strongly reduced [24-26]. Please note that we attribute the decreased foam permeability only to the mobility of the interfaces that is quantified by Bo and μ_s. It is reasonable to conclude that the increase in Bo and μ_s in the presence of particles is partially caused by clogging effects.

Correspondingly, Bo increases from 0.044 to 0.20 for $Bo =$ constant fits with Eq. (3), and μ_s increases from $0.74\times10^{-8} Pa.m.s$ to $3.47\times10^{-8} Pa.m.s$ for $\mu_s =$ constant fits with Eq. (3), indicating a decrease in interface mobility when the glass bead concentration in the foams increases from 0 g/L to 0.203 g/L. The effects of solid particles on the enhancement of interface rigidity have been previously reported [43]. Additionally, an investigation of the surface dilational rheology of mixed silica nanoparticle-CTAB interfacial layers showed the transfer or accumulation of solid particles at the liquid interface can increase the surface viscoelasticity [47]. The Plateau border loss coefficient, C_{PB}, increases from 1.91 to 29.19, whereas the vertex (node) loss coefficient, C_V, decreases from 16.08 to 4.96 for the fits with Eq. (4) when the glass bead concentration increases from 0 g/L to 0.203 g/L, again indicating a transition of the foam drainage regime.

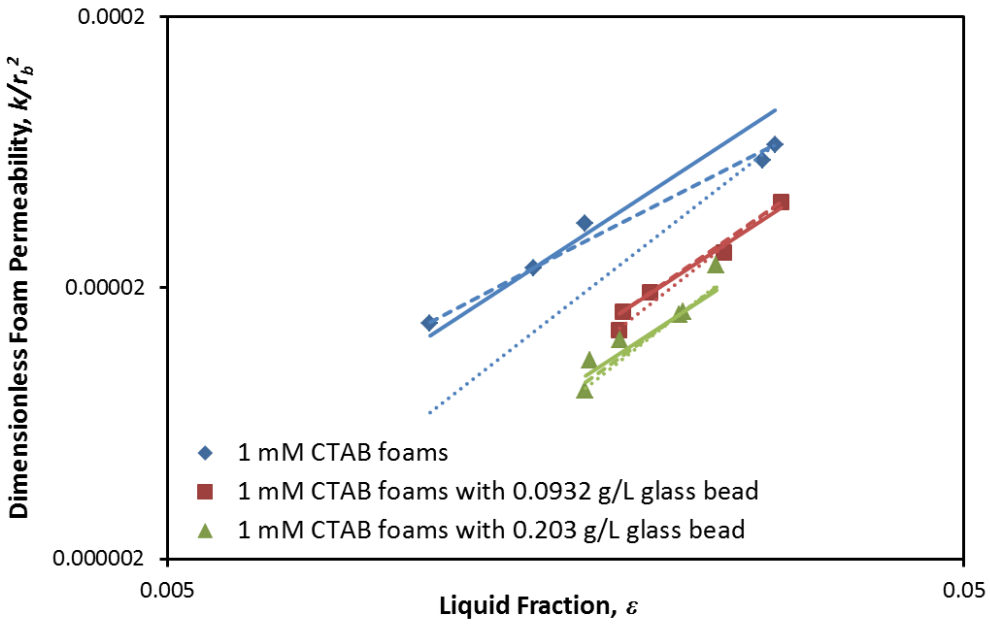

Figure 4. Dimensionless foam permeability as a function of the liquid fraction. Solid lines: fitting curves with Eq. (3) for $Bo =$ constant. Dotted lines: fitting curves with Eq. (3) for $\mu_s =$ constant. Dashed lines: fitting curves with Eq. (4) for $C_{PB}, C_V =$ constant. The Sauter mean bubble radii for 1 mM CTAB foams with 0 g/L, 0.0932 g/L and 0203 g/L glass beads in foams are 0.46 mm, 0.64 mm and 0.78 mm, respectively.

Table 1. Exponent, α, in Eq. (5) and constants in Eqs. (3) and (4)

System	α	Bo	$\mu_s \times 10^{-8} (Pa.m.s)$	C_{pb}	C_V
1 mM CTAB foams	0.34	0.044	0.74	1.91	16.08
1 mM CTAB foams with 0.0932 g/L glass beads	0.51	0.13	2.01	17.30	8.75
1 mM CTAB foams with 0.203 g/L glass beads	0.64	0.20	3.47	29.19	4.96

5. Conclusions

We conducted forced drainage experiments to study the effects of partially hydrophobic glass beads on the liquid drainage in CTAB foams. Two existing foam drainage equations for aqueous foams were successfully applied to simulate the forced drainage results for foams in the presence of solid particles. The simulation results show that the presence of solid particles triggers a transition from a node-dominated foam drainage regime to a Plateau border-dominated foam drainage regime because of the increased surface shear viscosity of the interface and viscous losses in the Plateau borders of the foams.

Acknowledgements

The authors gratefully acknowledge the China Scholarship Council (CSC) of the Chinese Government and The University of Queensland (UQ) for the CSC-UQ scholarship for JW.

References

[1] I. Cantat, S. Cohen-Addad, F. Elias, F. Graner, R. Hohler, O. Pitois, F. Rouyer, A. Saint-jalmes, Foams: Structure and Dynamics, CPI Group (UK) Ltd, Croydon, 2013.
[2] S. Hutzler, D. Weaire, S. Shah, Bubble sorting in a foam under forced drainage, Philosophical Magazine Letters, 80 (2000) 41-48.
[3] S. Hutzler, D. Weaire, Foam coarsening under forced drainage, Philosophical Magazine Letters, 80 (2000) 419-425.
[4] S. Hilgenfeldt, S.A. Koehler, H.A. Stone, Dynamics of Coarsening Foams: Accelerated and Self-Limiting Drainage, Physical Review Letters, 86 (2001) 4704-4707.
[5] A.E. Roth, C.D. Jones, D.J. Durian, Bubble statistics and coarsening dynamics for quasi-two-dimensional foams with increasing liquid content, PHYSICAL REVIEW E, 87 (2013) 042304.
[6] S.-J. Arnaud, L. Dominique, Time evolution of aqueous foams: drainage and coarsening, Journal of Physics: Condensed Matter, 14 (2002) 9397.
[7] V. Carrier, A. Colin, Coalescence in Draining Foams, Langmuir, 19 (2003) 4535-4538.
[8] A. Saint-Jalmes, Physical chemistry in foam drainage and coarsening, Soft Matter, 2 (2006) 836-849.
[9] R.A. Leonard, R. Lemlich, A study of interstitial liquid flow in foam. Part I. Theoretical model and application to foam fractionation, AIChE Journal, 11 (1965) 18-25.
[10] G. Verbist, D. Weaire, A.M. Kraynik, The foam drainage equation, Journal of Physics: Condensed Matter, 8 (1996) 3715.
[11] V. Goldshtein, I. Goldfarb, I. Shreiber, Drainage waves structure in gas-liquid foam, International Journal of Multiphase Flow, 22 (1996) 991-1003.
[12] S.A. Koehler, S. Hilgenfeldt, H.A. Stone, Liquid Flow through Aqueous Foams: The Node-Dominated Foam Drainage Equation, Physical Review Letters, 82 (1999) 4232-4235.
[13] L. Randriamanjatosoa, M. Zanin, S. Grano, Use of the foam drainage equation to model water flow in flotation froth, CHEMECA, Engineering Australia, Melbourne, Australia, 2007, pp. 300-306.
[14] S.J. Neethling, H.T. Lee, J.J. Cilliers, A foam drainage equation generalized for all liquid contents, Journal of Physics: Condensed Matter, 14 (2002) 331.
[15] S.A. Koehler, S. Hilgenfeldt, H.A. Stone, A Generalized View of Foam Drainage: Experiment and Theory, Langmuir, 16 (2000) 6327-6341.

[16] A. Britan, M. Liverts, G. Ben-Dor, S.A. Koehler, N. Bennani, The effect of fine particles on the drainage and coarsening of foam, Colloids and Surfaces A: Physicochemical and Engineering Aspects, 344 (2009) 15-23.
[17] R.M. Guillermic, A. Salonen, J. Emile, A. Saint-Jalmes, Surfactant foams doped with laponite: unusual behaviors induced by aging and confinement, Soft Matter, 5 (2009) 4975-4982.
[18] F. Carn, A. Colin, O. Pitois, M. Vignes-Adler, R. Backov, Foam Drainage in the Presence of Nanoparticle-Surfactant Mixtures, Langmuir, 25 (2009) 7847-7856.
[19] S. Guignot, S. Faure, M. Vignes-Adler, O. Pitois, Liquid and particles retention in foamed suspensions, Chemical Engineering Science, 65 (2010) 2579-2585.
[20] N. Louvet, R. Höhler, O. Pitois, Capture of particles in soft porous media, PHYSICAL REVIEW E, 82 (2010) 041405.
[21] F. Rouyer, C. Fritz, O. Pitois, The sedimentation of fine particles in liquid foams, Soft Matter, 6 (2010) 3863-3869.
[22] F. Rouyer, N. Louvet, C. Fritz, O. Pitois, Transport of coarse particles in liquid foams: coupling of confinement and buoyancy effects, Soft Matter, 7 (2011) 4812-4820.
[23] F. Carn, A. Colin, O. Pitois, R. Backov, Foam drainage study during plateau border mineralisation, Soft Matter, 8 (2012) 61-65.
[24] Y. Khidas, B. Haffner, O. Pitois, Capture-induced transition in foamy suspensions, Soft Matter, 10 (2014) 4137-4141.
[25] B. Haffner, Y. Khidas, O. Pitois, Flow and jamming of granular suspensions in foams, Soft Matter, 10 (2014) 3277-3283.
[26] F. Rouyer, B. Haffner, N. Louvet, Y. Khidas, O. Pitois, Foam clogging, Soft Matter, 10 (2014) 6990-6998.
[27] J.B.M. Hudales, H.N. Stein, The influence of solid particles on foam and film drainage, Journal of Colloid and Interface Science, 140 (1990) 307-313.
[28] S.W. Ip, Y. Wang, J.M. Toguri, Aluminum foam stabilization by solid particles, Canadian Metallurgical Quarterly, 38 (1999) 81-92.
[29] V.A. Nierstrasz, G. Frens, Marginal Regeneration and the Marangoni Effect, Journal of Colloid and Interface Science, 215 (1999) 28-35.
[30] E. Lorenceau, N. Louvet, F. Rouyer, O. Pitois, Permeability of aqueous foams, THE EUROPEAN PHYSICAL JOURNAL E, 28 (2009) 293-304.
[31] A. Saint-Jalmes, Y. Zhang, D. Langevin, Quantitative description of foam drainage: Transitions with surface mobility, THE EUROPEAN PHYSICAL JOURNAL E, 15 (2004) 53-60.
[32] P. Stevenson, Dimensional analysis of foam drainage, Chemical Engineering Science, 61 (2006) 4503-4510.
[33] A.V. Nguyen, Liquid Drainage in Single Plateau Borders of Foam, Journal of Colloid and Interface Science, 249 (2002) 194-199.
[34] P. Stevenson, C. Stevanov, Effect of Rheology and Interfacial Rigidity on Liquid Recovery from Rising Froth, Industrial & Engineering Chemistry Research, 43 (2004) 6187-6194.
[35] M. Durand, G. Martinoty, D. Langevin, Liquid flow through aqueous foams: From the plateau border-dominated regime to the node-dominated regime, Phys. Rev. E: Stat. Phys., Plasmas, Fluids, Relat. Interdiscip. Top., 60 (1999) R6307-R6308.
[36] D. Weaire, N. Pittet, S. Hutzler, D. Pardal, Steady-state drainage of an aqueous foam, Physical Review Letters, 71 (1993) 2670-2673.
[37] G. Verbist, D. Weaire, A Soluble Model for Foam Drainage, EPL (Europhysics Letters), 26 (1994) 631.
[38] A.V. Nguyen, H.J. Schulze, Colloidal science of flotation, Marcel Dekker, New York, 2004.
[39] H.C. Cheng, R. Lemlich, Errors in the measurement of bubble size distribution in foam, Industrial & Engineering Chemistry Fundamentals, 22 (1983) 105-109.
[40] R. Aveyard, B.P. Binks, J.H. Clint, Emulsions stabilized solely by colloidal particles, Advances in Colloid and Interface Science, 100–102 (2003) 503-546.

[41] R. Aveyard, B.P. Binks, P.D.I. Fletcher, T.G. Peck, C.E. Rutherford, Aspects of aqueous foam stability in the presence of hydrocarbon oils and solid particles, Advances in Colloid and Interface Science, 48 (1994) 93-120.
[42] P.R. Garrett, J. Davis, H.M. Rendall, An experimental study of the antifoam behavior of mixtures of a hydrocarbon oil and hydrophobic particles, Colloids and Surfaces A: Physicochemical and Engineering Aspects, 85 (1994) 159-197.
[43] G. Johansson, R.J. Pugh, The influence of particle size and hydrophobicity on the stability of mineralized froth, International Journal of Mineral Processing, 34 (1992) 1-21.
[44] S. Schwarz, S. Grano, Effect of particle hydrophobicity on particle and water transport across a flotation froth, Colloids and Surfaces A: Physicochemical and Engineering Aspects, 256 (2005) 157-164.
[45] T.N. Hunter, R.J. Pugh, G.V. Franks, G.J. Jameson, The role of particles in stabilising foams and emulsions, Advances in Colloid and Interface Science, 137 (2008) 57-81.
[46] A. Dippenaar, The destabilization of froth by solids. I. The mechanism of film rupture, International Journal of Mineral Processing, 9 (1982) 1-14.
[47] L. Liggieri, E. Santini, E. Guzman, A. Maestro, F. Ravera, Wide-frequency dilational rheology investigation of mixed silica nanoparticle-CTAB interfacial layers, Soft Matter, 7 (2011) 7699-7709.

Chapter 8: Conclusions and Recommendations for Future Research

1. Conclusions

This thesis has focused on the modeling of foam column kinetics, the effects of interfacial properties on foamability and foam stability and the effect of solid particles on foam drainage. The following conclusions can be reached based on the research presented here:

(1) A novel kinetic model has been proposed to interrelate the growth, drainage and collapse of foams to simulate the foam collapse and the evolution of foam height, liquid fraction, and the transport of liquid and gas in growing foams by analogy with reaction kinetics. Models to describe the foam column kinetics were summarized and categorized as zeroth, first and second order, according to the dependence of the foam collapse rate on the foam volume or height. The model predictions of foam growth and collapse show good agreement with the reported experimental results.

(2) Investigation of the foamability of the surfactant blend (i.e., SDS and DOH) revealed an anomalous effect of DOH on the foamability of SDS solutions. The remarkable decrease in foamability of SDS solutions caused by the addition of DOH cannot be easily explained by the theories of surface tension and surface viscoelasticity. Instead, alternative mechanisms were proposed to resolve these unexpected results. Below the DOH solubility limit, the displacement of SDS molecules by DOH molecules at the air-water interface results in a reduced surface potential, leading to a lower foamability, whereas the antifoam effects of DOH droplets account for the decreased foamability above the DOH solubility limit. The model developed in Chapter 3 was used to simulate the experimental results and interpret the antifoam effects of DOH.

(3) Examination of the effects of a nonpolar collector on the stability of two-phase froth showed that the presence of diesel oil, even in trace amounts (2 ppm), can effectively decrease the foam growth rate by accelerating the foam decay process. Two mechanisms were proposed to elucidate the observed antifoam effects of diesel oil: (i) the spreading of diesel oil droplets at the liquid film interface, which is quantified by the spreading pressure, and (ii) the molecular interactions between diesel oil and the frother molecules. Additionally, the model developed in Chapter 3 was used to simulate the experimental results and interpret the antifoam effects of diesel oil.

(4) The study addressing the rupture of a standing foam column stabilized by an anionic surfactant, that is, SDS with DOH and NaCl, indicates different roles of surface

viscoelasticity and intermolecular forces in foam stability. The presence of DOH in the SDS solutions was found to significantly increase the surface viscoelasticity and foam stability, despite the decreased surface potential caused by the displacement of SDS molecules by DOH molecules at the air-water interface. The retarded foam drainage and enhanced liquid film stability result in the relatively high stability of SDS-DOH foams compared with SDS foams. For SDS-NaCl mixtures with the same value of the mean ionic product (1 mM), the increased concentration of NaCl in SDS solutions reduces the surface potential and the Debye length because of the screening effect caused by the binding of sodium counter ions to the sulfate head groups. The foam stability decreases as a result of the weakened repulsive interactions between the two interfaces of the liquid films, despite the presence of the same surface concentration of SDS molecules, as indicated by the same equilibrium surface tension. Again, the model developed in Chapter 3 was used to simulate the experimental results and interpret the foam collapse behavior.

(5) Forced drainage experiments were conducted to study the liquid flow within the foams stabilized by a cationic surfactant (CTAB) in the presence of partially hydrophobic glass beads of floatable size ($d_{0.8} = 86.6\mu m$). A significant decrease in foam permeability was observed and ascribed to the presence of solid particles in the foams. Additionally, a transition of foam drainage was triggered according to the scaling behavior (power law) between the drainage velocity and the imposed flow rate. Moreover, two foam drainage equations for aqueous foams were applied to simulate the experimental data and interpret the transition. The simulation results showed that the presence of solid particles in the foams increases the rigidity of the interfaces and the viscous losses in the channels (Plateau borders) of the foams, resulting in a decrease in foam permeability.

2. Recommendations for future research

The present study represents an ongoing effort to study foam behavior and its governing mechanisms. Despite substantial research in this area, the behaviors of foam remain poorly understood. Indeed, thus far, there exists no general theory to explain foam properties for all types of foam systems. A variety of mechanisms have been proposed, but none can individually determine the foam properties. Thus, the complicated interplay of these mechanisms should always be considered when discussing foam properties. For foams in the presence of solid particles, the situation is even more complex because of the effect these particles exert on the interfacial properties and particle-particle interactions. Nevertheless,

investigation of the two-phase foam properties will undoubtedly establish useful benchmarks and contribute to our understanding of three-phase froth behavior. For future research, the following recommendations are made:

(1) The present study has shown that foam column kinetics can be simulated if the foam drainage parameters *m* and *n*, the superficial gas velocity, j_g, and the equilibrium foam height, $H_{\max}$, are known. In future studies, it may be possible to relax the conditions used in modeling the foam column kinetics if $H_{\max}$ is predictable.

(2) To further understand the mechanisms governing foamability and foam stability, it would be desirable to study the interplay and magnitude of these mechanisms in the different stages of foam life. For example, when the liquid film thickness is exceeds the range of the electrostatic repulsions, the surface viscoelasticity becomes crucial, but the disjoining pressure does not play a critical role in the film stability.

(3) Studying the effect of solid particles (e.g., glass beads) on foam drainage (CTAB foams) is relevant to froth flotation, in which the wash water is commonly applied to the froth layer to improve the product's grade. In future studies, more attention should be given to real froth systems, where both mineral particles and chemical reagents play roles in froth stability.

Appendix

Appendix A. Matlab code for numerical solutions of Eq. (17) – (23) in Chapter 3

A1. Function file: Foam_f.m

```
% Foam growth kinetics function routine: Mass balance only
%
% Mass balance only model
%
% Foam decay dynamics is:
%            F -> L3 + G3   (k2)
%
% Uses Foam_d.m as the driver routine
%
function f = Foam_f(t,y)

% Local variable assignment
e = y(1);       % Liquid fraction in the foam                  [1]
H = y(2);       % m of Foam height                             [2]
L3 = y(3);      % m of Liquid height from bursting bubbles     [3]
G3 = y(4);      % m of Gas from bursting bubbles               [4]
L2 = y(5);      % m of Liquid height from un-bursting bubbles  [5]
G2 = y(6);      % m of Gas from un-bursting bubbles            [6]

% Constants and parameters to be set
u  = 1e-3;        % interstitial liquid dynamic viscosity (Pa.s)
rol = 1000;       % interstitial liquid density (kg.m^-3)
rb = 1e-3;        % mean bubble radius (m)
tau = 0.031;      % equilibrium surface tension (N.m^-1)
g = 9.81;         % acceleration due to gravity (m.s^-1)
m = 0.0065;       % dimensionless number used in Eq. (1)
n = 1.58;         % dimensionless index used in Eq. (1)
p = 1.28;         % dimensionless number used in Eq. (1)
q = 0.46;         % dimensionless index used in Eq. (1)
jg = 8e-5;        % surperficial gas velocity (m.s^-1) jg = 8e-5; 11e-5;
15e-5 and 22e-5
hmax = 15.468e-2;  % maximum equilibrium foam height (m) hmax = 15.46e-2;
21.53e-2; 25.99e-2 and 32.98e-2
A = 7e-4;         % cross-section of foam column (m^2)
jf = 1.33e-10;    % superficial liquid velocity up the column (m/s) jf =
1.33e-10; 3.16e-10; 7.35e-10 and 2.09e-9

% Algebraic equations, in precedence order

k2 = jg/(1-e)/hmax^2;    % Foam decay rate constant (1/(s.m)) [7]

% RHS of differential equations
f(1) = (p*rol*g*rb*e^(1+q)/q/tau*((e*jg/(1-e)-jf)*u/rol/g/rb^2/m/e^n-
1))*(jg/(1-e)-k2*H^2);             % [f1]
f(2) = jg/(1-e)-k2*H^2;            % [f2]
f(3) = e*k2*H^2;                   % [f3]
f(4) = (1-e)*k2*H^2;               % [f4]
f(5) = e*(jg/(1-e)-k2*H^2);        % [f5]
f(6) = (1-e)*(jg/(1-e)-k2*H^2);    % [f6]
f=f';
```

A2. Drive file: Foam_d.m

```
% Foam Growth Model
% Mass balance only model
% Extensive model
% clear memory of any previous data
clear all
% Set the integration range and initial conditions
t0 = 0; tf = 5000;          % integration interval (s)
y0(1) = (1.58-1)/(1.58+1); % boundary condition of liquid fraction of the
foam, e ()
y0(2) = 0;                  % boundary condition of foam height, H (m)
y0(3) = 0;                  % boundary condition of liquid from bursting
bubbles, L3 (m)
y0(4) = 0;                  % boundary condition of gas from bursting
bubbles,G3 (m)
y0(5) = 0;                  % boundary condition of liquid from un-bursting
bubbles, L2 (m)
y0(6) = 0;                  % boundary condition of gas from bursting
bubbles,G2 (m)
% Set the error per step tolerance
toler = 1e-6;           % integration tolerance

% Set start of execution time
starttime = cputime;

% Set the integrator options
opts=odeset('AbsTol',toler,'RelTol',toler);

% Call solver
[t,y]=ode45('Foam_f',[t0,tf],y0,opts);

% Compute execution time of solution
elap = cputime - starttime;

% Print out the execution time
fprintf('Execution time = %5.3f seconds\n',elap)

% Plot results
y1 = y(:,1)*100;
plot(t,y1);
xlabel('Time (s)');
ylabel('Liquid Fraction in the Foam (%)');
ylim([0,30])

figure;

y2 = y(:,2)*100;
plot (t, y2);
xlabel('Time (s)');
ylabel('Foam Height, H (cm)');
ylim([0,20])

figure;
```

```
y3 = y(:,3)*7e-4*1e6;
plot (t, y3);
xlabel('Time (s)');
ylabel('Liqud Volume from Bursting Bubbles, L3 (mL)');
ylim([0,0.25])

figure;

y4 = y(:,4)*7e-4*1e6;

plot (t, y4);
xlabel('Time (s)');
ylabel('Gas Volume from Bursting Bubbles, G3 (mL)');
ylim([0,200])

figure;

y5 = y(:,5)*7e-4*1e6;
plot (t, y5);
xlabel('Time (s)');
ylabel('Liquid Volume in the Foam, L2 (mL)');
ylim([0,1.2])

figure;

y6 = y(:,6)*7e-4*1e6;
plot (t, y6);
xlabel('Time (s)');
ylabel('Gas Volume in the Foam, G2 (mL)');
ylim([0,110])


%legend('e ','H (m)','L1 (mL)','G1 (mL)','L3 (ml)','G3 (ml)')

% End of code
```

Appendix B. Surface tension oscillations of SDS-DOH solutions at a frequency of 0.05 Hz for the calculations of dynamic surface elasticity and viscosity of Figure 9 in Chapter 4

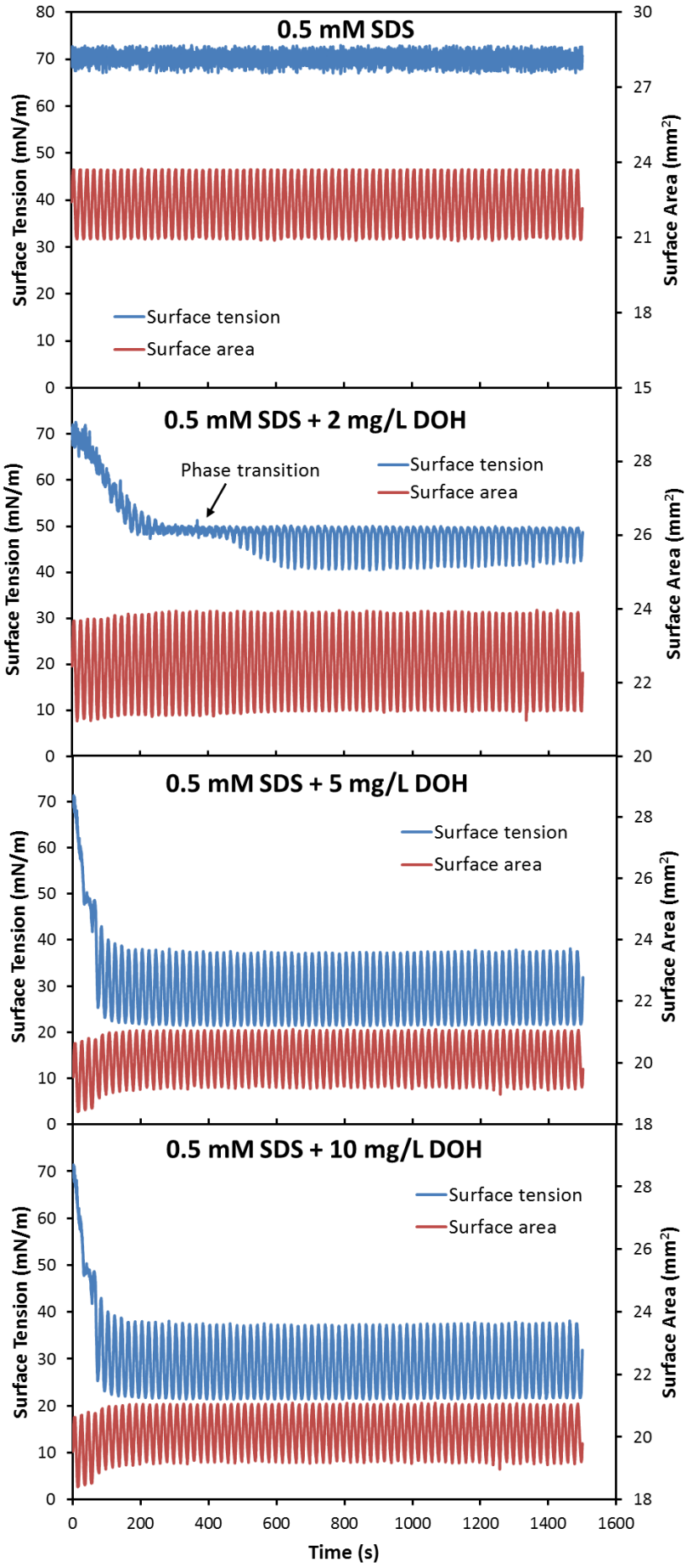
0.5 mM SDS
Surface tension
Surface area
0.5 mM SDS + 2 mg/L DOH
Phase transition
Surface tension
Surface area
0.5 mM SDS + 5 mg/L DOH
Surface tension
Surface area
0.5 mM SDS + 10 mg/L DOH
Surface tension
Surface area
Surface Tension (mN/m)
Surface Area (mm²)
Time (s)
0
200
400
600
800
1000
1200
1400
1600

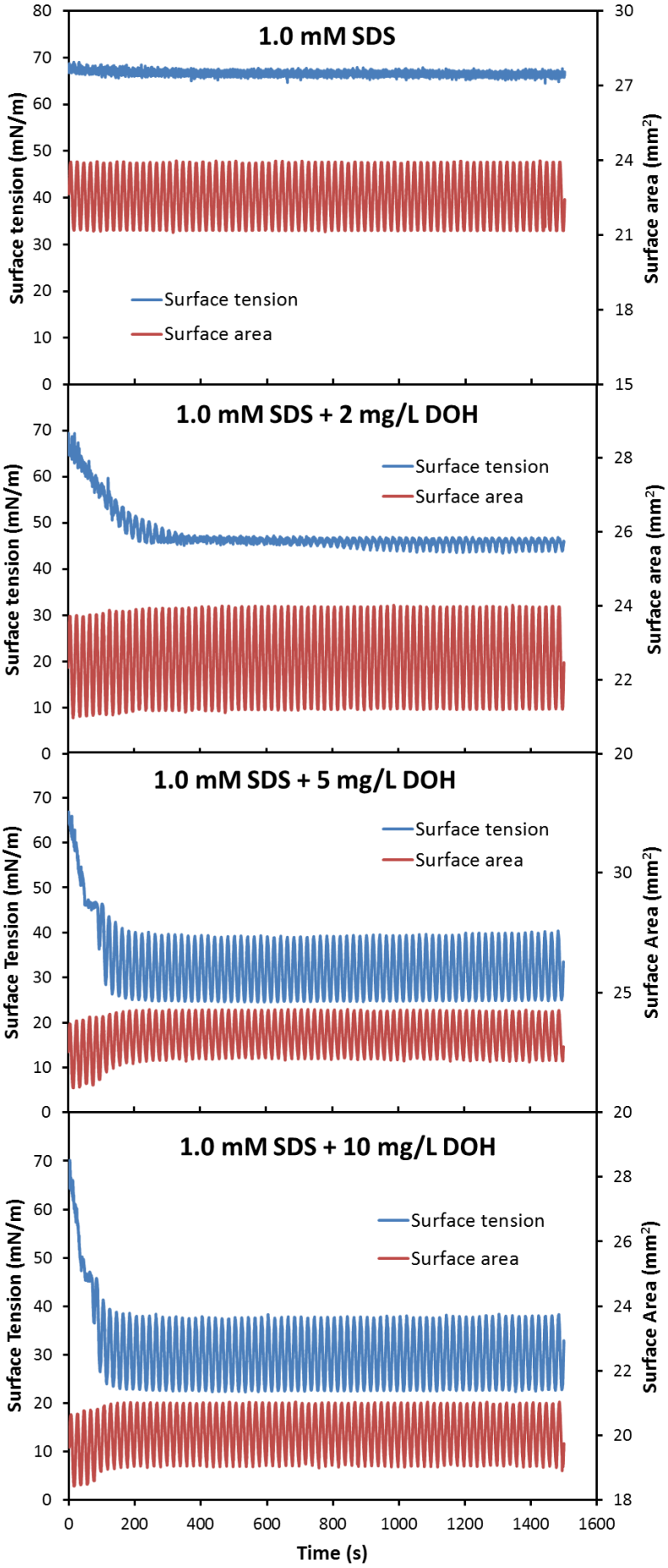
1.0 mM SDS
Surface tension
Surface area
Surface tension (mN/m)
Surface area (mm²)
1.0 mM SDS + 2 mg/L DOH
Surface tension
Surface area
Surface tension (mN/m)
Surface area (mm²)
1.0 mM SDS + 5 mg/L DOH
Surface tension
Surface area
Surface Tension (mN/m)
Surface Area (mm²)
1.0 mM SDS + 10 mg/L DOH
Surface tension
Surface area
Surface Tension (mN/m)
Surface Area (mm²)
Time (s)

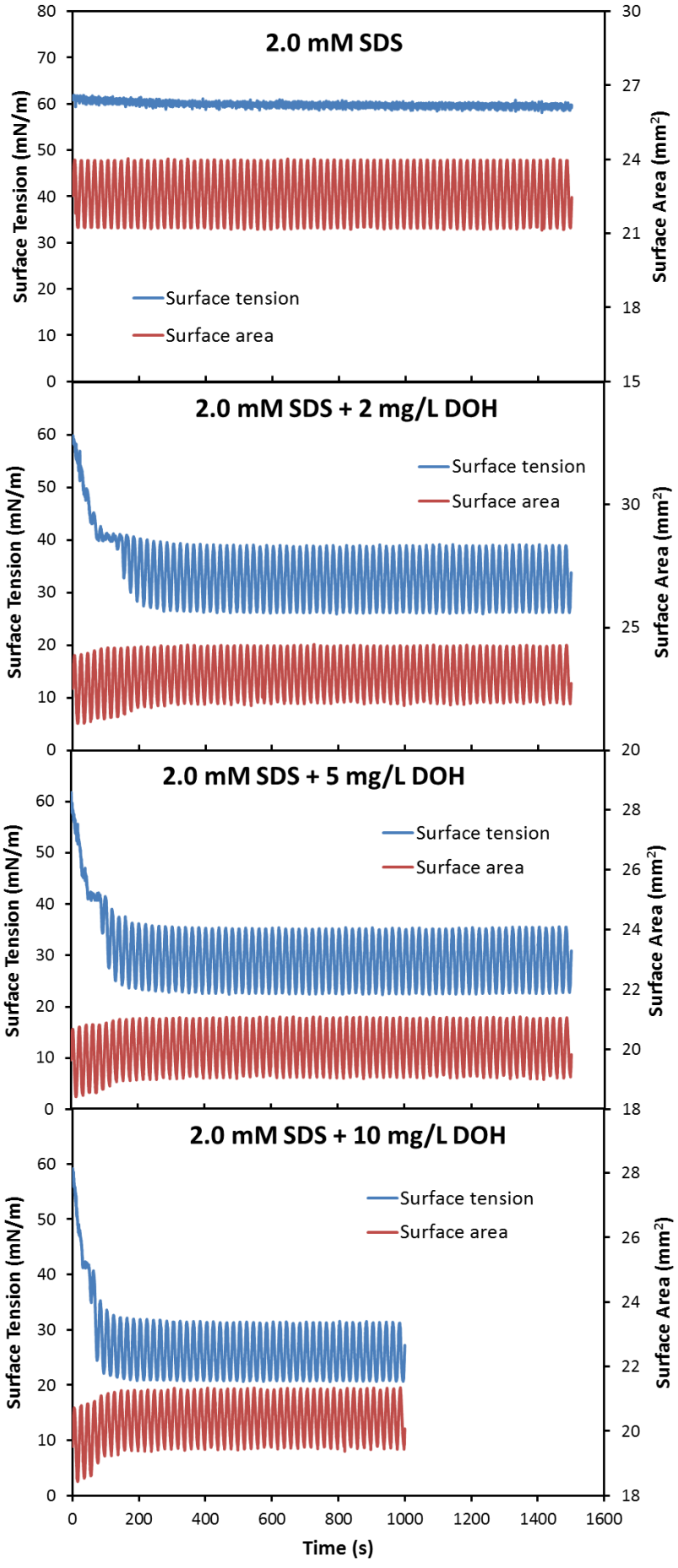
2.0 mM SDS
Surface tension
Surface area
2.0 mM SDS + 2 mg/L DOH
Surface tension
Surface area
2.0 mM SDS + 5 mg/L DOH
Surface tension
Surface area
2.0 mM SDS + 10 mg/L DOH
Surface tension
Surface area
Surface Tension (mN/m)
Surface Area (mm²)
Time (s)
0
200
400
600
800
1000
1200
1400
1600